

University of Alberta

Vortex dynamics and supercurrents in Bi-2212 superconducting single
crystals and films

by

Rongchao Ma

A thesis submitted to the Faculty of Graduate Studies and Research
in partial fulfillment of the requirements for the degree of

Doctor of Philosophy

Department of Physics

©Rongchao Ma

Fall 2009

Edmonton, Alberta

Permission is hereby granted to the University of Alberta Libraries to reproduce single copies of this thesis and to lend or sell such copies for private, scholarly or scientific research purposes only. Where the thesis is converted to, or otherwise made available in digital form, the University of Alberta will advise potential users of the thesis of these terms.

The author reserves all other publication and other rights in association with the copyright in the thesis and, except as herein before provided, neither the thesis nor any substantial portion thereof may be printed or otherwise reproduced in any material form whatsoever without the author's prior written permission.

Examining Committee

Jan A. Jung, Physics

K. H. Chow, Physics

Vadim A. Kravchinsky, Physics

Yu Jeffrey Gu, Physics

Thomas H. Etsell, Chemical and Materials Engineering

Davor Pavuna, Physics, Ecole Polytechnique Federale de Lausanne

Abstract

The magnetic properties of $Bi_2Sr_2CaCu_2O_{8+x}$ (BSCCO) single crystals and thin films have been studied systematically with a contactless Hall probe system. The BSCCO single crystals of $T_c \simeq 92$ K were grown using a crucible-free optical floating-zone technique. The thin film disks of $T_c \simeq 82$ K were grown using magnetron sputtering technique. Our findings are as follows:

1. The vortex penetration process is strongly time dependent. The penetration time scale varies and depends on the temperature, the applied field and the geometry of the sample.
2. The persistent current relaxations and the effective energy barrier against vortex motion is investigated in a ring-shaped $Bi_2Sr_2CaCu_2O_x$ single crystal. The results show a transition from a strongly non-logarithmic regime to a logarithmic one with increasing temperature. The vortex dynamics in the non-logarithmic regime are insensitive to changes in the microstructure (decreasing oxygen content), but the relaxations in the logarithmic regime are strongly affected by the microstructure.
3. A peak in the temperature dependence of the trapped vortex field is observed at a temperature below the vortex melting line. Logarithmic and non-logarithmic dependence on time were observed in the magnetic relaxations at temperatures below and above the peak, respectively. The results suggest the presence of the vortex-depinning transition at temperatures below the melting line of BSCCO.
4. Vortex penetration, vortex relaxation and vortex-depinning transition in YBCO single crystal are found qualitatively similar to that of BSCCO superconductor, but quantitatively different. These difference are supposed to be caused by the strong anisotropy in BSCCO superconductor.

Acknowledgment

I would like to express my deep thanks to professor Jan A. Jung for giving me the opportunity to explore the fascinating magnetic properties in high temperature superconductors, for his continuous support during the course of the research and the amount of time he devoted in reading and modifying the papers. I would also like to thank professor Kim H. Chow for his support and help during the research, for carefully reading the papers and the invaluable comments.

I wish to express my sincere thank to the members of my examining committee, professors Vadim A. Kravchinsky, Yu Jeffrey Gu, Thomas H. Etsell from University of Alberta, and professor Davor Pavuna from Ecole Polytechnique Federale de Lausanne, for their invaluable comments and suggestions on my research and thesis.

I would also like to thank all the colleagues in our lab: Dr. Mehmet Egilmiz for help in the research and in preparing the thesis defense; Dr. Ahmad Mansour, Dr. Isaac Fan and Dr. Mohmad Sayer for help in the research; C. E. Winterfield for help in the measurement; Dr. Huseyin Serhat Alagoz and Dr. Shaikh Tawhid Mahmud for help.

I am grateful to the following persons who have made the completion of this thesis possible:

David Lawrie, David C. Fortin and John P. Davis for correcting the English in this thesis.

Bill Burris for help in the computer language. Greg Popwhich, Don Mullin, Steve Rogers, Gilbert Lachat and Tony Walford for help in the equipments.

D. Prabhakaran, at Oxford University, for providing the BSCCO crystals.

Hiroki Tadatomu, at Osaka University, for providing the YBCO crystal.

J. C. Phillips, at Rutgers University, for the invaluable comments on the paper.

Finally, I wish to thank all the staff, faculty, and friends who have helped me directly and indirectly during my study and research at the University of Alberta.

Rongchao Ma

Fall 2009
Edmonton

Contents

1	Overview	2
2	Introduction	11
2.1	Backgrounds	13
2.1.1	Quantized Vortex	13
2.1.2	Energy Barriers to Vortex Entry	16
2.1.3	Flux Pinning	18
2.1.4	Magnetic Relaxation	20
2.1.5	Vortex Lattice Melting	24
2.2	Project Objectives	25
3	Experimental Methods	36
3.1	Sample Preparation	36
3.1.1	Bi-2212 Single Crystal	37
3.1.2	Bi-2212 thin film	37
3.2	Measuring procedure	41
3.2.1	Hall Probe System	42
3.2.2	Scan Profile	43
3.2.3	Decay Measurement	46
4	Vortex Penetration in Bi-2212 Superconductors	49
4.1	Introduction	49
4.2	Temperature Dependence of Vortex Penetration	50

4.3	Dependence of Vortex Penetration on Applied Field	53
4.4	Time Dependence of Vortex Penetration	53
4.5	Conclusions	58
5	Persistent Supercurrents and Vortex Dynamics in a Ring-shaped Bi₂Sr₂CaCu₂O_x Single Crystal	62
5.1	Introduction	62
5.2	Temperature Dependence of the Persistent Current Density	64
5.3	Decay of Persistent Current	66
5.4	Effective Energy Barrier	68
5.5	Effects of Oxygen	71
5.6	Conclusions	72
6	Depinning-induced Transition in Bi-2212 Superconductors	76
6.1	Introduction	76
6.2	Phase Diagram	78
6.3	Decay Rates	81
6.4	Effects of Vacuum Annealing	87
6.5	Conclusions	88
7	Magnetic Properties in YBa₂Cu₃O_{6+x} Single Crystal	93
7.1	Introduction	93
7.2	Experimental Details	94
7.3	Temperature Dependence and Time Dependence of Vortex Penetration	94
7.4	Phase Diagram	96
7.5	Decays	99
7.6	Decay Rates	102
7.7	Conclusions	102
8	Summary and Conclusions	106
8.1	Vortex Penetration	106

8.2	Vortex Dynamics with Persistent Currents	108
8.3	Vortex Depinning Transition	109
8.4	Magnetic Properties in YBCO Crystal	111
8.5	Outlook	111

List of Tables

2.1	Meaning of μ in the collective pinning model.	23
5.1	Annealing conditions of the BSCCO crystal. μ_1 and μ_2 are the vortex critical exponents at temperatures below and above T^* , respectively. .	68
6.1	Annealing conditions of BSCCO crystal. T and t are the annealing temperature and the annealing time, respectively, in an argon or vacuum environment	85

List of Figures

2.1	Quantized vortices in type-II superconductors. (a) Magneto-optical images of vortices [19] in a $NbSe_2$ superconducting crystal at 4.3 K after cooling in magnetic field of 3 Oe. $\Phi = n \left(\frac{h}{2e}\right)$. Ψ is the order parameter (or G-L wave function), ξ is the coherence length and λ is the penetration depth. (b) Schematic representation of the microstructure of a vortex.	14
2.2	Vortex pancakes in strong anisotropic superconductor, where a, b and c are the crystal axes.	15
2.3	Energy barrier $U_{eff}(J) \approx U_0(J_{c0}/J)^\mu$ in type-II superconductors [50], where U_0 is the barrier height in the absence of a driving force, and J_{c0} is the critical current density at which the barrier vanishes.	21
2.4	Schematic representation of vortex melting line in the strongly layered high- T_c superconductors, where H_{c1} is lower critical lower critical field, and H_{c2} is the upper critical field.	26
3.1	Bi-2212 single crystal ring ($\phi 1$).	38
3.2	Schematic representation of the thin film magnetron sputtering system.	39
3.3	Bi-2212 thin film disk ($\phi 10$).	40
3.4	Trapped magnetic field profile in a Bi-2212 single crystal ring. By scanning the Hall Probe above the sample, we can get the distribution of the trapped magnetic field.	44
3.5	Saturation line of Bi-2212 superconductor	45

3.6	Decay measurements. By fixing the Hall Probe above the sample, we can measure the trapped magnetic field as a function of time.	47
4.1	(A) Temperature dependence of the field trapped in the BSCCO single crystal. The field was trapped by applying a constant magnetic field $H_{appl} = 250$ G which was subsequently reduced to zero after a time interval t . $H_m(T)$ is the temperature dependence of the saturation line. (B) The corresponding temperature dependence of the field trapped in the BSCCO thin film after applying a constant field of 125 G.	51
4.2	Trapped field as a function of applied field over different time intervals t in a Bi2212 single crystal. (A) Measured at 22 K. (B) Measured at 28 K.	54
4.3	Vortex penetration curves of the $Bi_2Sr_2CaCu_2O_{8+x}$ single crystal. (A) The penetration curves measured under the same applied magnetic field $H_a = 500$ G, but at different temperatures $T = 22$ K, 25 K, 28 K respectively. (B) The penetration curves measured under the same temperature $T=25$ K, but at different applied magnetic field $H_a = 250$ G, 500 G, 750 G respectively.	55
4.4	Vortex penetration curves of the $Bi_2Sr_2CaCu_2O_{8+x}$ thin film. (A) The penetration curves measured under the same applied magnetic field $H_a = 50$ G, but at different temperatures $T = 26$ K, 52 K, 58 K, 64 K respectively. The inset are the dependence of trapped field on temperature under a constant applied magnetic field. (B) The penetration curves measured under the same temperature $T = 26$ K, but at different applied magnetic field $H_a = 50$ G, 125 G, 250 G, 625 G respectively.	56

5.1	The dependence of the persistent current density $J(T)$ on temperature measured in as-grown BSCCO (sample A0) between 1s and 10^4 s after the critical state was established. For $J_m(T)$ recorded after 1s the data could be fitted with the equations $J_m = (2.5 \times 10^5 A/cm^2)[1 - T/(46.7K)]^{3.7}$ and $J_m = (4.2 \times 10^3 A/cm^2)[1 - T/(92K)]^2$ below and above 36 K, respectively.	65
5.2	Dependence of the persistent current density on time measured at different temperatures between 24 and 46 K in the as-grown BSCCO (A0) crystal.	67
5.3	The effective energy barrier $U_{eff}(J)$ as a function of the persistent current density J calculated for the as-grown and vacuum annealed BSCCO crystal. The suppression of the current density J_m due to annealing is responsible for the shift of $U_{eff}(J)$ to low current density. The values of the critical exponents $\mu_{1,2}$ are shown in Table 4.1. The inset: Typical curve of the thermal factor $g(T)$ as a function of temperature.	69
5.4	Dependence of the persistent current density on temperature 1s after the critical state was established, measured for as-grown and vacuum annealed BSCCO single crystal (Solid lines are guides to the eye). . .	70
6.1	(a) Temperature dependence of the field trapped in the BSCCO single crystal by applying different constant magnetic fields between 50 and 1500 G during a time interval t^* of 120 s. $H_m(T)$ represents the temperature dependence of the saturation line. Line A joins the maxima of the trapped field. (b) Temperature dependence of the logarithmic decay rates $S=d(\ln H_{tr})/d(\ln t)$ of the trapped field calculated for a short initial time intervals up to 10-20 s. The arrows indicate temperatures of the maxima in the trapped field. (c) Dependence of the field trapped in the BSCCO crystal on time measured at different temperatures around the trapped field maximum.	79

6.2	(a) Temperature dependence of the field trapped in a BSCCO thin film by applying magnetic fields between 25 and 500 G during a time interval t^* of 120 s. $H_m(T)$ represents the temperature dependence of the saturation line. Line A joins the maxima of the trapped field. (b) Temperature dependence of the logarithmic decay rates $S=d(\ln H_{tr})/d(\ln t)$ of the trapped field calculated for short initial time intervals up to 10-20 s. The arrows indicate temperatures of the maxima in the trapped field. (c) Dependence of the field trapped in the BSCCO film on time measured at different temperatures around the trapped field maximum.	80
6.3	(a) Decays of the field trapped at a fixed temperature $T_f = 25$ K in the BSCCO crystal, after applying external fields of 250, 750 and 1250 G. (b) Decays of the field trapped at a fixed temperature $T_f = 52$ K in the BSCCO film, after applying external fields of 25, 50, 75 and 100 G. The insets show the dependence of the trapped field, obtained by applying different external fields, on temperature.	82
6.4	Evolution of the temperature dependence of the field trapped in the BSCCO crystal with the annealing temperature in vacuum. The field was trapped by applying a constant magnetic field of 250 G. The results for sample A2 are not shown. They are identical to those for sample A1. Solid curves represent the saturated lines.	86
6.5	Schematic representation of the temperature dependence of the depinning and the saturated lines.	88
7.1	(a) Temperature dependence of the z-component of the field trapped in the YBCO single crystal. The field was trapped by applying a constant magnetic field $H_{appl} = 500$ G which was subsequently reduced to zero after a time interval t . $H_m(T)$ is the temperature dependence of the saturation line. (b) Temperature dependence of the x-component of the field trapped in the YBCO crystal after applying a constant field of 500 G.	95

7.2	(a) Temperature dependence of the z -component of the field trapped in the YBCO single crystal by applying different constant magnetic fields between 250 G and 1500 G during a time interval of $t^* = 120$ s. $H_m(T)$ represents the temperature dependence of the saturation line.	
	(b) The corresponding temperature dependence of x -component of the field trapped in the YBCO crystal by applying magnetic fields between 250 G and 1500 G during a time interval of $t^* = 120$ s.	97
7.3	(a) Dependence of the z -component of the field trapped in the YBCO crystal on time measured at different temperature around the trapped field maximum. (b) The corresponding time decay curves of the x -component measured for the YBCO crystal.	100
7.4	Temperature dependence of the logarithmic decay rates $S=d(\ln H_{tr})/d(\ln t)$ of the z -component of the trapped field calculated for a short initial time intervals up to 10-20 s for the YBCO crystal. Decay rates correspond to the points on the phase diagram of z -component.	101

List of Symbols

λ	Penetration depth
ξ	Coherence length
Φ_0	Flux quantum
T^*	Crossover temperature from 2D/0D to 3D
H_{c1}	Lower critical field
H_{c2}	Upper critical field
H_a	Applied magnetic field
T_{KT}	Kosterlitz-Thouless temperature
J_c	Critical current density (also J_m)
J_{c0}	Critical current density at which the barrier vanishes
GB	Geometrical barrier
S	Decay rate
U_{eff}	Effective energy barrier
T_c	Critical temperature
H_m	Melting field
h	Planck's constant
e	Charge of electron
μ	Critical exponent
B_{sf}	Self magnetic field
T_f	Fixed temperature
U	potential energy barrier height
k	Boltzmann constant
t_0	Effective hopping attempt time
U_0	Barrier height in the absence of a driving force

Chapter 1

Overview

This thesis has been divided into three sections, which deal with some important aspects of vortex entry, vortex dynamics and persistent currents. The major achievements are listed below:

(a) Surface barriers: The effect of surface barriers [1, 2] on the vortex penetration in type-II superconductors is an important topic and of high interest to both experimental and theoretical studies. The existing literatures on this topic is mostly focused on the vortex entry conditions which have been studied since the early 60s.[1, 2] More recently, the vortex entry conditions have been analyzed numerically by some theories on the basis of the time-dependent GL equations.[3, 4] The presence of the geometrical barrier was first proposed by Zeldov et al., who derived an analytical solution which governs the vortex penetration/entry and its dynamics in flat samples of type II superconductors under the condition that the applied magnetic field is perpendicular to the flat surface.[5] The results of this work have been confirmed by the experiments on Bi-2212 crystals using Hall sensor arrays. It has been found that the geometrical barrier retards the vortex penetration. Although these results clearly reveal the effect of the surface and geometrical barriers against the vortex entry, they have not provided any information about the time evolution of the vortex entry into a superconductor. This question is particularly important because potential device applications of

type-II superconductors may strongly depend on such information. Unfortunately, the literature has failed to provide the information on the time scale of this entry [3, 4, 6, 7]. This suggests that special experimental techniques are required to gain knowledge on this topic.

In the first section of this thesis, we proposed an effective method which determines the time scale of vortex penetration into the Bi-2212 superconductors (see Chapter 4). This technique has been successfully applied to the samples with different geometry and, therefore, different surface barrier conditions: Bi-2212 single crystals and thin films. For the first time we have quantified the time scale of the vortex entry into a prototypical HTS superconductor. In principle, our results could be applied to all kinds of type II superconductors as discussed in Chapter 7. To our knowledge, these findings are novel and are of particular interest to both theoretical and experimental researchers in the field of superconductivity.

(b) Vortex dynamics and persistent currents: In general, the understanding of the vortex dynamics is based on the results of the magnetization measurements carried out on the rectangular shaped samples.[8] Unfortunately, these measurements which give useful insight into the dependence of the vortex phases on magnetic field and temperature (i.e., the H-T phase diagrams) [8, 9, 10, 11, 12, 13], have not provided direct information about the relationship between the vortex pinning and the persistent current. This information has not been obtained either by measurement of the relaxation (time dependence) of the magnetization [8] or by Bean's critical state model [1, 14] applied to the spatial distribution of magnetization, which have been otherwise implemented successfully to study the vortex pinning and the corresponding vortex-density gradients in a superconducting sample. In this sense, a superconducting ring offers a unique opportunity to investigate the interaction between the magnetic vortices trapped in the ring's bulk and the persistent currents circulating around the ring.[15] The advantage of the ring-geometry is that the induced persistent current exerts a Lorentz force on the vortices driving them out of the

ring uniformly in the radial directions. Consequently this causes the dissipation of the persistent current. By applying and switching off larger external magnetic fields one could produce persistent currents at the critical level. Magnetic field trapped at the ring's center is proportional to the critical current density according to the Biot-Savart law. The magnitude of this field and its decay could be measured with a magnetic field sensor, such as a Hall sensor.

Early studies have shown that $\text{Bi}_2\text{Sr}_2\text{CaCu}_2\text{O}_8$ (BSCCO) superconductors have two vortex regimes [16, 17, 18, 19], at temperatures below and above the crossover temperature $T^* = 36$ K. Each of these regimes has a different vortex dynamics and pinning mechanism.[20, 21, 22, 23, 24, 25]

In Chapter 5, we used the technique described above to investigate the temperature dependence of the persistent current and its dissipation rate due to its interaction with magnetic vortices in a pure ring-shaped BSCCO single crystal whose microstructure (oxygen content) has been changed by vacuum annealing. This allowed us to obtain information on the value of exponent μ , a parameter showing the dependence of the energy barrier against vortex motion $U_{eff}(J) \propto (J_c/J)^\mu$ and the persistent current density J . Temperature dependence of the persistent current relaxations revealed a crossover in the dissipation rate from a strongly non-logarithmic regime at temperatures below T^* to a logarithmic one at temperatures above T^* . In the former regime the vortex dynamics is governed by the energy barrier $U_{eff}(J)$ with $\mu \simeq 1/7$ which depends little on changes in the microstructure, suggesting highly cooperative effects in the vortex structure. [26] In the latter regime, on the other hand, μ is strongly dependent on the microstructure, with its value dropping from 0.7 in an as-grown crystal down to 0.35 in a disordered crystal. These studies provided new results on the critical exponent μ for the pinning barriers of the vortex structure in Bi-2212 superconductor due to intrinsic disorder.

(c) Vortex depinning-induced phase transitions: The understanding of the mixed state of high- T_c superconductors, requires the exploration of possible phase

transitions between different vortex phases such as vortex solids (or glasses) and liquids.[8] The nature of these transitions is determined by a complicated interplay between thermal fluctuations, disorder and large anisotropy. In highly anisotropic BSCCO superconductors, Josephson plasma resonance (JPR) measurements [27], which can directly probe the interlayer coherence of the vortex state [28], revealed that the vortex could be decoupled above the melting line.

The magnetic phase diagram [8] is commonly plotted as H vs. T . For BSCCO superconductors [9], the magnetic phase diagram reveals two phases at high fields ($>400\text{Oe}$): a glassy phase at low temperatures (albeit with a pronounced 2D character) and a high temperature liquid phase starting at about 35K. At low fields ($<400\text{Oe}$), there is a Bragg glass (thought to be 3D) at low temperatures with a second order glass transition to an ordered crystalline phase at 35-40K and finally a first order melting transition to a liquid at high temperatures. Physically, this magnetic phase diagram represents the vortex structure inside the superconductor, that is, the internal magnetic field. The detailed vortex structure of the mixed state is determined by the flux pinning, the external magnetic field and the temperature. Furthermore, according to the Bean's critical state model [14], the internal magnetic field in the low T and low H region is not uniform and the local value of H is a strongly varying function of the position inside the superconductor even though the external magnetic field is uniform. Therefore, the conventional magnetic phase diagram cannot give proper information about the vortex system by simply referring it to the magnitude of the external magnetic field.

The presence of decoupling [29] or depinning transition [30, 31] has been suggested by some theories, but their presence has not been shown in experiments. A experiment aimed to identify these transitions should provide answer to the following questions: What happens to the vortex lattice and its pinning at temperatures just below the saturation/melting line? Does the pinning of the vortex-lattice decrease abruptly at the saturation line or does this process occur gradually when the temperature approaches the 2D to 3D crossover temperature.

In Chapter 6, we attempted to answer these questions. The approach that we used is as follows: we applied a constant external magnetic field, H_a , to a superconductor at different temperatures, which results in penetration of the vortices into the bulk of the superconductor. We then reduce H_a to zero and the vortex field trapped in the sample is detected by a Hall probe sensor. At or close to the melting field [32] $B_m(T)$, the superconductor is fully penetrated and the internal magnetic field is expected to be constant over the entire sample volume. Therefore, the vortex structure close to the melting field can be well represented by the measurement of the trapped magnetic field. At a fixed temperature, the trapped magnetic field increases with increasing external magnetic field and finally reaches a saturated value, which corresponds (not equals) to the melting field $B_m(T)$ (external field). We name the temperature dependence of the saturation field as the “saturation line”. As the trapped field is monitored as a function of temperature, the behavior of the vortex lattice can be inferred. Our experiments have provided the experimental evidence for presence of theoretically predicted decoupling/depinning transitions in the vortex matter of type II superconductors.

Our experiments also have revealed that the maxima in the trapped field in BSCCO crystal and BSCCO thin film occur at temperatures several degrees below the saturation line. The presence of maxima suggests that the partial depinning of magnetic vortices occur at temperatures above the maxima, leading to a gradual decrease of the trapped field with an increasing temperature, which eventually (at higher temperatures) merges with the saturation line. These findings are summarized in Figure 6.5 of Chapter 6, showing clearly the presence of depinning/decoupling region in the vortex phase diagram. To our knowledge this is the first experimental manifestation of such phase transition in the vortex matter and is of great interest of theorist in this area. In addition we have found large differences between the properties of BSCCO crystals and thin films. These discrepancies are attributed to the difference in the defect densities of the samples.

The measurements performed on BSCCO superconductors have been repeated on YBCO crystals (see Chapter 7). The results obtained agree qualitatively with those obtained on BSCCO. These findings clearly indicate that the results discussed above are universal.

Bibliography

- [1] C. P. Bean, J. D. Livingston, Phys. Rev. Lett. **12**, 14 (1964).
- [2] R. W. De Blois, W. De Sorbo, Phys. Rev. Lett. **12**, 499 (1964).
- [3] P. G. de Gennes, Sol. St. Comm. **3**, 127 (1965).
- [4] L. Kramer, Phys. Rev. **170**, 475 (1968).
- [5] E. Zeldov, A. I. Larkin, V. B. Geshkenbein, M. Konczykowski, D. Majer, B. Khaykovich, V. M. Vinokur, and H. Shtrikman, Phys. Rev. Lett. **73**, 1428 (1994).
- [6] Ryuzo Kato, Yoshihisa Enomoto, Sadamichi Maekawa, Phys. Rev. B **47**, 8016 (1993).
- [7] Carlos Bolech, Gustavo C. Buscaglia, and A. Lopez, Phys. Rev. B **52**, R15719 (1995).
- [8] G. Blatter, M. V. Feigel'man, V. B. Geshkenbein, A. I. Larkin, V. M. Vinokur, Rev. Mod. Phys. **66**, 1125 (1994).
- [9] H. Beidenkopf, N. Avraham, Y. Myasoedov, H. Shtrikman, E. Zeldov, B. Rosenstein, E. H. Brandt, and T. Tamegai, Phys. Rev. Lett. **95**, 257004 (2005).
- [10] M. Liu, Y. W. He, W. J. Wu, and Y. H. Yang, Phys. Rev. B **71**, 224508 (2005).
- [11] Sandeep Tyagi and Yadin Y. Goldschmidt, Phys. Rev. B **70**, 024501 (2004).
- [12] C. J. Olson, G. T. Zimanyi, A. B. Kolton, and N. Gronbech-Jensen, Phys. Rev. Lett. **85**, 5416 (2000).

- [13] D. Darminto, M. O. Tjia, T. Motohashi, H. Kobayashi, Y. Nakayama, J. Shimoyama, and K. Kishio, *Phys. Rev. B* **62**, 6649 (2000).
- [14] C. P. Bean, *Phys. Rev. Lett.* **8**, 250 (1962).
- [15] J. Jung, K. H. Chow, M. Egilmez, and A. Welsh, *Appl. Phys. Lett.* **87**, 262506 (2005).
- [16] A. Houghton, R. A. Pelcovits, and A. Sudbo, *Phys. Rev. B* **40**, 6763 (1989).
- [17] L. I. Glazman, A. E. Koshelev, *Phys. Rev. B* **43**, 2835 (1991).
- [18] D. S. Fisher, Matthew P. A. Fisher and David A. Huse, *Phys. Rev. B* **43**, 130 (1991).
- [19] P. L. Gammel, L. F. Schneemeyer, J. V. Wasczak, and D. J. Bishop, *Phys. Rev. Lett.* **61**, 1666 (1988).
- [20] A. Piriou, Y. Fasano, E. Giannini, and O. Fischer, *Phys. Rev. B* **77**, 184508 (2008).
- [21] V. F. Correa, J. A. Herbsommer, E. E. Kaul, F. de la Cruz, and G. Nieva, *Phys. Rev. B* **63**, 092502 (2001).
- [22] M. F. Goffman, J. A. Herbsommer, F. de la Cruz, T. W. Li and P. H. Kes, *Phys. Rev. B* **57**, 3663 (1998).
- [23] T. Verdene, H. Beidenkopf, Y. Myasoedov, H. Shtrikman, M. Rappaport, E. Zeldov, and T. Tamegai, *Phys. Rev. Lett.* **101**, 157003 (2008).
- [24] Yadin Y. Goldschmidt and Jin-Tao Liu, *Phys. Rev. B* **76**, 174508 (2007).
- [25] Yadin Y. Goldschmidt and Eduardo Cuansing, *Phys. Rev. Lett.* **95**, 177004 (2005).
- [26] J. C. Phillips, Private communication; Activation Energies of Vortex Glasses and Liquids in Strongly Disordered Superconductors, unpublished.

- [27] Y. Matsuda et al., Phys. Rev. Lett. 75, 4512 (1995).
- [28] M. Tachiki et al., Phys. Rev. B 50, 7065 (1994).
- [29] M. J. W. Dodgson, V. B. Geshkenbein, G. Blatter, Phys. Rev. Lett. **83**, 5358 (1999).
- [30] R. Sugano, T. Onogi, K. Hirata, and M. Tachiki, Phys. Rev. Lett. **80**, 2925 (1998).
- [31] R. Sugano et. al., Physica B **284**, 803 (2000).
- [32] E. Zeldov, D. Majer, M. Konczykowski, V. B. Geshkenbein, V. M. Vinokur and H. Shtrikman, Nature **375**, 373 (1995).

Chapter 2

Introduction

$Bi_2Sr_2Ca_{n-1}Cu_nO_{2n+4-x}$ ($n = 1, 2, 3$), or BSCCO, is a high T_c superconductor with a highly layered structure discovered in late 1980's [1, 2, 3]. BSCCO was the first high T_c superconductor which did not contain a rare earth element, and is also the first high T_c superconductor to be found applications in industry [4, 5].

This system continues to be interesting because of its strongly layered microstructure offers a potentially interesting system for studying the interplane coupling (2D-3D crossover) [6] and the pairing mechanism [7] in high- T_c superconductivity, which are currently not clear. The development of Bi-series superconductors is a very difficult task because of its inherent brittleness and the narrow range of the processing temperature required to produce the superconductive phase.[8] Several phases, such as Bi-2223, Bi-2212 and Bi-2201, usually coexist in the BSCCO superconductor.

The study of the magnetic properties of BSCCO superconductors is challenging because of the complexity of the vortex structure and the consequent vortex dynamics.[6] Up to now, there are still many open questions about vortex dynamics, some of them are the subject of this thesis:

1. Time dependence of vortex penetration

The motion of the vortices inside a superconductor is retarded because of the pres-

ence of the resistances and the vortex penetration process is time-dependent. The majority of the studies in vortex penetration are focused on the vortex entry and exit conditions, while systematic studies of the time dependence (time scale) of vortex penetration are currently not available.

2. Persistent currents and vortex dynamics

The pinning potential of a vortex is a function of current because of the interaction between the vortex and the current. For BSCCO superconductors, no unique functional relation between the pinning potential and current has been found in the intermediate region ($20K \leq T \leq 40K$). On the other hand, the mechanism for the crossover at $T^* \approx 30K$ of the melting line is not clear.

3. Vortex-depinning induced phase transitions

Theoretical calculations have shown that for the highly anisotropic superconductor BSCCO, there is an almost vertical depinning line T_{dp} dividing the vortex solid phase into two phases. On the other hand, the theoretic calculations suggest that a vortex decoupling transition [9] appears in the pancake-vortex lattice of layered superconductors with a finite Josephson coupling a few degrees below the melting line. Unfortunately, experiments have not confirmed explicitly these theoretical suggestions.

In this chapter, we will start by providing background information on vortices in high T_c superconductors and BSCCO. Then we describe the project objectives of this thesis. In chapter 2, we introduce the experimental details used in this thesis. In chapter 3, we designed a special experimental measuring procedure to test the time scale of the vortex penetration into the $Bi_2Sr_2CaCu_2O_{8+x}$ superconductors under various conditions. In chapter 4, we study the interaction between the current and the vortices, and then the vortex structure and its properties in the vicinity of the

crossover temperature T^* in the BSCCO superconductor. In chapter 5, we investigated the pinning and the phase transition of the vortex system at temperatures just below the saturation line of BSCCO superconductor. In chapter 6, we investigated the vortex penetration and the vortex phase transition in YBCO single crystal. Finally, we give a short summary to the results of this thesis in chapter 7.

2.1 Backgrounds

2.1.1 Quantized Vortex

Type-II superconductor has two critical field, the lower critical field, H_{c1} , and the upper critical field, H_{c2} . The applied fields H_a near to the surface of the superconductor is subjected to the repulsive force from the field generated by the surface screening supercurrent [10], which expels the applied field out of the superconductor to maintain the superconductor as a perfect diamagnetic body when the applied magnetic field is $H_a < H_{c1}$. As the applied field H_a increases to a value such that $H_{c1} < H_a < H_{c2}$, the type-II superconductor has a negative surface energy, or negative free energy in the interface between the normal region (caused by the magnetic field) and the superconducting region. As a result, the coexistence of the superconducting phase with a magnetic field has a lower energy, that is, the coexistence turns out to be favorable in energy for preserving the superconducting state. In this case, the superconductor prefers to let part of the applied magnetic field penetrate into its body in the form of quantized vortices to reduce the energy. In the absence of disorder, the quantized vortices form a regular lattice of parallel lines [11, 12, 13, 14, 15, 16, 17, 18, 20, 21], each carrying a single flux quantum $\phi_0 = h/2e$. (Figure 2.1), where h is Planck's constant, and e is the charge of electron.

BSCCO superconductors have highly layered microstructures.[22] The vortices in these superconductors are generally in the form of disconnected “disks” or “pancakes” (Figure 2.2) because of the limitation in the coherence length and the space between the layers of the microstructure of these superconductors.[6, 23] As a result, the vortex

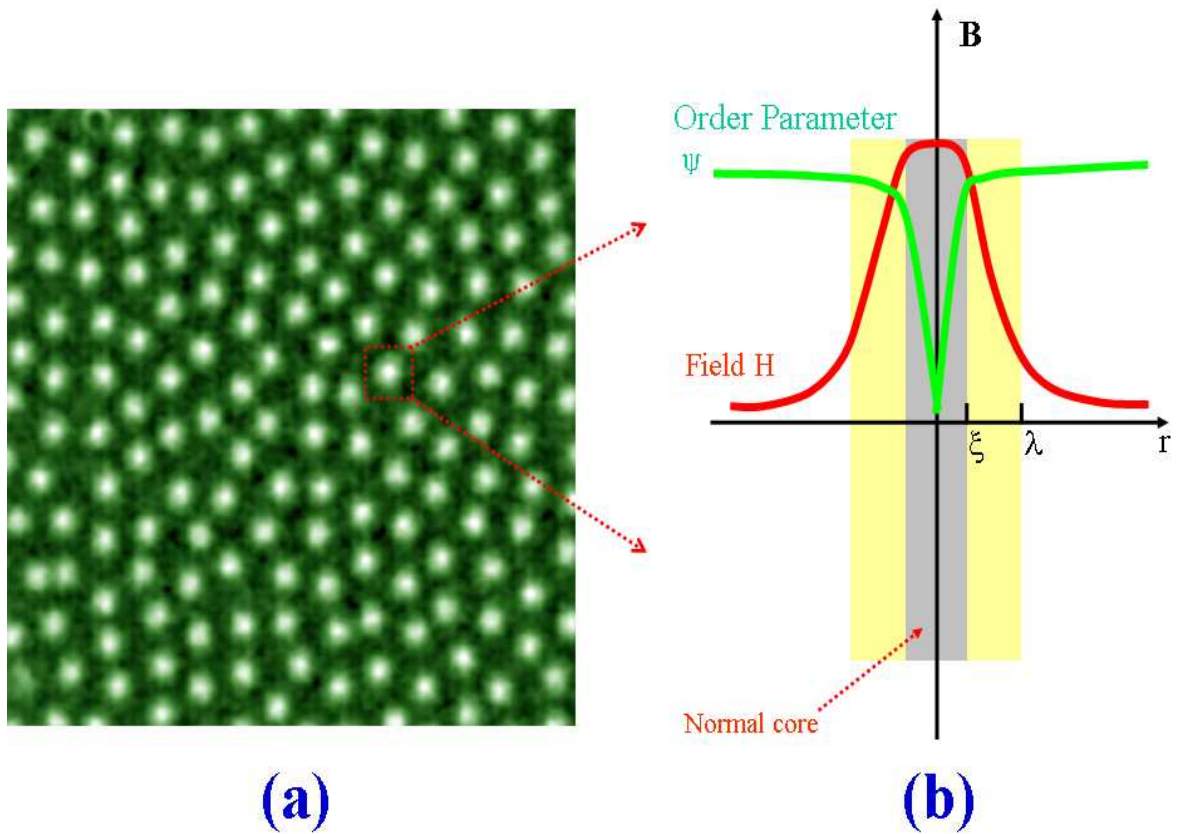


Figure 2.1: Quantized vortices in type-II superconductors. (a) Magneto-optical images of vortices [19] in a $NbSe_2$ superconducting crystal at 4.3 K after cooling in magnetic field of 3 Oe. $\Phi = n \left(\frac{h}{2e} \right)$. Ψ is the order parameter (or G-L wave function), ξ is the coherence length and λ is the penetration depth. (b) Schematic representation of the microstructure of a vortex.

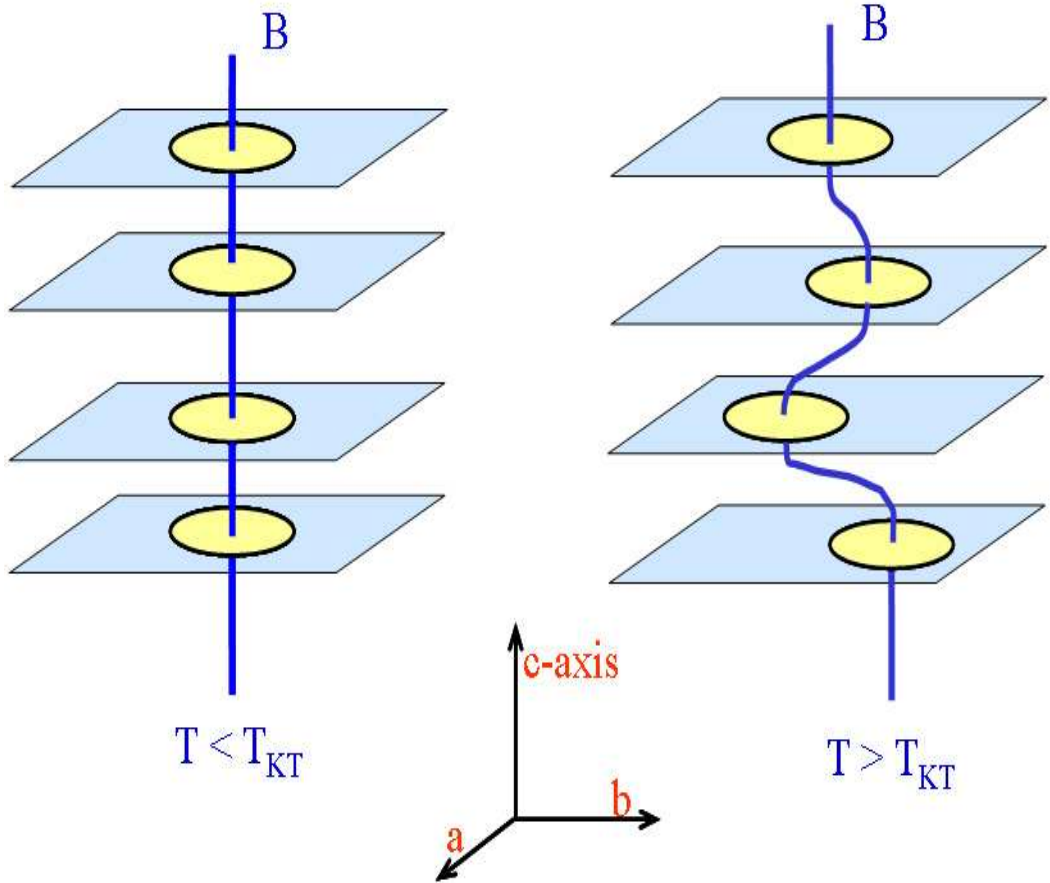


Figure 2.2: Vortex pancakes in strong anisotropic superconductor, where a , b and c are the crystal axes.

dynamics in these superconductors is much more complicated.

BSCCO superconductors are strongly type-II and their lower critical field H_{c1} is very low ($H_{c1}(0) \approx 650G$).[6] The Meissner phase, in which the magnetic field is expelled out, of these superconductors is then bounded in a very small region and their phenomenology is dominated by the presence of vortices over most of the phase diagram. Thus, all the technologically relevant BSCCO materials are hard superconductors operating in the mixed state. This mixed state is where the superconducting phase and the quantized vortices coexist. The study of magnetic properties in the mixed state becomes very important as the magnetic properties of type-II superconductors govern its current carrying ability.

2.1.2 Energy Barriers to Vortex Entry

The energy barriers here means the the resistances to the vortice motion in a type-II superconductor. Energy barriers prevents the vortex penetration into the bulk of a type-II superconductor. Vortex entry is the process in which a vortex start to penetrate into a type-II superconductor. In the study of vortex peneration in type-II superconductors, it is a challenging problem to find out the vortex entry conditions [24] at which the Abrikosov vortices start to penetrate into the superconductor under the driving force of the external magnetic field. This is a fundamentally important step in describing the magnetic behavior of type-II superconductors because the vortex entry will destroy the Meissner state and transfer the superconductor into mixed state. Currently, most of the researches have been devoted to the effects of surface barriers on the vortex penetration in these materials.[24, 25, 26, 27, 28, 29]

The vortex-entry conditions were first studied by De Gennes in terms of Gibbs free energy for the testing vortex.[24] Kramer investigated the vortex-entry conditions by analyzing the stability of the Meissner state with respect to the order parameter and electromagnetic fluctuations.[25] A number of other works studied the vortex-entry conditions by solving the time-dependent GL equation numerically [26, 27].

Bean-Livingston Barrier

Generally speaking, there are two separate forces, the repulsive Lorentz force and the attractive image force [30, 31, 32], exert on a vortex when it is created within a type-II superconductor lying parallel and near to the surface.

The repulsive Lorentz force is caused by the external field (H) that penetrates into the superconductor as $He^{-d/\lambda}$, or the surface screening currents, where d is the distance between the vortex and the surface, and λ is penetration depth. If H is of the same sign as the field of the vortex, a repulsive Lorentz force is produced which attempts to push the vortex into the bulk of the sample. The Lorentz force can be

written as:

$$f_L = \Phi_0 j = \Phi_0 \frac{H}{\lambda} e^{-\frac{d}{\lambda}} \quad (2.1)$$

where j is the current density and Φ_0 is the quantum of the flux.

The attractive image force [30] is caused by the boundary condition that, the current normal to the surface must be zero. This condition can be easily satisfied by adding an image vortex of opposite sign outside the surface, which attracts the vortex to the surface. Let $2d$ be the distance between a vortex and its image, the image force can be written as:

$$f_{im} = -\frac{\Phi_0^2}{2\pi\mu_0\lambda^3} K_1\left(\frac{2d}{\lambda}\right) \quad (2.2)$$

where μ_0 is the permeability of free space, and $K_1\left(\frac{2d}{\lambda}\right)$ is the modified Bessel function of the second kind.

Note that for any nonzero H , the repulsive force will eventually dominate the image contribution for $d \gg \lambda$. The addition of the above two forces lead to an energy barrier to the vortex motion.

Connolly et al. found that in Bi-2212 single-crystal disks, flux preferentially flows along linear defects into the interstitial platelet regions up to a characteristic field H_p , above which flux enters the disks.[33] They identified this as the field of first penetration of pancake vortices over the Bean-Livingston barrier around the disks. Wang et al. found that for vortex penetration in BSCCO materials, the Bean-Livingston surface-barrier effect dominates only at the temperatures above 15 K, while below 15K, the Bean bulk-pinning energy barrier determines the vortex penetration field.[34, 35]

Geometric Barriers

The geometric barrier [36, 37, 38] is a shape dependent barrier, which was first introduced by Zeldov et al. [36], and then was extensively discussed by Brandt.[39] The

introduction of the concept of “geometrical barrier” (GB) makes it possible to investigate vortex structure in high-temperature superconductors. We can simply describe it as follows [36, 40]:

Consider a thin superconducting sample with rectangular cross section of width $2W$ ($-W < x < W$) and thickness d ($d \ll W$). A magnetic field H_a is applied perpendicular to the surface of the sample. Near the sharp corners the local field is enhanced considerably compared to H_a , and then penetrates into the sample first at these points. This cancels out part of the opposing forces due to the Bean-Livingston barrier. However, for the flux line to enter the bulk of the sample, the length of flux line L_f has to be considerably longer than d , that is, $L_f > d$. The flux line is then stretched by an amount $\Delta = L_f - d$. In this sense, the energy cost of creating the flux line near the surface is raised due to the sample geometry. Since this effect is strongly shape dependent, it could be shown that there is no geometrical barrier in the case of an elliptical cross section.[40]

The geometrical barrier results in retarded vortex penetration, and is expected to dominate the observed magnetic behavior of high- T_c superconductors at elevated temperatures where critical currents are relatively low. The experimental observations of vortex penetration and dynamics in Bi-2212 single crystals is in very good agreement with the theoretical derivations.[36] The geometric barrier has also been recognized experimentally by hysteretic magnetisation experiments in type-II superconductors in the absence of bulk pinning.[39]

2.1.3 Flux Pinning

The vortices in a type-II superconductor can be pinned down by the pinning centers (defects). The pinning of the vortices with various crystal imperfections is responsible for the existence of a critical current density J_c , which is usually defined as the current density at which an arbitrarily small voltage is observed.[6, 41] Vortices interact with the pinning centers because the superconducting properties of the latter are different from that of the bulk superconductor. The strength of the interaction is a function of

the magnitude of this difference. The difference may be small and can manifest itself as a difference in critical temperature, critical field, or Ginsburg-Landau parameter κ . The difference may be large when the pinning center is non-superconducting. The pinning of vortices can be simply explained by the condensation energy $U_0 = \frac{1}{2}\mu H_c^2 V$ of type-II superconductor, that is, the superconducting system has a lower total energy when the vortex sits on the defects.

Because of the short coherence length of the high- T_c superconductors, the oxygen vacancies on the CuO_2 planes are sufficient to locally depress the superconducting order parameter, and become the effective pinning centers.[41] Kes obtained a depinning current density for BSCCO of $5 \times 10^6 A/cm^2$ at $T = 0$ K and a pinning energy of 34 K in temperature units.[42]

The oxygen vacancies are distributed on the CuO_2 planes randomly. The calculations have shown that if the vortices are perfectly periodic and rigid, they would not be effectively pinned by any random collection of pinning sites.[41] Fortunately, the vortices are elastic over a limited temperature range, therefore, the paths of the individual flux lines can deviate from the ideal periodic Abrikosov lattice to lower their energy by passing through the pinning sites which is more favored in energy. But at the same time, the elastic energy of the vortex lines is increased because of the deformation in the vortex lines. The equilibrium flux-line configuration will be that distorted arrangement which minimizes the sum of these two energies. This idea was first suggested by Larkin and Ovchinnikov and is now developed as the so-called “collective pinning theory” [43].

For the strongly layered BSCCO superconductor, the interaction between the vortices within the plane can be ignorable for a weak magnetic field, and the pinning is then a 3D collective pinning.[6] With increasing magnetic field, the intraplanar interaction becomes increasingly important and we can ignore the coupling interaction between neighbouring pancake vortices in different layers, creating a vortex system that crosses over from 3D to 2D collective pinning.[44] In this case all pancake vortices within the radius $R_c > a_0$ are pinned collectively, where R_c is the collective pinning

radius.

2.1.4 Magnetic Relaxation

Because of thermal activation, quantum tunneling or mechanical vibrations, vortices can move out of their pinning sites spontaneously [6], causing the so-called magnetic relaxation. The hopping time, t , can be written out by the so-called Arrhenius relation:

$$t = t_0 e^{\frac{U}{kT}} \quad (2.3)$$

where U is the potential-energy barrier height, k is the Boltzmann constant, T is the temperature and t_0 is the effective hopping attempt time. When current presents, the hopping process is increased by the Lorentz force [6]:

$$F = \frac{1}{c} J \times B \quad (2.4)$$

where J is the current density and B is the field. Therefore, U should be a decreasing function of J (Figure 2.3).

Anderson and Kim have considered the pinning of the simplest possible model with a linear J -dependence of the barrier energy [45, 46]:

$$U = U_0 \left(1 - \frac{J}{J_{c0}} \right) \quad (2.5)$$

where U_0 is the barrier height in the absence of a driving force, and J_{c0} is the critical current density at which the barrier vanishes. This linear approximation is a reasonable approximation near J_{c0} and is a fair description for conventional superconductors for which $U_0 \gg kT$. This model is applicable to the situation where the interactions between vortices is small, but in application to any other system or regime one can expect major modification, which will be discussed later. From Eq.(2.5) one can

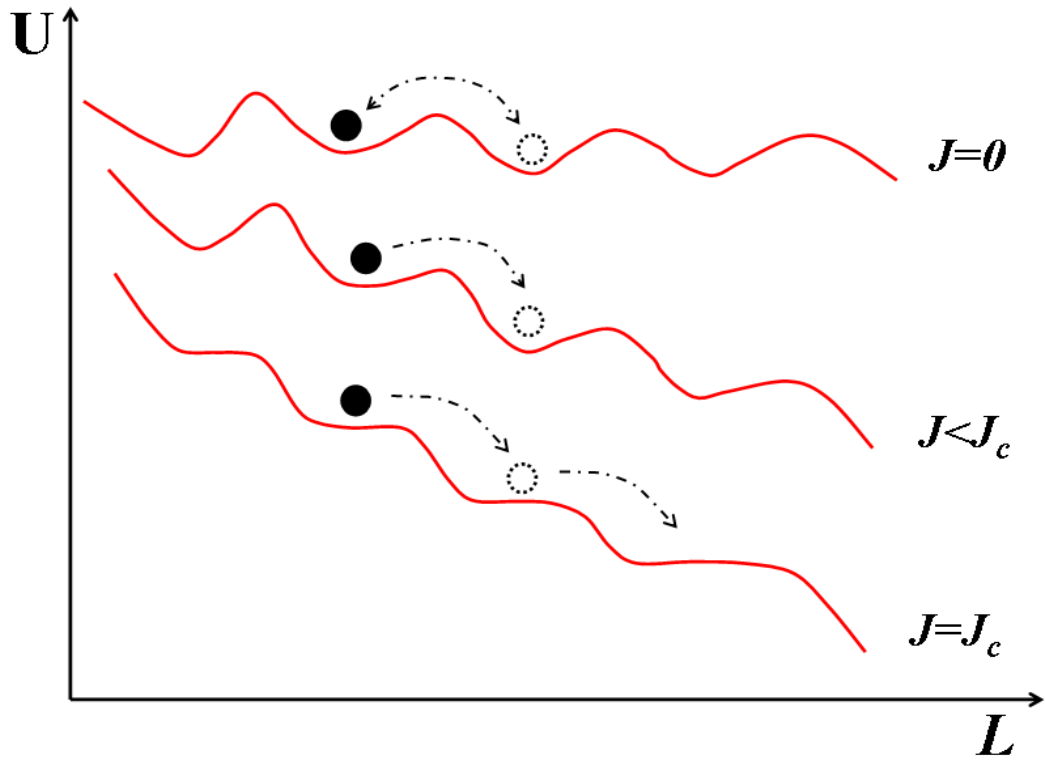


Figure 2.3: Energy barrier $U_{eff}(J) \approx U_0(J_{c0}/J)^\mu$ in type-II superconductors [50], where U_0 is the barrier height in the absence of a driving force, and J_{c0} is the critical current density at which the barrier vanishes.

obtain the famous logarithmic time dependence of the current density:

$$J = J_{c0} \left[1 - \frac{kT}{U_0} \ln \left(1 + \frac{t}{t_0} \right) \right] \quad (2.6)$$

It is very useful to define the so-called “normalized relaxation rate” [6]:

$$S = \frac{1}{M} \frac{dM}{d(\ln t)} = \frac{d(\ln M)}{d(\ln t)} = \frac{d(\ln J)}{d(\ln t)} \quad (2.7)$$

Combining Eq.(2.7) with Eq.(2.6), we have:

$$S = \frac{-kT}{U_0 - kT \ln(t/t_0)} \quad (2.8)$$

The logarithmic flux creep theory has been well confirmed for conventional low-temperature superconductors.[47, 48, 49] However, for layered high- T_c superconductors such as the BSCCO superconductor, the relaxation deviates away from the logarithmic pattern even at the initial stage of the magnetic relaxation. In order to explain this phenomenon, one has to consider the nonlinear J -dependence of the barrier energy. [6]

Beasley et al. first realized that the energy barrier $U_{eff}(J)$ should have a nonlinear dependence on the current density J . [49] Feigel'man et al. proposed the following inverse power-law barrier [50]:

$$U_{eff}(J) = U_0 \left(\frac{J_{c0}}{J} \right)^\mu \quad (2.9)$$

where μ is a critical exponent μ , from which one can identify the vortex structure in the superconductor. The detailed correspondence between the μ and the pinning mechanism is shown in Table 2.1.

The above inverse power-law barrier can be derived from the collective vortex pinning theory.[50] In order to have $U(j_c) = 0$, the above equation is generally modified

Table 2.1: Meaning of μ in the collective pinning model.

Geometric dimension	μ	Pinning Mechanism
3D	1/7	Single vortex
	3/2	Small vortex bundle
	7/5	Large bundle
2D	8/9	Small vortex bundles
	1/2	Large vortex bundles

to the following form [50]:

$$U_{eff}(J) = U_0 \left[\left(\frac{J_{c0}}{J} \right)^\mu - 1 \right] \quad (2.10)$$

In addition to this, Zeldov et al. have proposed a logarithmic barrier [51, 52]:

$$U_{eff}(J) = U_0 \ln \left(\frac{J_{c0}}{J} \right) \quad (2.11)$$

This barrier is useful in high- T_c superconductor.

A central result from the “inverse power-law barrier” is the following “interpolation formula” [6]:

$$J(T, t) = \frac{J_{c0}}{\left[1 + \frac{\mu k T}{U_0} \ln \frac{t}{t_0} \right]^{1/\mu}} \quad (2.12)$$

where t_0 is the logarithmic time scale. The factor μ in the denominator is introduced in order to interpolate between the usual Anderson formula (for $J_c - J \ll J_c$ at short times) and the long-time behavior.

The above interpolation formula Eq.(2.12) can be also derived from vortex glass theory [53, 54]. In this theory, the flux system undergoes a thermodynamic phase transition from a vortex-glass state in which vortices are localized in a metastable state by interactions with the pinning centers and the other vortices. In its simplest version, the vortex-glass model predicts μ to be a universal exponent less than one, while the collective creep theory [50] predicted a complicated dependence of μ on field and temperature.

Combining Eq. (2.7) and (2.12), we have the normalized relaxation rate:

$$S = \frac{kT}{[U_0 + \mu kT \ln(t/t_0)]} \quad (2.13)$$

Since $M \propto J$, one can easily convert M into J . Using the thermally activated flux motion theory, Beasley et al. obtained the relaxation rate of the magnetization M [49]:

$$\frac{dM}{dt} = \frac{Ba\omega_0}{\pi d} \exp\left\{-\frac{U_{eff}(J)}{k_B T}\right\} \quad (2.14)$$

where B is the magnetic induction, a is the hopping distance, $\omega = 2\pi/\tau_0$ is the microscopic attempt frequency, d is the thickness of the sample, and k_B is the Boltzmann constant. This theory was developed by Maley [55] who built an equation that can be used to calculate the current dependence of the effective activation energy $U_{eff}(J, T)$ from the relaxation measurements at different temperatures with the equation:

$$U_{eff}(J, T) = -k_B T \left[\ln\left(\frac{dJ}{dt} \frac{1}{J_m}\right) - C \right] \quad (2.15)$$

where $C = \ln(a\omega/\pi d)$ is a constant. From Eq.(2.15) we see that the temperature dependence of $U_{eff}(J, T)$ is not significant at each temperature. To keep the piecewise continuity of the $U_{eff}(J, T)$ segments, one can choose the optimum value of C for all the segments and divide them by the thermal factor $g(T)$, which contains the temperature dependence of the superconducting parameters.[56, 57, 58] This will shift all the segments onto the same smooth curve. Finally, the effective activation energy $U_{eff}(J, T)$ and the current density J is fitted with the inverse power-law Eq.(2.10) [59, 60] and from the μ value, we can identify the corresponding vortex structure.

2.1.5 Vortex Lattice Melting

Similar to the atoms in the lattices of a solid, a vortex can deviate away from its equilibrium position because of thermal motion at finite temperatures.[6] This motion becomes stronger as the temperature or the applied field increases. Eventually,

the vortex-lattice will melt at a certain critical temperature T_m (or $H_m(T)$). Under different temperatures T_m , we get different melting fields. By connecting all the melting points on the $H - T$ phase diagram, we obtain the so called “melting line”. The melted vortex system is called a “vortex-liquid”, in which a zero resistance supercurrent cannot exist because of the motion of the vortices.

For the highly layered BSCCO superconductor, the vortices are disconnected “disks” or “pancakes” and the vortex melting behavior is much more complicated [6]. As shown in Figure 2.4, there is a very sharp drop [61] in the melting field B_m at $T < T^* \approx 30K$. After experiencing a crossover at around 32K, the melting field switches to a slower drop with increasing temperature. The physics of this crossover in the melting field has not been clear until now.[44, 62, 63, 64]

Since a consistent theory for a 3D bulk melting transition is still currently lacking [6], the position and the shape of the vortex-lattice melting line is usually determined by the Lindermann criterion $\langle u^2(T_m) \rangle_{th} \approx c_L^2 a_0^2$. In the intermediate-field range $H_{c1} < H_a < H_{c2}$, the transition line takes the form $B_m(T) \approx (5.6c_L^4/Gi)H_{c2}(0)(1 - T/T_c)^2$, where $c_L \approx 0.1 \sim 0.4$, and Gi is the Ginzberg number.

2.2 Project Objectives

The magnetic properties of BSCCO superconductors are intriguing because of the complexity of the vortex structure and the consequent vortex dynamics.[6] Up to now, some areas are still unclear and more detailed understanding of the behavior of the vortex structure is highly desirable. In this thesis, we study the following three topics:

1. Time dependence of vortex penetration

The majority of the studies in vortex penetration are focused on the vortex entry and exit conditions [24, 25, 26, 27, 28, 29]. However, inside a superconductor, a moving vortex is still affected by the surface barriers, as well as other resistances, such as

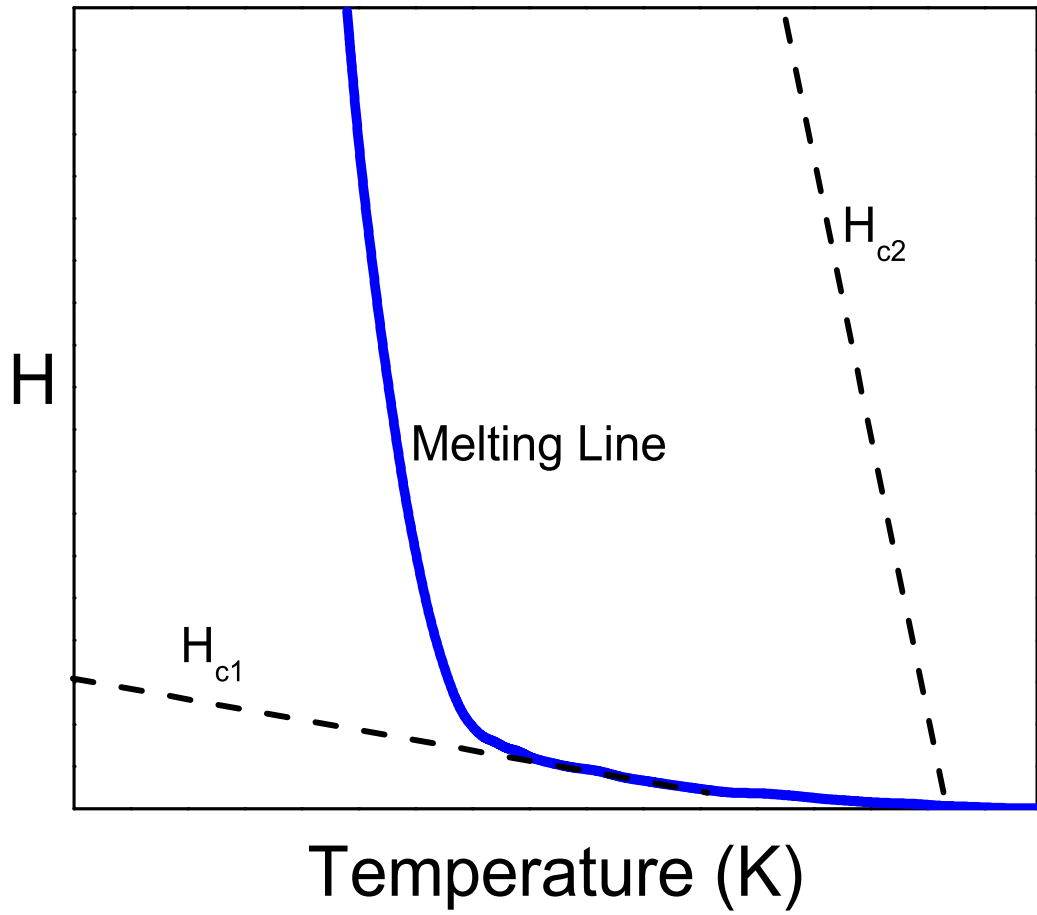


Figure 2.4: Schematic representation of vortex melting line in the strongly layered high- T_c superconductors, where H_{c1} is lower critical lower critical field, and H_{c2} is the upper critical field.

the pinning force [6] and the damping force.[65] All of these forces contribute to slow down the vortex motion. From the time dependent form of the GL theory [66, 67], one knows that a moving vortex gives rise to a “core” mass and an “electromagnetic” mass per unit length. The motion of the vortices would be retarded because of the presence of the resistances, according to mechanics. The vortex-penetration process cannot occur instantly and, therefore, must be time-dependent. Now the question arises: how long does it take for the penetrating field to reach a saturated value under a certain applied magnetic field?

The investigation of the time dependence of the vortex penetration process is important both in theoretical understanding and in practical applications of the type-II superconductor.[6] Systematic studies of the time dependence of vortex penetration are currently not available. For this purpose, we designed a special experimental measuring procedure that tests the time scale of the vortex penetration into the $Bi_2Sr_2CaCu_2O_{8+x}$ superconductors under various conditions.

2. Persistent currents and vortex dynamics

Because of the the interaction between the current and the vortices caused by the Lorentz force, the pinning potential U_{eff} is a function of current J . [6] For BSCCO superconductors, at temperatures below 20 K and above 40 K the dependence of the effective potential U_{eff} on J is described by the functions $U_{eff}(J) \propto \ln(J_c/J)$ and $U_{eff}(J) \propto (J_c/J)^{2/3}$, respectively. In the intermediate region ($20K \leq T \leq 40K$), no unique functional relation between U_{eff} and J has been found [68]. Clearly, more detailed understandings of the interaction between the current and the vortices, and the dependence of U_{eff} on J are needed.

On the other hand, the temperature dependence of the vortex melting line in the $Bi_2Sr_2CaCu_2O_8$ (BSCCO) superconductor exhibits a crossover behavior as the temperature is decreased.[41, 69, 70, 71]. Experiments [61] have confirmed a very sharp drop of the melting field B_m at $T < T^* \approx 30K$, which is explained as the 2D

to 3D transition temperature [44], or 0D to 3D transition temperature.[62, 63, 64] However, recent studies in BSCCO superconductors indicate that the crossover may be caused by the pinning transition.[73, 74, 75] One way to study these problems is to exert forces on the vortices by coupling the vortices to a current.

In this section, our purpose is to get more detailed understanding of the interaction between the current and the vortices, so we can understand the vortex structure and its properties in the vicinity of the crossover temperature T^* in the BSCCO superconductor. These studies were carried out in a ring shaped Bi-2212 superconductor under a series of annealings in vacuum.

3. Vortex-depinning induced phase transitions

It is already known that the vortex lattice encounters the melting transition into a vortex-liquid phase at a temperature T_m below T_c if the vortex fluctuations are sufficiently large.[6] It is still not clear what happens before melting, or what properties it has in the lower field region below the vortex melting line. The previous studies indicate that two distinct thermodynamic phases are present in the lower field region below $H_m(T)$, which is contrary to the common belief that a single Bragg glass phase prevails throughout this part of the phase diagram [76]. Theoretical calculations have shown that for the highly anisotropic superconductor BSCCO, there is an almost vertical depinning line T_{dp} dividing the vortex solid phase into two phases. This is evidenced by a sharp change in slope of the T -dependence of the vortex lattice, showing more than half of the vortices in the system are depinned at any time.[77, 78] Some results imply a depinning line of similar topology within the Bragg glass phase below $H_m(T)$ [49, 79, 80, 81, 81, 82, 83]. On the other hand, some theories suggest that a vortex decoupling transition [9] appears in the pancake-vortex lattice of layered superconductors with a finite Josephson coupling a few degrees below the melting line. In view of this, it looks as if the vortex depinning transition is a decoupling transition. Unfortunately, experiments have not confirmed explicitly these

theoretical suggestions. Recently, Beidenkopf et al.(2005) claimed it is a crossover from Bragg glass to vortex crystal (lattice) when a thermodynamic line in this region of a BSCCO superconductor was found.[44] Therefore, the physics in this region requires a more fundamental reconsideration.

In this section, our goal is try to understand what happens to the vortex lattice and its pinning at temperatures just below the melting line of the BSCCO superconductor.

Bibliography

- [1] C. Michel, M. Hervieu, M. M. Borel. *Z. Phys. B* **68**, 421 (1987).
- [2] H. Maeda, Y. Tanaka, M. Fukutumi, and T. Asano, *Jpn. J. Appl. Phys.* **27 (2)**, L209 (1988).
- [3] S. M. Green, Yu Mei, A. E. Manzi, H. L. Luo, R. Ramesh and G. Thomas, *J. Appl. Phys.* **66 (2)**, 728 (1989).
- [4] C. L. Briant, E. L. Hall, K. W. Lay, I. E. Tkaczyk, *J. Mater. Res.* **9 (11)**, 2789 (1994).
- [5] Timothy P. Beales, Jo Jutson, Luc Le Lay and Michele Molgg, *J. Mater. Chem.* **7**, 653 (1997).
- [6] G. Blatter, M. V. Feigel'man, V. B. Geshkenbein, A. I. Larkin, V. M. Vinokur, *Rev. Mod. Phys.* **66**, 1125 (1994).
- [7] K. H. Bennemann and J. B. Ketterson Eds., *The Physics of Superconductors* (Springer, New York, 2003), Vol. 1.
- [8] David Larbalestier, Alex Gurevich, D. Matthew Feldmann and Anatoly Polyanski, *Nature* **414**, 368 (2001).
- [9] M. J. W. Dodgson, V. B. Geshkenbein, G. Blatter, *Phys. Rev. Lett.* **83**, 5358 (1999).
- [10] W. Meissner and R. Ochsenfeld, *Naturwissenschaften* **21**, 787 (1933).

- [11] A. A. Abrikosov, Soviet Phys. JETP **5**, 1174 (1957).
- [12] W. H. Kleiner, L. M. Roth and S. H. Autler, Phys. Rev. **133**, A1226 (1964).
- [13] D. Gribier, B. Jacrot, L. Madhav Rao, B. Farnoux, Phys. Lett. **9**, 106 (1964).
- [14] G. Sarma, Compt. Rend. Acnd. Sci. Paris **258**, 1461 (1964).
- [15] U. Essmann, H. Trauble, Sci. Am. **224**, 75 (1971).
- [16] P. L. Gammel, D. J. Bishop, G. J. Dolan, J. R. Kwo, C. A. Murray, L. F. Schneemeyer, J. V. Waszczak, Phys. Rev. Lett. **59**, 2592 (1987).
- [17] C. A. Murray, P. L. Gammel, D. J. Bishop, Phys. Rev. Lett. **64**, 2312 (1990).
- [18] F. London, Superfluids (John Wiley and Sons, New York, 1950), p. 152.
- [19] P. E. Goa, H. Hauglin, M. Baziljevich, E. Il'yashenko, P. L. Gammel and T. H. Johansen, Supercond. Sci. Technol. **14**, 729 (2001).
- [20] L. Onsager, Proceeding of the International Conference on Theoretical Physics, Kyoto and Tokyo, 1954), pp. 935-936.
- [21] S. Bascom, Jr. Deaver, William M. Fairbank, Phys. Rev. Lett. **7**, 43 (1961).
- [22] Jr. Charles P. Poole, Horacio A. Farach, Richard J. Creswick and Ruslan Prozorov, Superconductivity (Elsevier, Second edition, 2007), p. 218.
- [23] W. E. Lawrence, S. Doniach, in Kanda (ed.) Proc. 12th Int. Conf. Low Temp. Phys. (Kyoto, 1970: Keigaku, Tokyo, 1971), p. 361.
- [24] P. G. de Gennes, Sol. St. Comm. **3**, 127 (1965).
- [25] L. Kramer, Phys. Rev. **170**, 475 (1968).
- [26] Ryuzo Kato, Yoshihisa Enomoto, Sadamichi Maekawa, Phys. Rev. B **47**, 8016 (1993).

- [27] Carlos Bolech, Gustavo C. Buscaglia, and A. Lopez, Phys. Rev. B **52**, R15719 (1995).
- [28] D. Yu. Vodolazov, Phys. Rev. B **62**, 8691 (2000).
- [29] B. L. Plourde, D. J. Van Harlingen, D. Yu. Vodolazov, R. Besseling, M. B. Hesselberth, and P. H. Kes, Phys. Rev. B **64**, 014503 (2001).
- [30] C. P. Bean, J. D. Livingston, Phys. Rev. Lett. **12**, 14 (1964).
- [31] L. Burlachkov, Phys. Rev. B **47**, 8056 (1993).
- [32] L. Burlachkov, V. B. Geshkenbein, A. E. Koshelev, A.I. Larkin, and V.M. Vinokur, Phys. Rev. B **50**, 16770 (1994).
- [33] M. R. Connolly, M. V. Milosevic, S. J. Bending, and T. Tamegai, Phys. Rev. B **78**, 132501 (2008).
- [34] Y. M. Wang, M. S. Fuhrer, and A. Zettl, S. Nagashima, K. Oka, and Y. Nishihara, Phys. Rev. B **71**, 132507 (2005).
- [35] Y. M. Wang, A. Zettl, S. Ooi, and T. Tamegai, Phys. Rev. B **65**, 184506 (2002).
- [36] E. Zeldov, A. I. Larkin, V. B. Geshkenbein, M. Konczykowski, D. Majer, B. Khaykovich, V. M. Vinokur, and H. Shtrikman, Phys. Rev. Lett. **73**, 1428 (1994).
- [37] M. V. Indenbom, G. D'Anna, M. O. Andre, V. V. Kabanov, and W. Benoit, Physica C **235-240**, 201 (1994).
- [38] M. Benkraouda and J. R. Clem, Phys. Rev. B **53**, 5716 (1996).
- [39] E. H. Brandt, Physics and material science of vortex state, flux pinning and dynamics., volume 356 of NATO ASI. Kluwer Academic Publisher, the Netherlands, 1999.
- [40] Kristian Fosheim and Asle Sudbo, Superconductivity: physics and applications (John Wiley and Sons Ltd., NJ USA, 2004), p.232.

- [41] Michael Tinkham, Introduction to Superconductivity (McGraw-Hill, Inc., USA second edition, 1996), p.11/p.120.
- [42] P. H. Kes, Flux pinning and the summation of pinning forces, Concise Encyclopedia of magnetic and superconducting materials (J. Evetts ed.), Pergamon, Oxford (1992), p.170.
- [43] A. I. Larkin and Yu. V. Ovchinnikov, J. Low Temp. Phys. **34**, 409 (1979).
- [44] H. Beidenkopf, N. Avraham, Y. Myasoedov, H. Shtrikman, E. Zeldov, B. Rosenstein, E. H. Brandt, and T. Tamegai, Phys. Rev. Lett. **95**, 257004 (2005).
- [45] P. W. Anderson, Phys. Rev. Lett. **9**, 309 (1962).
- [46] P. W. Anderson and Y. B. Kim, Rev. Mod. Phys. **36**, 39 (1964).
- [47] Y. B. Kim, C. F. Hempstead, and A. R. Strnad, Phys. Rev. **131**, 2486 (1963).
- [48] Y. B. Kim, C. F. Hempstead, and A. R. Strnad, Rev. Mod. Phys. **36**, 43 (1964).
- [49] M. R. Beasley, R. Labusch, and W. W. Webb, Phys. Rev. **181**, 682 (1969).
- [50] M. V. Feigel'man, V. B. Geshkenbein, A. I. Larkin, V. M. Vinokur, Phys. Rev. Lett. **63**, 2303 (1989).
- [51] E. Zeldov, N. M. Amer, G. Koren, A. Gupta, R. J. Gambino, and M. W. McElfresh, Phys. Rev. Lett. **62**, 3093 (1989).
- [52] E. Zeldov, N. M. Amer, G. Koren, A. Gupta, M. W. McElfresh, and R. J. Gambino, Appl. Phys. Lett. **56**, 680 (1990).
- [53] Alexis P. Malozemoff and Matthew P. A. Fisher, Phys. Rev. B **42**, 6784 (1990).
- [54] Matthew P. A. Fisher, Phys. Rev. Lett. **62**, 1415 (1989).
- [55] M. P. Maley, J. O. Willis, Phys. Rev. B **42**, 2639 (1990).

- [56] Hai-hu Wen, H. G. Schnack, R. Griessen, B. Dam, J. Rector, *Physica C* **241**, 352 (1995).
- [57] J. R. Thompson, L. Krusin-Elbaum, L. Civale, G. Blatter, C. Field, *Phys. Rev. Lett.* **78**, 3181 (1997).
- [58] C. J. van der Beek, P. H. Kes, M. P. Maley, M. J. V. Menken, A. A. Menovsky, *Physica C* **195**, 307 (1992).
- [59] D. R. Nelson, V. M. Vinokur, *Phys. Rev. Lett.* **68**, 2398 (1992).
- [60] D. R. Nelson, V. M. Vinokur, *Phys. Rev. B* **48**, 13060 (1993).
- [61] P. L. Gammel et al., *Phys. Rev. Lett.* **61**, 1666 (1988).
- [62] A. Piriou, Y. Fasano, E. Giannini, and O. Fischer, *Phys. Rev. B* **77**, 184508 (2008).
- [63] V. F. Correa, J. A. Herbsommer, E. E. Kaul, F. de la Cruz, and G. Nieva, *Phys. Rev. B* **63**, 092502 (2001).
- [64] M. F. Goffman, J. A. Herbsommer, F. de la Cruz, T. W. Li and P. H. Kes, *Phys. Rev. B* **57**, 3663 (1998).
- [65] John Bardeen, M. J. Stephen, *Phys. Rev.* **140**, A1197 (1965).
- [66] M. J. Stephen, H. Suhl, *Phys. Rev. Lett.* **13**, 797 (1964).
- [67] H. Suhl, *Phys. Rev. Lett.* **14**, 226 (1965).
- [68] M. Nideröst et al., *Phys. Rev. B* **53**, 9286 (1996).
- [69] A. Houghton et al., *Phys. Rev. B* **40**, 6763 (1989).
- [70] L. I. Glazman, A. E. Koshelev, *Phys. Rev. B* **43**, 2835 (1991).
- [71] D. S. Fisher et al., *Phys. Rev. B* **43**, 130 (1991).

- [72] M. Tinkham, Introduction to Superconductivity, 2nd edition, McGraw-Hill, Inc., USA (1996), p. 344.
- [73] T. Verdene, H. Beidenkopf, Y. Myasoedov, H. Shtrikman, M. Rappaport, E. Zeldov, and T. Tamegai, Phys. Rev. Lett. **101**, 157003 (2008).
- [74] Yadin Y. Goldschmidt and Jin-Tao Liu, Phys. Rev. B **76**, 174508 (2007).
- [75] Yadin Y. Goldschmidt and Eduardo Cuansing, Phys. Rev. Lett. **95**, 177004 (2005).
- [76] G. Blatter and V. B. Geshkenbein, The Physics of Superconductors (Springer, New York, 2003), Vol. 1, Chapter 10, p.725.
- [77] R. Sugano, T. Onogi, K. Hirata, and M. Tachiki, Phys. Rev. Lett. **80**, 2925 (1998).
- [78] R. Sugano et. al., Physica B **284**, 803 (2000).
- [79] C. D. Dewhurst and R. A. Doyle. Phys. Rev. B **56**, 10832 (1997).
- [80] Y. Yamaguchi, G. Rajaram, N. Shirakawa, A. Mumtaz, H. Obara, T. Nakagawa, and H. Bando, Phys. Rev. B **63**, 014504 (2000).
- [81] Yuji Matsuda, Marat B. Gaifullin, Ken-ichi Kumagai, Makoto Kosugi, and Kazuto Hirata, Phys. Rev. Lett. **78**, 1972 (1997).
- [82] S. Ooi, T. Shibaushi, T. Tamegai, Physica B **284-288**, 775 (2000).
- [83] S. Ooi, T. Mochiku, K. Hirata, Physica C **378**, 523 (2002).

Chapter 3

Experimental Methods

The materials used in this thesis are $Bi_2Sr_2Ca_1Cu_2O_{8-x}$ (Bi-2212) single crystals and thin films. The first and the difficult step in our study is the sample preparation[1]. It is extremely hard to get good samples with high T_c and high J_c . Bi-2212 is a highly anisotropic materials with a short coherence and the vortex matter is very sensitive to temperature. During the measurement, the temperature has to be precisely controlled. Therefore, the experimental methods are important in the study of BSCCO superconductors. In this chapter, we will describe the experimental aspects of sample growth and measurement used in this thesis.

3.1 Sample Preparation

In order to grow high quality BSCCO samples, the nominalized composition has to be consistent with the following heat treatment conditions because of the volatility of the components in the BSCCO superconductor. The preparation process is sensitive to the temperature [2], the oxygen environment [1] and the sintering duration.[3] All these have to be considered in a consistent way.

3.1.1 Bi-2212 Single Crystal

BSCCO crystals of $T_c \simeq 92$ K were grown in the Clarendon Laboratory of Oxford University using a crucible-free optical floating-zone technique. Therefore, they are extra “clean” materials and have very small flux pinning ability.

In order to measure the magnetic properties of the BSCCO superconductors in the Hall probe system, we prepared the samples in circular shapes, such as disks and rings. Small pieces of Bi-2212 single crystals were cut from a bigger as-grown crystal with scalpels, and then shaped into disks or rings (Figure 3.1) under a microscope. The crystal disks were 0.5 mm thick and had outer diameters of 1.0 mm. The crystal ring was 0.5 mm thick and its inner and outer diameters were ~ 0.5 and 1.0 mm, respectively. The axes of both the ring and disk were parallel to the c-axis of the crystal.

3.1.2 Bi-2212 thin film

The Bi-2212 sputtering targets of nominal composition $Bi_{1.9}Pb_{0.2}Sr_2CaCu_2O_{8+x}$ were prepared by solid state reaction methods. Since the Bi-2212 phase is most stable [1] at 850-870 °C, the temperature range is very small, so the sintering temperature must be controlled very accurately.

The BSCCO thin film samples of $T_c \simeq 82$ K were deposited on (100) MgO substrates of size 10×10 mm² in a magnetron sputtering system (Figure 3.2), which allows one to deposit thin films over a large area.

The magnetron sputtering system consists of a cryo-pumped vacuum chamber with a base pressure of 1×10^{-7} Torr. There are three rf magnetron sputtering guns which can work with either a DC or an AC power source. The substrates are attached to a nickel plate with silver paste which allows uniform heating.

During the sputtering process the substrates were configured in an “off-axis” position (Figure 3.2), which can be heated up to 800 °C by a heater below the plate. A temperature controller was used to control the substrate temperature with a stability of $\pm 1^\circ C$. The two working gas suppliers (Ar and O₂) could be adjusted by two digital

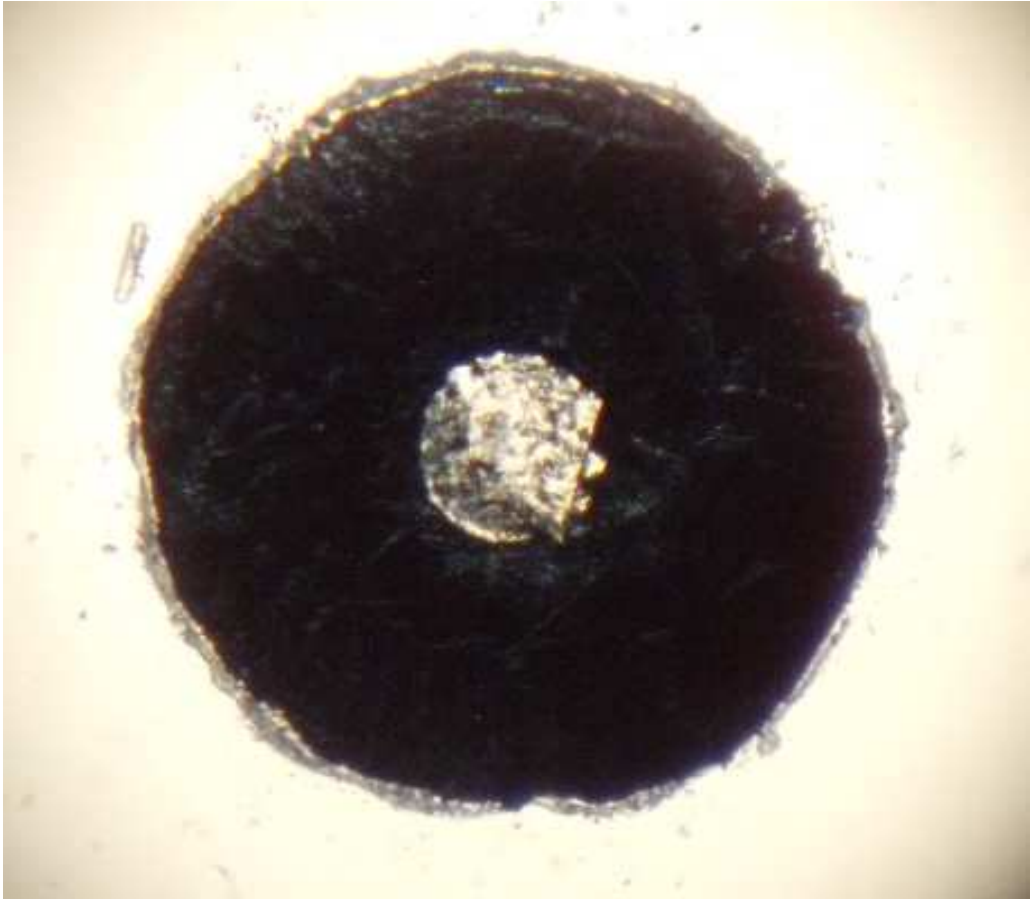


Figure 3.1: Bi-2212 single crystal ring ($\phi 1$).

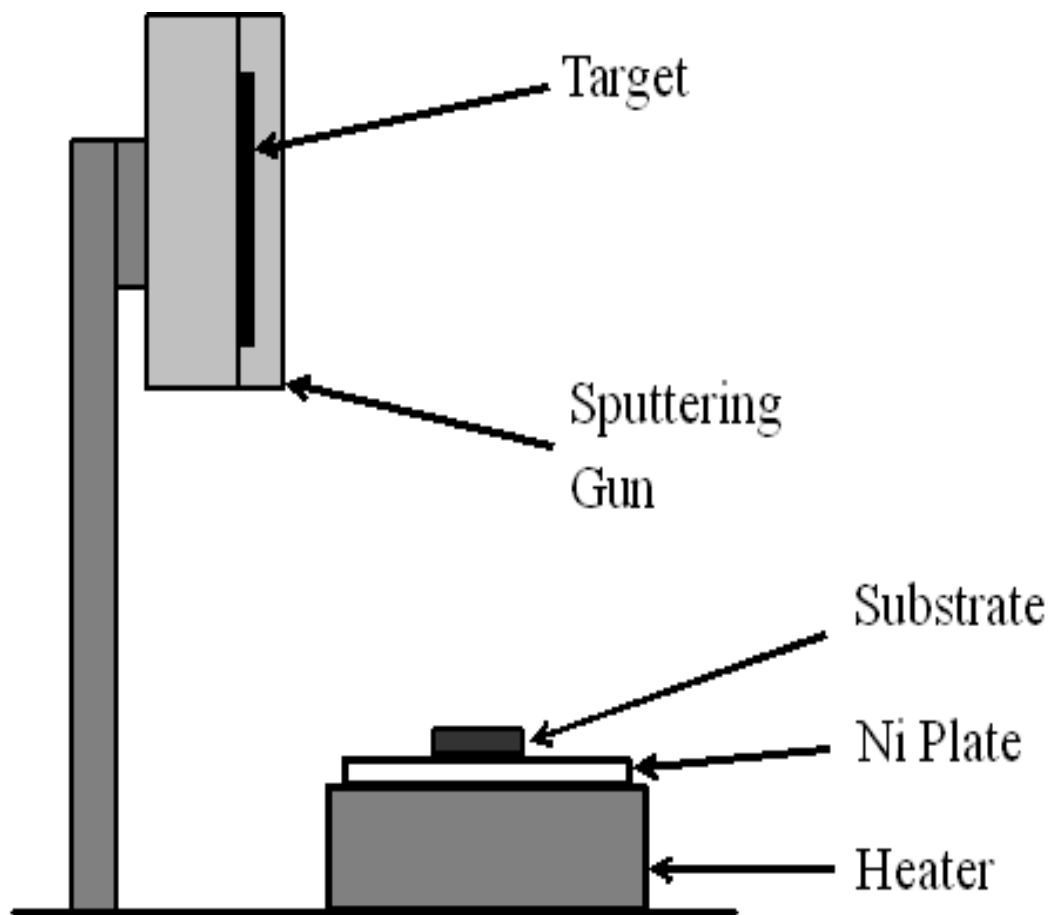


Figure 3.2: Schematic representation of the thin film magnetron sputtering system.

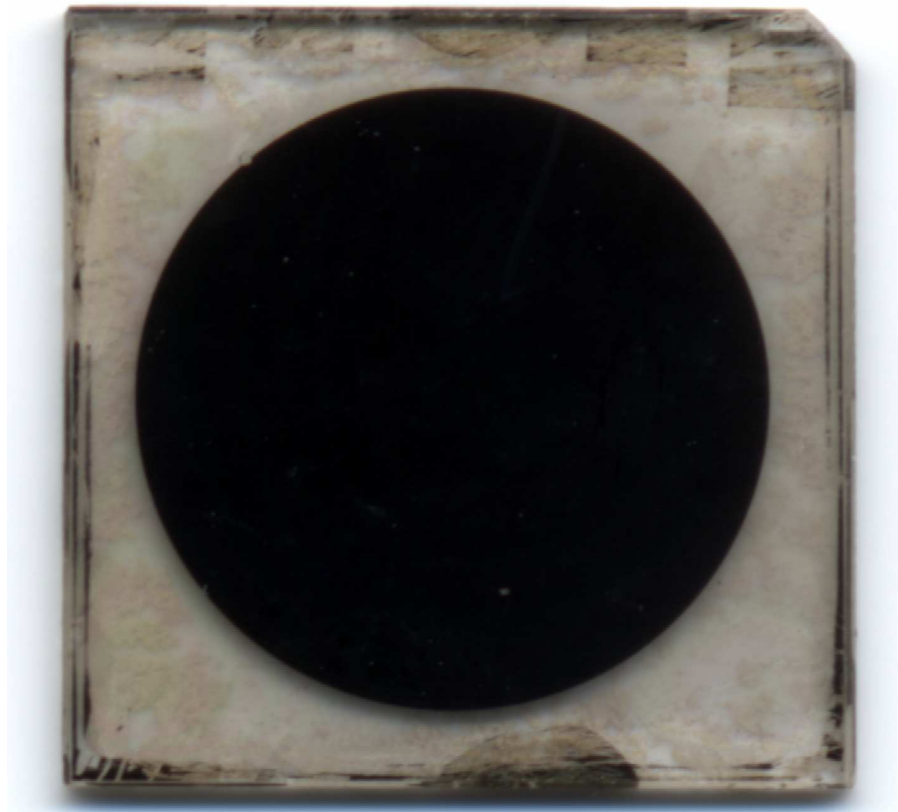


Figure 3.3: Bi-2212 thin film disk ($\phi 10$).

meters separately. Sputtering was usually carried out in an argon-oxygen mixed gas with a ratio of 3:1, while the substrate temperature was maintained at 680 °C. The deposited films were sintered at 800 °C for one hour on average.

The highest T_c we obtained using the above stated procedure was 82 K. This is far from the T_c of Bi-2212 single crystal 92 K; the reason could be the lattice constant mismatch between Bi-2212 ($a = 5.4095 \text{ \AA}$) and MgO ($a = 4.216 \text{ \AA}$).

The as-grown thin film samples were finally patterned into the disks of diameter 10 mm and 220 nm thick by the photolithography methods in the University of Alberta NanoFab. The c-axes of the BSCCO thin films were oriented normal to the surface of the substrates (Figure 3.3).

3.2 Measuring procedure

For highly anisotropic superconductors, the experiments [4] have confirmed that the vortex matter is very sensitive to temperature. The vortex melting line in these superconductors exhibits a crossover from 3D to 0D melting behavior as the temperature is decreased. In the 0D case, the melting field drops almost vertically with increasing temperature. The melting line has a dramatic effect on the temperature dependence of the critical current J_c in the high- T_c superconductors [5], which was found to be very similar to that of B_m . This important issue requires that special attention be paid to precise temperature control in the measurement of BSCCO superconductors.

In our study, the measurements involve the vortex dynamics when persistent currents are present. Since the vortex-pinning potential $U_{eff}(J)$ is a function of current density J through the interaction between the current and the vortices [6], $U_{eff}(J)$ can be described by the power-law dependence, i.e. $U_{eff}(J) \propto (J_c/J)^\mu$. This allows one to use the critical exponent μ to identify the vortex structure. The understanding of the interaction between the current and the vortices caused by the Lorentz force is highly desirable in the application of superconductivity.

The most frequently used measuring methods in superconductors are R-T (Resistance vs temperature) transport measurements, and DC/AC magnetization measurements. In the R-T measurement, the Joule heat from the contacts usually affects the reliability of the results, and it is also hard to distinguish between very low resistance and the superconductivity. However, the standard measuring methods for the magnetic properties in superconductors are the magnetization measurements [7], which generally give information about the diamagnetization (or surface screening effect) with the applied magnetic field and the total vortices trapped in the bulk. They cannot give any direct information about the flux pinning ability when the persistent currents are present. Consequently, one cannot obtain any useful information about the persistent current relaxation. On the other hand, in magnetization measurements the J_c of the sample is calculated from the magnetization with the Bean model [8, 9]; its validity is usually affected by the theoretical critical model itself. Especially when

studying the magnetic properties of a superconductor, all of these measuring methods are “indirect measurements”. Therefore, an alternative technique needs to be used. A superconductive ring is a good choice for this purpose. Indeed, the superconductive rings play a particular important role in the study of superconductivity.

3.2.1 Hall Probe System

Considering the fact that the persistent circulating current in a superconductor generates a magnetic field, one can calculate the persistent circulating current from the measured magnetic field according to the Biot-Savart law.[10] Generally, a persistent current in a superconducting ring shaped sample is generated by applying a magnetic field to the ring which is subsequently removed. The persistent current decays due to the interaction between the current and the vortices. By measuring the trapped field in the superconductive rings we can obtain information about the persistent current relaxations and the exponential parameter μ , in the scaling relation between the effective energy barrier and the persistent current density. In our lab, the study of the magnetic properties of the superconductors is carried out on a Hall probe system by directly measuring the trapped fields in the superconductor.

The disk or ring shaped samples are mounted on a sample holder, which can be cooled down to around 10 K. A constant external magnetic field H_a (up to 1.5 kG, generated by a copper-wound solenoid in a direction parallel to the axis of the ring or the disk) was applied to the zero-field-cooled samples at temperatures below T_c and subsequently reduced to zero after some time interval t . The magnitude of the resulting trapped field was recorded with an axial Hall sensor of sensitivity ± 2 mG, placed 2.5 mm above the sample at room temperature. Since the Hall probe itself is sensitive to temperature, embedding the Hall probe close to the sample can be problematic. On the other hand, it is much easier to operate the Hall probe in air.

At higher temperatures, the trapped field drops to a very low value, and the fluctuation is large. So, in all the measurements, we require that the temperature deviation is within 0.05 K. The measurements of the trapped field were performed as

functions of temperature for different applied fields, and the duration of the applied field.

The advantage of this measuring system is that it allows a contactless evaluation of the persistent current in the superconductor from the trapped magnetic field by using the Biot-Savart law.

3.2.2 Scan Profile

The first thing we can do with the Hall probe system is to scan the “profile” - the magnetic field distribution in the sample. Before the measurement, a DC magnetic field H_a generated by a solenoid was applied perpendicular to the surface of the sample (a-b plane of the crystal). For the purpose of full penetration, the applied field was held constant for a certain time interval and then switched off. A stepper motor drives the sensitive Hall probe and scans along the diameter of the sample. A computer connected to the system records the component of the magnetic field perpendicular to the ring-shaped sample and the corresponding positions of the Hall probe. The magnetic field distribution is then plotted automatically by the computer, as shown in Figure 3.4.

The lower critical field, $H_{c1}(T)$, and the upper critical field, $H_{c2}(T)$, of type-II superconductors are well-defined functions of temperature, T , and external magnetic field, H . The conventional magnetic phase diagram [1] is commonly plotted as H vs. T . At or close to the melting field $B_m(T)$, the superconductor is fully penetrated and the internal magnetic field is expected to be constant over the entire sample volume. Therefore, the vortex structure close to the melting field can be well represented by the measurement of trapped magnetic field. At a fixed temperature, the trapped magnetic field increases with increasing external magnetic field and finally reaches a saturated value, which corresponds (not equal) to the melting field $B_m(T)$ (external field). Similar to the name “melting line”, we will refer to the series of the saturated trapped field as “saturation line” (See Figure 3.5).

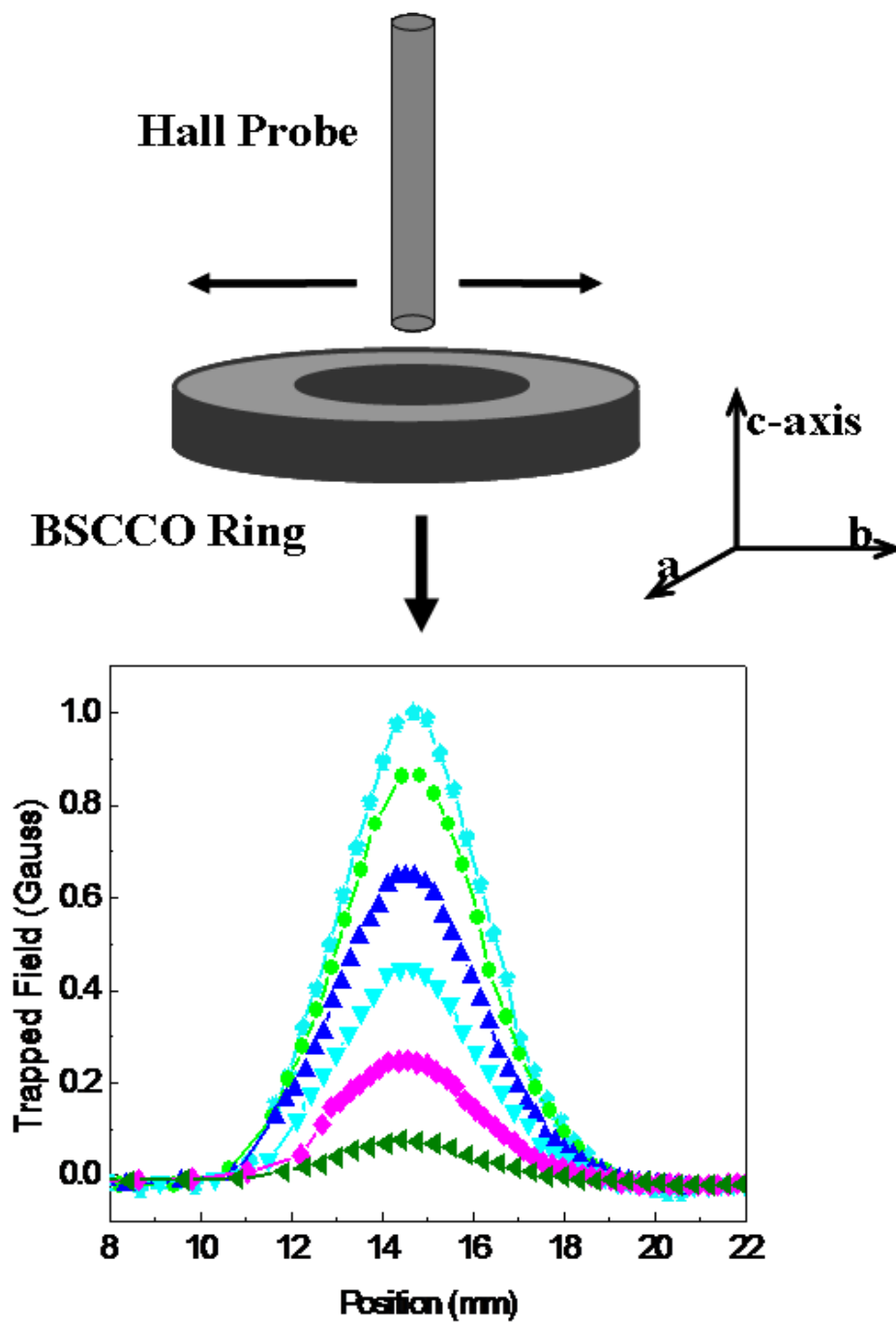


Figure 3.4: Trapped magnetic field profile in a Bi-2212 single crystal ring. By scanning the Hall Probe above the sample, we can get the distribution of the trapped magnetic field.

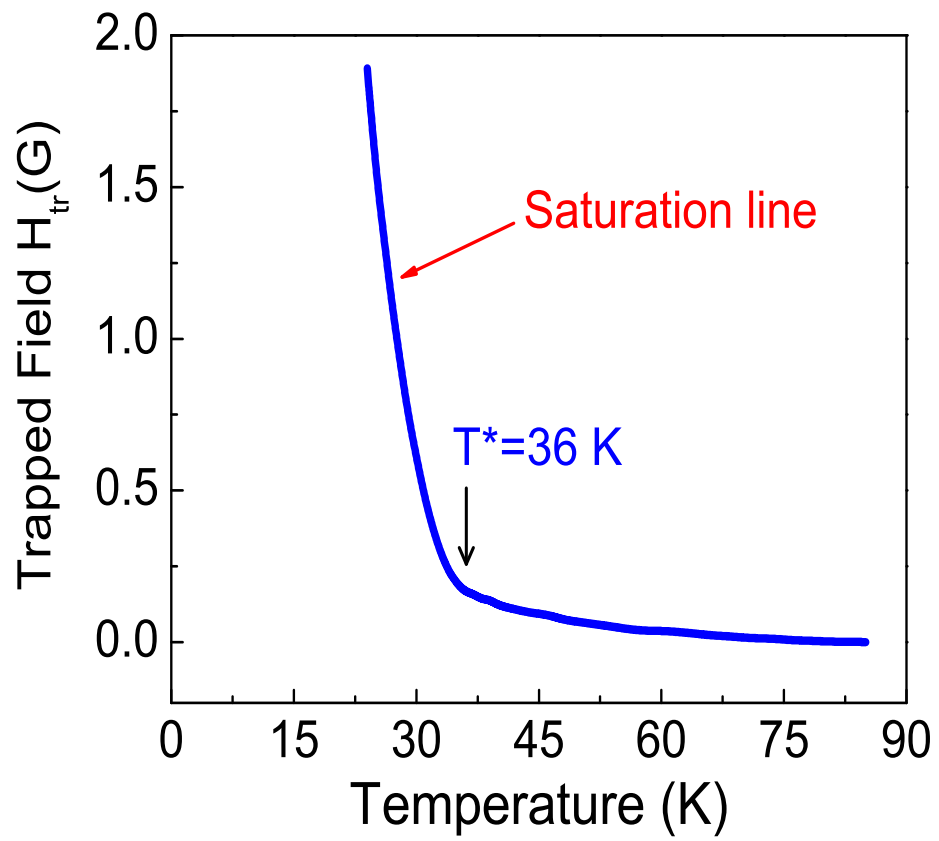


Figure 3.5: Saturation line of Bi-2212 superconductor

3.2.3 Decay Measurement

The second thing we can do with the Hall probe is to measure the time evolution of the magnitude of the trapped field in the sample (Figure 3.6). At first, we scan the magnetic profile and find out the position where the maximum trapped field is located, and then we fix the Hall probe at this maximum field position. After, a magnetic field H_a (generated by a solenoid) is applied perpendicular to the surface of the sample (a-b plane of the crystal) for a certain time interval and is subsequently switched off. The computer starts to record the value of the trapped field and the corresponding time continuously. In this way, we can measure the trapped field as a function of time, that is, the decay of the persistent current in the superconductor.

The decays were measured at different applied fields and temperatures. The dependence of the trapped field on time t helps us to visualize the pinning potentials of the vortices in the superconductor. This will be studied in detail in Chapter 4.

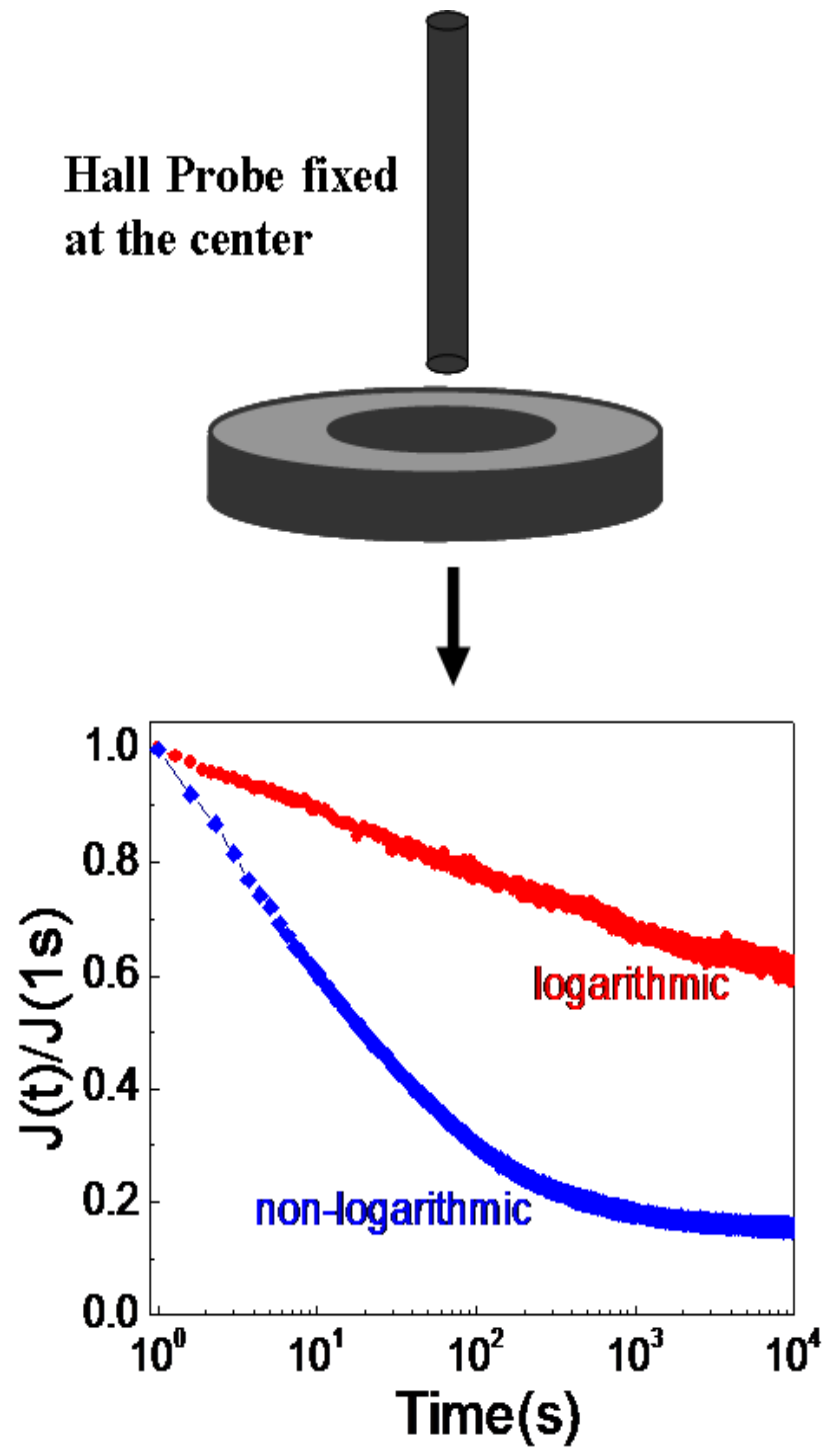


Figure 3.6: Decay measurements. By fixing the Hall Probe above the sample, we can measure the trapped magnetic field as a function of time.

Bibliography

- [1] S. M. Green and Yu Mei and A. E. Manzi and H. L. Luo and R. Ramesh and G. Thomas, *J. Appl. Phys.* **66**, 728 (1989).
- [2] Z. Mori, K. Sakai, H. Ota and R. Aoki, *J. Low Temp. Phys.* **105**, 1283 (2004).
- [3] H. K. Lee, K. W. Lee, K. Park, N. M. Huang, O. K. Oh, J. S. Kim, K. H. Yoo, Y. B. Kim, C. S. Kim, Y. K. Cho, J. C. Park, S. I. Suck, *J. Appl. Phys.* **66**, 1881 (1989).
- [4] P. L. Gammel et al., *Phys. Rev. Lett.* **61**, 1666 (1988).
- [5] G. Balestrino et al., *J. of Supercond.* **3**, 211 (1990).
- [6] M. Nideröst et al., *Phys. Rev. B* **53**, 9286 (1996).
- [7] H. Beidenkopf, N. Avraham, Y. Myasoedov, H. Shtrikman, E. Zeldov, B. Rosenstein, E. H. Brandt, and T. Tamegai, *Phys. Rev. Lett.* **95**, 257004 (2005).
- [8] C. P. Bean, *Phys. Rev. Lett.* **8**, 250 (1962).
- [9] C. P. Bean, *Rev. Mod. Phys.* **36**, 31 (1994).
- [10] David J. Griffiths, *Introduction to Electrodynamics*, Third Edition, p215 (1999), Prentice Hall, New Jersey.
- [11] G. Blatter et al., *Rev. Mod. Phys.* **66**, 1125 (1994).

Chapter 4

Vortex Penetration in Bi-2212 Superconductors

The vortex entry conditions [1, 2, 3, 4] have been well studied. The results have shown that the vortex penetration process is affected by the pinning, the temperature, the applied field and the geometry [5] of the sample. However, the study on the time scale of vortex penetration is currently unavailable. In this chapter, we design a special measuring procedure to study the time dependence of vortex penetration into the $Bi_2Sr_2CaCu_2O_{8+x}$ single crystal and thin films.

4.1 Introduction

For a type-II superconductor, as an applied magnetic field H_a increases to a value such that $H_{c1} < H_a < H_{c2}$, the magnetic field can penetrate into the superconductor in the form of quantized vortices [6, 7, 8, 9, 10, 11, 12, 13, 14, 15], each carrying a single flux quantum $\phi_0 = h/2e$. The vortex penetration process occurs at the surface first, and afterward goes further into the interior because of the edge barriers, which includes the “surface barrier” [16, 17] and the “geometrical barrier” (GB) [5]. The vortex entry conditions were first studied by De Gennes [1], and then by Kramer [2]. A number of other works studied the vortex entry conditions by solving the

time-dependent GL equation numerically [3, 4]. Besides the surface barrier to the vortex-penetration, a moving vortex in a type-II superconductor experiences other resistances, such as the pinning force [18] and the damping force [19]. The motion of the vortex is then retarded [20]. Thus, the vortex-penetration process cannot occur instantly and must be time-dependent. Now the question arises: how long does it take for the penetrated field to reach a saturated value under a particular applied magnetic field?

The investigation of the time dependence of the vortex penetration process is important both in the theoretical understanding and in the practical application of type-II superconductors [18]. In this chapter, we will use a specially designed experimental measuring procedure to test the time scales of vortex penetration into the $Bi_2Sr_2CaCu_2O_{8+x}$ superconductors under various conditions.

4.2 Temperature Dependence of Vortex Penetration

The $Bi_2Sr_2CaCu_2O_{8+x}$ single crystal and thin film samples with geometric shapes of disks and rings were prepared as detailed in Chapter 2.

Figure 4.1 shows the temperature dependence of the trapped field obtained by applying a constant magnetic field over different time intervals t , as well as the measurements of the “saturation line”. The meaning of “saturation line” is explained in Chapter 2, that is, the temperature dependence of the maximum field that can be trapped in a sample at each temperature (represented by the solid line in Figures 4.1(A) and (B)). The temperature dependence of the trapped field, after a constant magnetic field is applied and subsequently removed, exhibits a maximum at temperatures close to the saturation line. At higher temperatures the trapped fields merge with those at the saturation line. The maximum in the trapped field and its evolution with an increasing t have been observed to be qualitatively similar in both the single crystal and thin film samples.

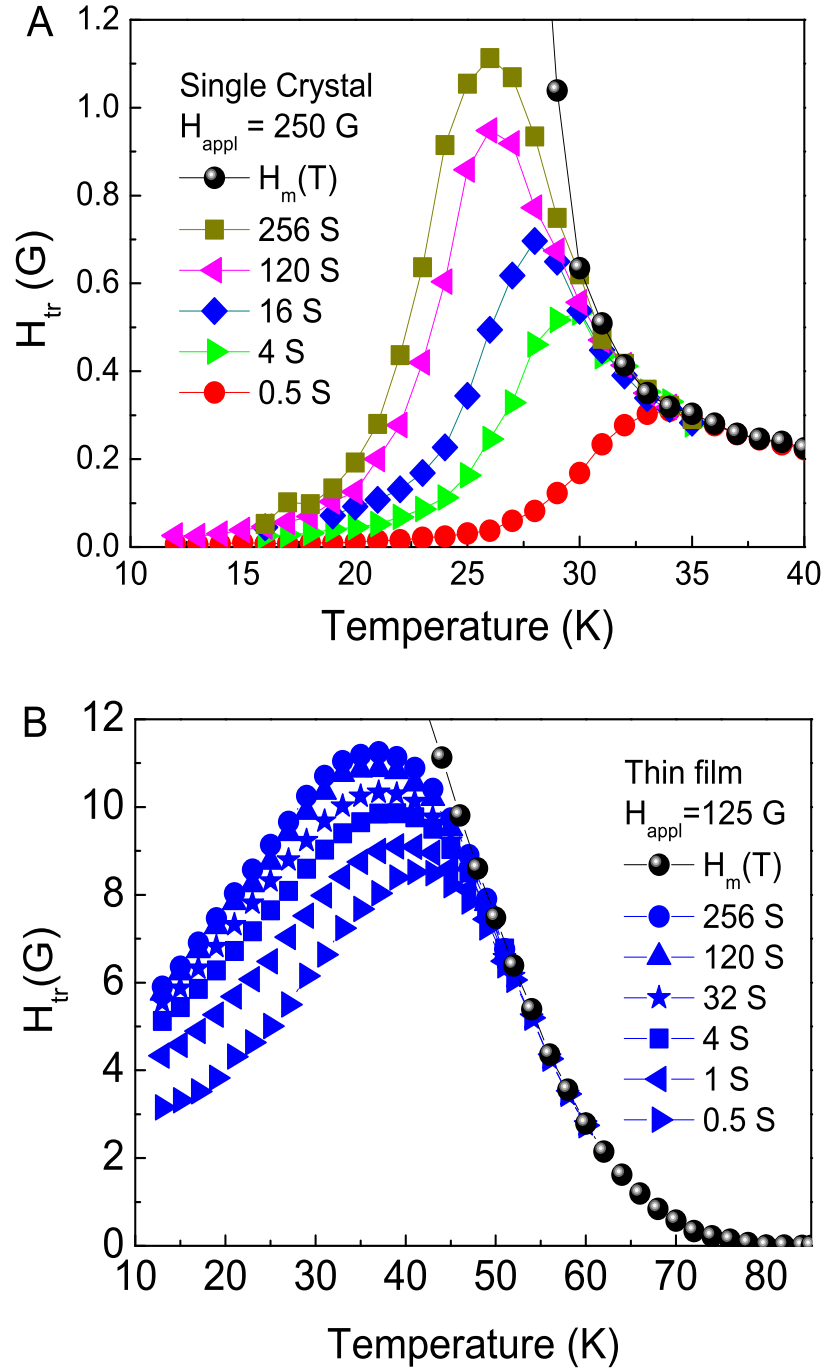


Figure 4.1: (A) Temperature dependence of the field trapped in the BSCCO single crystal. The field was trapped by applying a constant magnetic field $H_{appl} = 250$ G which was subsequently reduced to zero after a time interval t . $H_m(T)$ is the temperature dependence of the saturation line. (B) The corresponding temperature dependence of the field trapped in the BSCCO thin film after applying a constant field of 125 G.

The observed dependence of the trapped field on temperature could be the result of the interplay between the surface screening effects [21] and the surface and bulk pinning of the vortices [24, 25, 26]. At low enough temperatures, the strong surface screening currents limit the vortex entry into the superconductor. In this case, only a small number of vortices can penetrate into the bulk and their pinning results in a small trapped field. On the other hand, according to Bean and Livingston [16], a vortex close to the surface (inside the superconductor) feels an attractive image force to the surface and a repulsive force from the external field. The sum of these two forces decreases exponentially away from the surface; therefore, it is a short range force which only works at the initial stage of the vortex-penetration process when the vortex is close to the surface. However, the surface screening effect weakens with increasing temperature, allowing more vortices to be pinned in the superconductor. One, therefore, would expect that when a constant magnetic field is applied at different temperatures and subsequently removed, the resulting trapped field would gradually increase with increasing temperature and reach a maximum at the saturation line. In fact experiments show that the maxima in the trapped field in BSCCO crystals and BSCCO films occur at temperatures several degrees below the saturation line. The presence of the maximum suggests that the partial depinning of magnetic vortices [27, 28] occurs at temperatures above the maximum, leading to a gradual decrease of the trapped field with increasing temperature, which eventually merges with the saturation line.

The vortex penetration starts from the edge according to the Bean mode; consequently, the material at the center of a sample should have no effect on the vortex penetration process. Therefore, it is expected that there should be no big qualitative difference for the vortex penetration between the ring and the disk at the lower temperatures. Our measurements in the crystal ring (not shown here) have similar figures to those in the crystal disk, indicating that the strong surface screening currents and the Bean-Livingston barrier limit the vortex entry into the superconductor. The vortices are mainly trapped close to the edge.

Figure 4.1 also shows that at a fixed temperature, the trapped field in the thin film saturates in a shorter time interval. This can be explained by the fact that the thin film has a very small thickness (z -axis), and, therefore, the surface barrier perpendicular to the z -axis is smaller. When the external magnetic field is applied parallel to the z -axis, the Bean-Livingston barrier against the vortices motion should be weak, and the vortices can penetrate into the thin film more easily compared to the crystal which has a larger thickness. Thus, the trapped field in the thin film samples saturates in a shorter time interval.

4.3 Dependence of Vortex Penetration on Applied Field

Figure 4.2 shows the trapped fields as a function of the applied fields over different time intervals t . The trapped field increases with increasing time interval t . At higher applied fields, the rate at which the trapped field increases also increases.

Both Figure 4.1 and Figure 4.2 show the vortex penetration into the BSCCO superconductors are strongly time dependent. The penetration time scale depends on the temperature, the applied field and the geometry of the sample. In the following section we will measure the trapped field as a function of the time interval t during which an external magnetic field is applied to the sample. This $H_a - t$ measurement can show the time dependence of the vortex penetration process in a more explicit way. Let us refer to the curves corresponding to this process as “vortex penetration curves”.

4.4 Time Dependence of Vortex Penetration

Figure 4.3 shows the vortex-penetration curves measured in the crystal. The curves in (A) are measured under the same applied field $H_a = 250\text{G}$, but at different temperatures $T = 22\text{K}$, 25K , 28K , respectively. The curves in (B) are measured at the

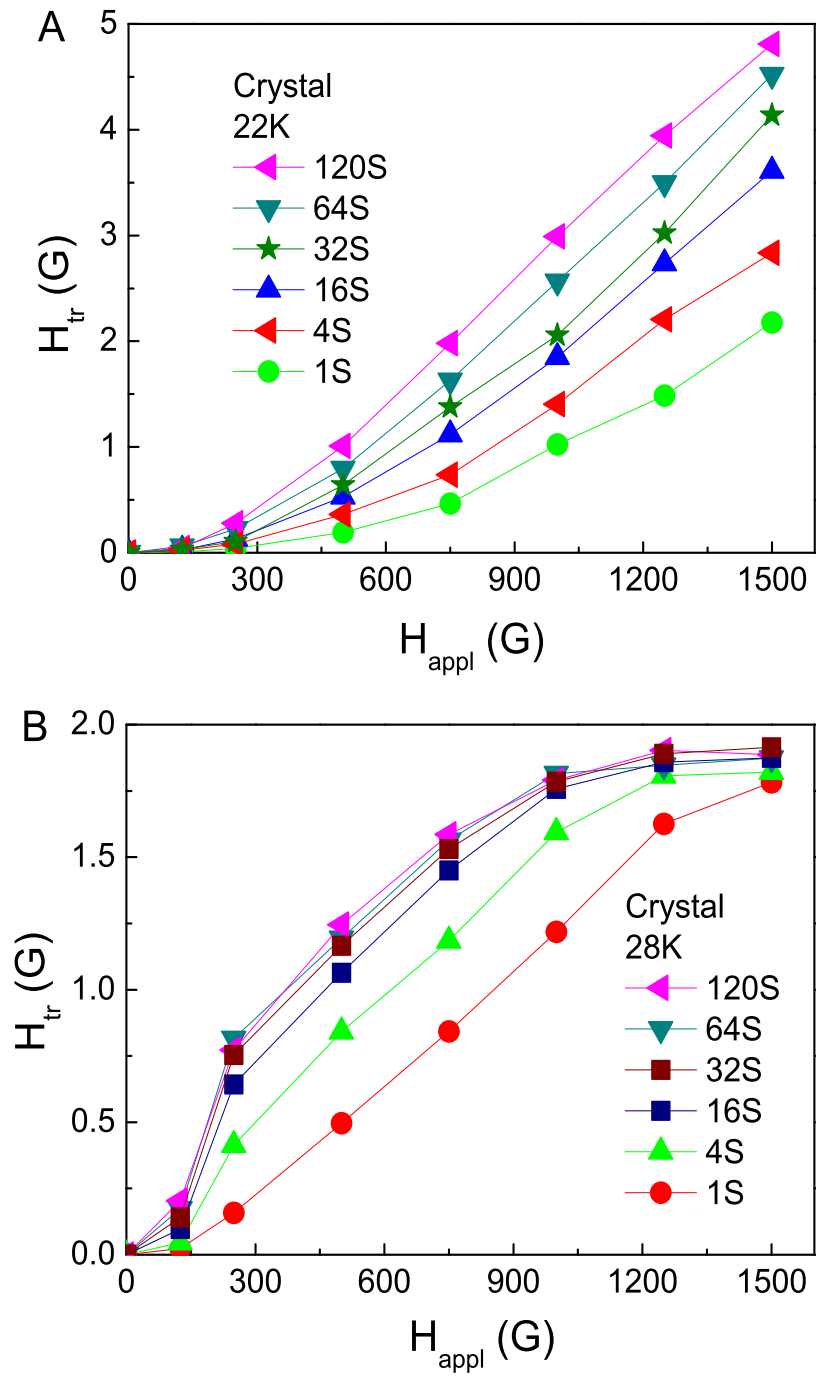


Figure 4.2: Trapped field as a function of applied field over different time intervals t in a Bi2212 single crystal. (A) Measured at 22 K. (B) Measured at 28 K.

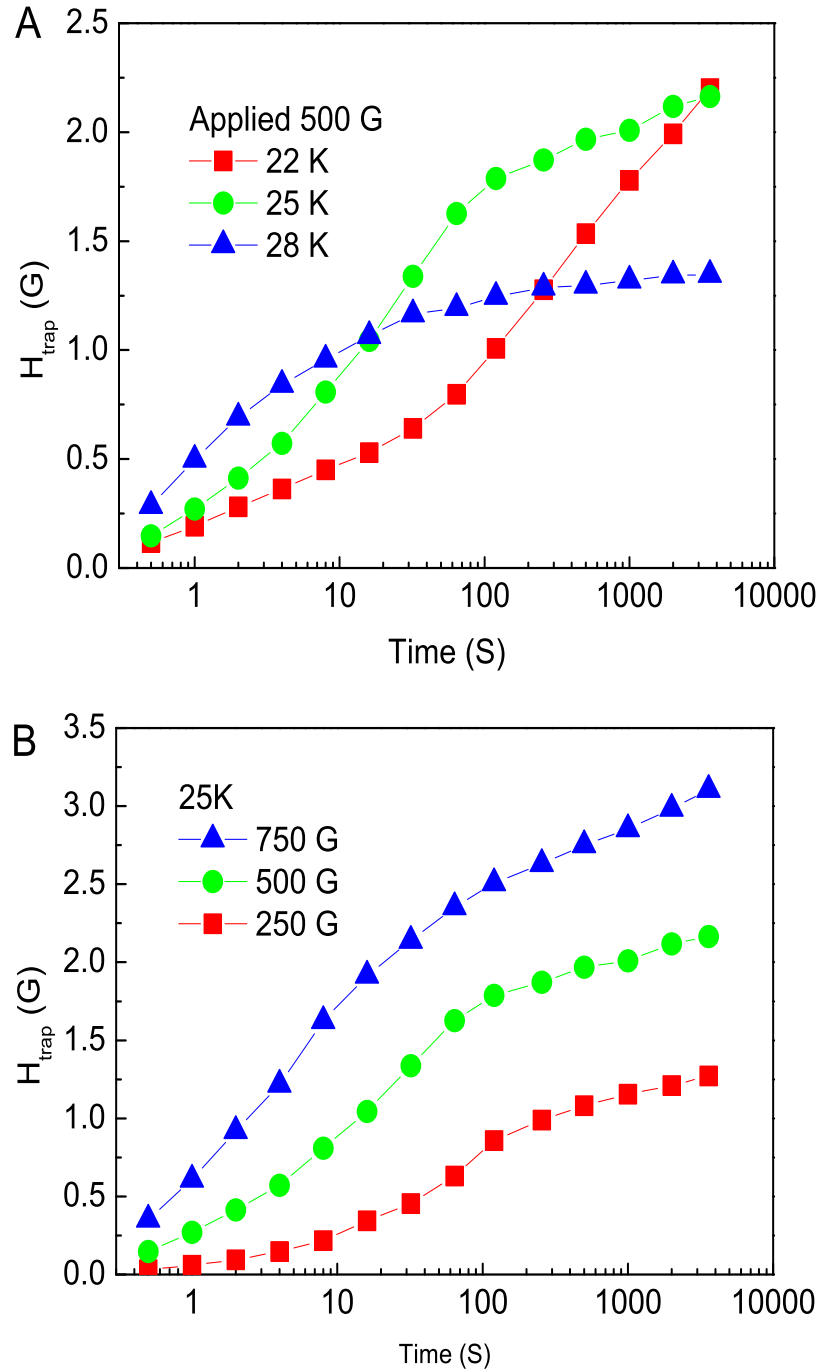


Figure 4.3: Vortex penetration curves of the $Bi_2Sr_2CaCu_2O_{8+x}$ single crystal. (A) The penetration curves measured under the same applied magnetic field $H_a = 500$ G, but at different temperatures $T = 22$ K, 25 K, 28 K respectively. (B) The penetration curves measured under the same temperature $T=25$ K, but at different applied magnetic field $H_a = 250$ G, 500 G, 750 G respectively.

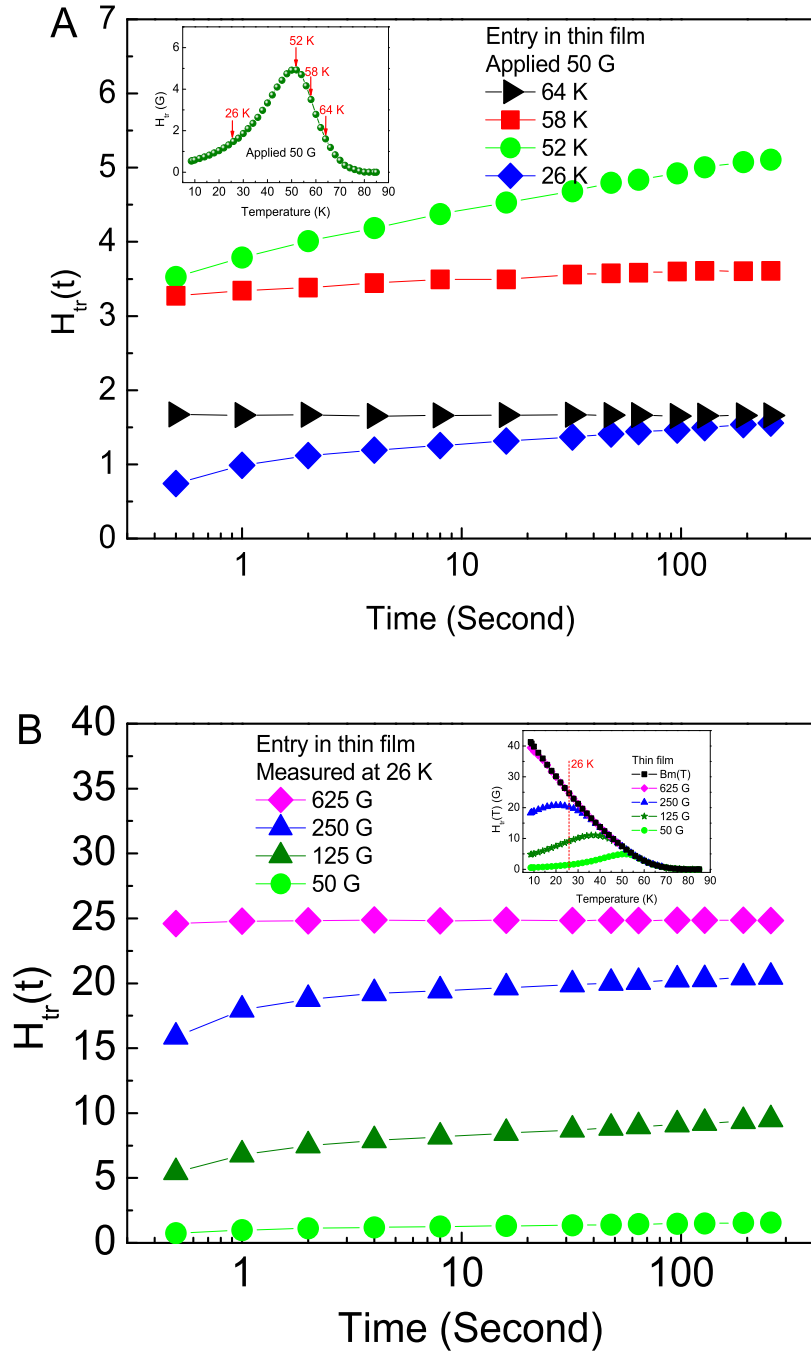


Figure 4.4: Vortex penetration curves of the $Bi_2Sr_2CaCu_2O_{8+x}$ thin film. (A) The penetration curves measured under the same applied magnetic field $H_a = 50$ G, but at different temperatures $T = 26$ K, 52 K, 58 K, 64 K respectively. The inset are the dependence of trapped field on temperature under a constant applied magnetic field. (B) The penetration curves measured under the same temperature $T = 26$ K, but at different applied magnetic field $H_a = 50$ G, 125 G, 250 G, 625 G respectively.

same temperature $T=25\text{K}$, but under different applied magnetic field $H_a = 250\text{G}$, 500G , 750G , respectively. Vortex penetration is very fast for the first few seconds and then slows down to approach the upper limit asymptotically. We plot the x-axis of the graph logarithmically to get a better view of the trend. Both figures show that the vortex penetration curves have a “concave” shape over the short duration part, which subsequently turns into a “convex” shape at some crossover time. As the sample goes to higher temperatures or higher applied fields, the crossover shifts to lower temperatures until finally it becomes unobservable.

The “concave” shape in the vortex penetration curves may be caused by the surface screening effect and the edge barriers [22]. Since the surface screening effect is strong at lower temperature, the vortex penetration speed $dB/d(\ln t)$ is reduced and results in the “concave” shape on the penetration curve. On the other hand, as stated in Ref.[16], the vortex close to a surface feels the Bean-Livingston forces, which decrease exponentially from the surface. The conclusion is that it is a short range force which only works at the initial stages of the vortex-penetration process where the vortex is close to the surface. As a vortex goes into the interior of the crystal, where $x \gg \lambda$ (λ is the penetration depth), the Bean-Livingston force drops and becomes negligible. This results in a fast increase in speed in the trapped field. The shape of the penetration curve is then changed into the “convex” shape of the longer duration part of the curve.

Since the surface screening effect weakens with increasing temperature, it allows the vortices to penetrate into the superconductor faster at higher temperatures, shifting the crossover to a shorter time. At a high enough temperature, the crossover is close to zero and finally becomes unobservable. The surface screening effect has an upper limit at a certain temperature. For a larger applied magnetic field, the vortices are subjected to a larger driving force and overcome the surface barrier. The penetration is then faster and the crossover appears over a shorter time interval. Therefore, when the applied field is large enough, the crossover will be shifted to a very short time interval and finally disappear.

Figure 4.4 shows the vortex penetration curves in a thin film sample. One can easily see that all the vortex penetration curves in our thin film sample are in the “convex” shape, and there is no “concave” shape. As discussed before, a concave vortex penetration curve is caused by the strong surface barriers to vortex motion. However, a thin film sample has a very small thickness (z -axis) and the surface barrier perpendicular to the z -axis is very small. If an external magnetic field is applied parallel to the z -axis of a thin film sample, the surface barrier is weak and the “concave” shape vortex penetration curves should not occur.

4.5 Conclusions

In summary, we found that the vortex-penetration process in BSCCO superconductors is time dependent and strongly related to the edge barrier of the sample. Since the physics revealed in our measurements are not restricted to the specified microstructure of BSCCO superconductors, the time dependent vortex-penetration process is suggested to be a general physical property of the system, which should be observable in other superconductors.

Bibliography

- [1] P. G. de Gennes, Sol. St. Comm. **3**, 127 (1965).
- [2] L. Kramer, Phys. Rev. **170**, 475 (1968).
- [3] Ryuzo Kato, Yoshihisa Enomoto, Sadamichi Maekawa, Phys. Rev. B **47**, 8016 (1993).
- [4] Carlos Bolech, Gustavo C. Buscaglia, and A. Lopez, Phys. Rev. B **52**, R15719 (1995).
- [5] E. Zeldov et al., Phys. Rev. Lett. **73**, 1428 (1994).
- [6] A. A. Abrikosov, Soviet Phys. JETP **5**, 1174 (1957).
- [7] W. H. Kleiner, L. M. Roth and S. H. Autler, Phys. Rev. **133**, A1226 (1964).
- [8] D. Gribier, B. Jacrot, Rao L. Madhav and B. Farnoux, Phys. Lett. **9**, 106 (1964).
- [9] G. Sarma, Compt. Rend. Acnd. Sci. Paris **258**, 1461 (1964).
- [10] U. Essmann and H. Trauble, Sci. Am. **224**, 75 (1971).
- [11] P. L. Gammel, D. J. Bishop, G. J. Dolan, J. R. Kwo, C. A. Murray, L. F. Schneemeyer, and J. V. Waszczak, Phys. Rev. Lett. **59**, 2592 (1987).
- [12] C. A. Murray, P. L. Gammel, and D. J. Bishop, Phys. Rev. Lett. **64**, 2312 (1990).
- [13] F. London, Superfluids (John Wiley and Sons, New York, 1950), p.152.

- [14] L. Onsager, Proceeding of the International Conference on Theoretical Physics, Kyoto and Tokyo, 1954), pp. 935-936.
- [15] S. Bascom, Jr. Deaver, William M. Fairbank, Phys. Rev. Lett. **7**, 43 (1961).
- [16] C. P. Bean, J. D. Livingston, Phys. Rev. Lett. **12**, 14 (1964).
- [17] R. W. De Blois, W. De Sorbo, Phys. Rev. Lett. **12**, 499 (1964).
- [18] G. Blatter, M. V. Feigel'man, V. B. Geshkenbein, A. I. Larkin, V. M. Vinokur, Rev. Mod. Phys. **66**, 1125 (1994).
- [19] John Bardeen, M. J. Stephen, Phys. Rev. **140**, A1197 (1965).
- [20] A. S. Joseph, W. J. Toasch, Phys. Rev. Lett. **12**, 219 (1964).
- [21] W. Meissner and R. Ochsenfeld, Naturwissenschaften **21**, 787 (1933).
- [22] A. A. F. Olsen, H. Hauglin, T.H. Johansen, P.E. Goa, D. Shantsev, Physica C **408-410**, 537 (2004).
- [23] A. B. Pippard, Philos. Mag. **19**, 217 (1969).
- [24] L. Burlachkov, Phys. Rev. B **47**, 8056 (1993).
- [25] S. T. Weir, W. J. Nellis, Y. Dalichaouch, B. W. Lee, M. B. Maple, J. Z. Liu, R. N. Shelton, Phys. Rev. B **43**, 3034 (1991).
- [26] N. Chikumoto, M. Konczykowski, N. Motohira, A. P. Malozemoff, Phys. Rev. Lett. **69**, 1260 (1992).
- [27] Ryoko Sugano, Toshiyuki Onogi, Kazuto Hirata, Masashi Tachiki, Physica B **284-288**, 803 (2000).
- [28] R. Sugano, T. Onogi, K. Hirata, and M. Tachiki, Phys. Rev. Lett. **80**, 2952 (1998).
- [29] Thierry Giamarchi and Pierre Le Doussal, Phys. Rev. Lett. **72**, 1530 (1994).

- [30] H. Kupfer, A. Will, R. Meier-Hirmer, Th. Wolf, and A. A. Zhukov, Phys. Rev. B **63**, 214521 (2001).
- [31] Michel J. P. Gingras and David A. Huse, Phys. Rev. B **53**, 15139 (1996).
- [32] Alexis P. Malozemoff and Matthew P. A. Fisher, Phys. Rev. B **42**, 6784 (1990).
- [33] Thomas Nattermann, Phys. Rev. Lett. **64**, 2454 (1990).

Chapter 5

Persistent Supercurrents and Vortex Dynamics in a Ring-shaped $\text{Bi}_2\text{Sr}_2\text{CaCu}_2\text{O}_x$ Single Crystal

A superconducting ring offers a unique possibility to investigate the interaction between the magnetic vortices trapped in the ring's bulk and the persistent currents circulating around the ring [1] and, consequently, the nature of the vortex structure and its pinning in the presence of the persistent current. This allows one to obtain useful information about the persistent current relaxations [2] and the value of the exponent μ , a parameter in the scaling relation between the effective energy barrier against vortex motion U_{eff} and the persistent current density J .

In this chapter, we measure the persistent current relaxations in the ring-shaped single crystals of $\text{Bi}_2\text{Sr}_2\text{CaCu}_2\text{O}_x$ and study the changes in the vortex structure with an increasing concentration of oxygen vacancies obtained through vacuum annealing.

5.1 Introduction

Applications of the magneto-transport properties of superconductors require the knowledge of the interaction between the persistent current flowing through a supercon-

ductor and the magnetic vortices trapped in its bulk [2]. This interaction modifies the vortex pinning potential U_{eff} and causes the decay of the persistent current. In general, the dependence of U_{eff} on the current density J is described by the power-law dependence [3], i.e. $U_{eff}(J) \propto (J_c/J)^\mu$, where J_c is the critical current density. The values of the exponent μ in this equation, which depend on the type of the vortex structure involved, have been provided by theories of vortex pinning [3]. Unfortunately, the magnetization measurements which give useful insight into the dependence of the vortex phases on magnetic field and temperature (i.e., the H-T phase diagrams) [2, 4, 5, 6, 7, 8], do not provide direct information about the relationship between the vortex pinning and the persistent current. This information has not been obtained either by measurement of the relaxation (time dependence) of the magnetization [2] or by Bean's critical state model [9, 10] applied to the spatial distribution of magnetization, which have been otherwise implemented successfully to study the vortex pinning and the corresponding vortex-density gradients in a superconducting sample.

In fact one should consider the possibility of investigating the interaction between persistent currents and vortices using ring-shaped superconducting samples [1]. This is because an external magnetic field $H \geq H_{c1}$ applied to the superconducting ring in a direction along the ring's axis, and subsequently turned off, generates the persistent current circulating around the ring in addition to the magnetic vortices trapped in the ring's bulk [11]. The advantage of the ring geometry is that the induced persistent current exerts a Lorentz force on the vortices driving them out of the ring uniformly in the radial directions. Consequently, this causes the dissipation of the persistent current. By applying and switching off larger external magnetic fields one could produce persistent currents at the critical level. Magnetic field trapped at the ring's center is proportional to the critical current density according to the Biot-Savart law. The magnitude of this field and its decay could be measured with a magnetic field sensor, such as a Hall sensor.

The ring-shaped samples and the technique described above have been employed

by us to investigate the motion (and pinning) of the vortices subjected to the Lorentz force applied by the persistent current, and the resulting relaxation (time decay) of the persistent current in high purity single crystals of $\text{Bi}_2\text{Sr}_2\text{CaCu}_2\text{O}_8$ (BSCCO). BSCCO is a highly anisotropic cuprate with two vortex regimes [12, 13, 14, 15], at temperatures below and above the crossover temperature $T^* = 36$ K. Each of these regimes has a different vortex dynamics and pinning mechanism [16, 17, 18, 19, 20, 21]. We have tested this system in order to obtain information on the effective energy barrier against the motion of vortices U_{eff} in the ring-shaped as-grown BSCCO crystal, and its dependence on the persistent current density, as well as its dependence on temperature in low and high temperature ranges. An effective approach that could be applied to clarify the differences in the vortex dynamics at temperatures below and above T^* is to change the sample's microstructure by reducing oxygen content in the system [8] and, consequently, T_c using successive vacuum annealings at high temperatures. The measurements of the persistent current and its relaxation performed on the annealed ring-shaped BSCCO crystal have shown that a small reduction of the oxygen content (which causes a large drop of the persistent current density to a very low value) leads to dramatic changes in the vortex lattice at temperatures above T^* , but leaves the vortex structures almost intact at temperatures below T^* .

5.2 Temperature Dependence of the Persistent Current Density

The $\text{Bi}_2\text{Sr}_2\text{CaCu}_2\text{O}_{8+x}$ single crystal ring shaped samples were prepared as detailed in Chapter 2.

The measurements of the temperature dependence of the persistent current density J_m close to the critical state in the ring-shaped as-grown BSCCO crystal shows a very sharp drop of J_m with increasing temperature at low temperatures below $T^* = 36$ K (see Figure 4.1). At temperatures above T^* J_m decreases slowly with increasing temperature. T^* has been interpreted before as the 2D to 3D crossover temperature

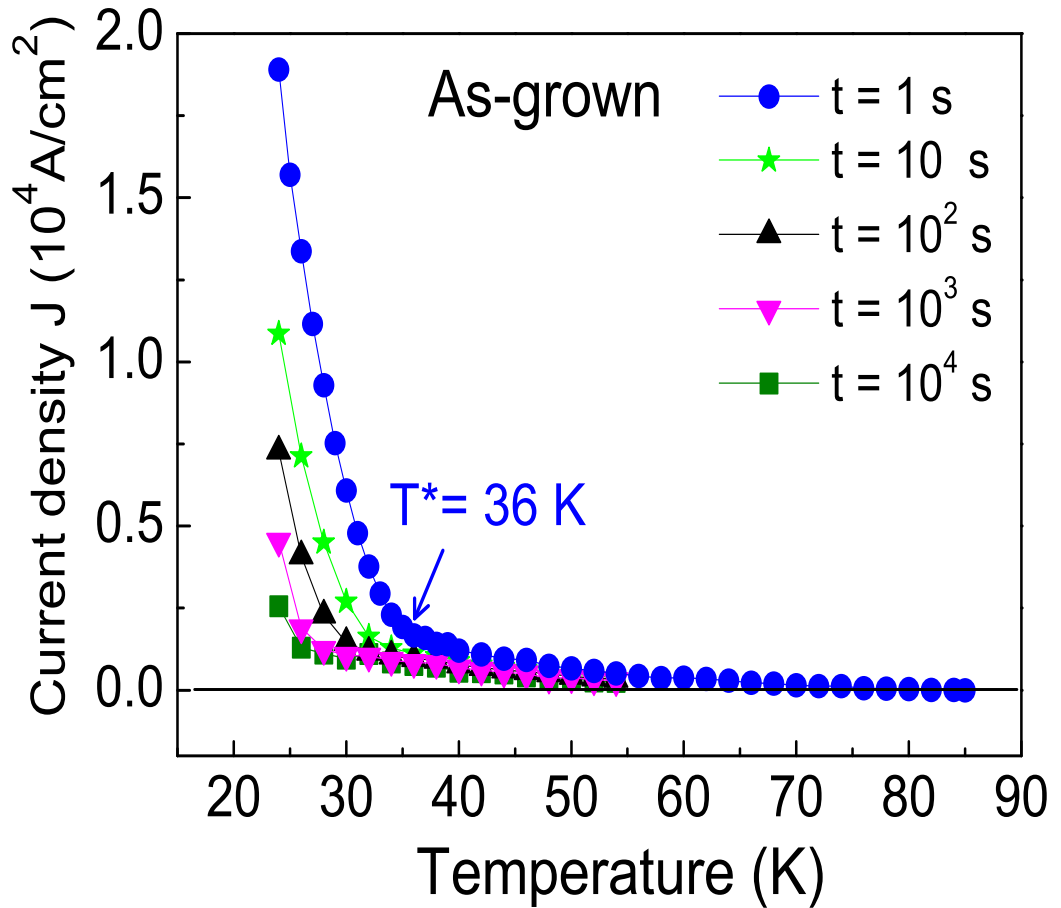


Figure 5.1: The dependence of the persistent current density $J(T)$ on temperature measured in as-grown BSCCO (sample A0) between 1s and 10^4 s after the critical state was established. For $J_m(T)$ recorded after 1s the data could be fitted with the equations $J_m = (2.5 \times 10^5 A/cm^2)[1 - T/(46.7K)]^{3.7}$ and $J_m = (4.2 \times 10^3 A/cm^2)[1 - T/(92K)]^2$ below and above 36 K, respectively.

[15], the 0D to 3D transition temperature [16, 17, 18] or as the temperature at which the pinning properties change [19, 20, 21]. Measurement of the time decays of the persistent current from the critical level confirms the latter, and shows indeed very fast decays of the persistent current at temperatures below T^* , in contrast to much slower ones at temperatures above T^* (see Figure 4.2). Figure 4.2 shows the temperature dependence of the persistent current J recorded at different times between 1 and 10^4 s after the critical state was established in the ring-shaped as-grown BSCCO crystal. After 10^4 s a giant reduction of the persistent current magnitude by almost 85-90% was detected at temperatures below T^* . This is in contrast to a much smaller drop of the persistent current by about 40% which was detected at temperatures above T^* .

The Lorentz force exerted by the persistent current on the vortices reduces the pinning energy barrier U_{eff} resulting in the vortex motion, consequently, large dissipation of the persistent current. Since the magnetic field B_{sf} trapped in the ring's center is directly proportional to the current density J_m according to the Biot-Savart law, the time decay of $B_{sf}(T, t)$ at a particular temperature should follow the same law as the time decay of $J_m(T, t)$.

5.3 Decay of Persistent Current

Figure 4.3 shows the decay of the persistent current from the critical current level, measured in the ring-shaped as-grown BSCCO crystal at several different temperatures below and above T^* . At temperatures below T^* the decays are non-logarithmic over a time period between 1 and 10^4 s; however, above T^* they become quasi-logarithmic. The super-fast non-logarithmic decays are in agreement with the general frameworks of the collective flux creep theory [22, 3] and the vortex-glass theory [23, 24]. These theories predict that the long-range order of the flux-line lattice could be destroyed by the random pinning centers but the short-range order still exists resulting in the collective pinning in a finite volume.

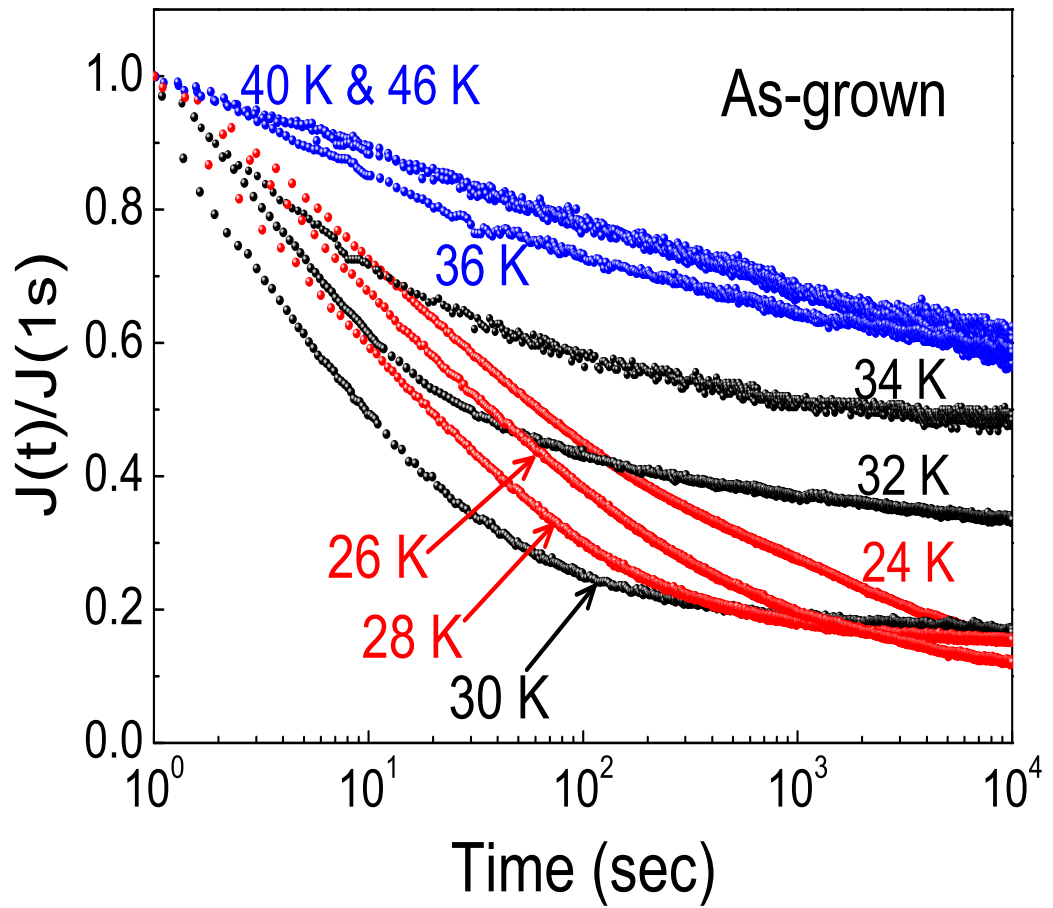


Figure 5.2: Dependence of the persistent current density on time measured at different temperatures between 24 and 46 K in the as-grown BSCCO (A0) crystal.

Table 5.1: Annealing conditions of the BSCCO crystal. μ_1 and μ_2 are the vortex critical exponents at temperatures below and above T^* , respectively.

Name	Environment	T(°C)	t(hours)	$\mu_1(\pm 0.01)$	$\mu_2(\pm 0.01)$
A0	As-grown	-	-	0.16	0.69
A1	Argon	300	2	0.16	0.53
A2	Vacuum	300	5	0.16	0.53
A3	Vacuum	357	2	0.14	0.52
A4	Vacuum	400	1	0.12	0.51
A5	Vacuum	450	1	0.18	0.35

5.4 Effective Energy Barrier

The persistent current decay rates dJ/dt have been used to calculate the dependence of the effective energy barrier against vortex motion $U_{eff}(J, T)$ on the persistent current density J over a time period between 1 and 10^4 seconds. The plot of $U_{eff}(J, T)$ versus J consists of multiple segments. Each segment is calculated at each temperature of the measurement from equation [25]: $U_{eff}(J, T) \simeq -kT\{\ln[|(dJ/dt)/J_m|] - C\}$, where J_m is the current density measured at 1s, k is Boltzmann's constant, and C is an adjustable constant. Normally, these segments do not form a continuous curve. In order to maintain "piecewise" continuity of this curve at all temperatures, the value of C was adjusted and U_{eff} was divided by a thermal factor $g(T) \leq 1$ which contains the temperature dependence of the superconducting parameters [26, 27]. Choosing the optimum value of $C = 20$ for all the segments causes them to fall on the same smooth curve. Curve A0 in Figure 4.3 represents the dependence of $U_{eff}(J) = U_{eff}(J, T)/g(T)$ for the ring-shaped as-grown BSCCO sample. It indicates that the dependence of the effective energy barrier on J could be described by the power-law, i.e. $U_{eff}(J) \propto (J_c/J)^\mu$ with $\mu_1 \simeq 1/7$ and $\mu_2 \simeq 2/3$ below T^* (high currents) and above T^* (low currents), respectively.

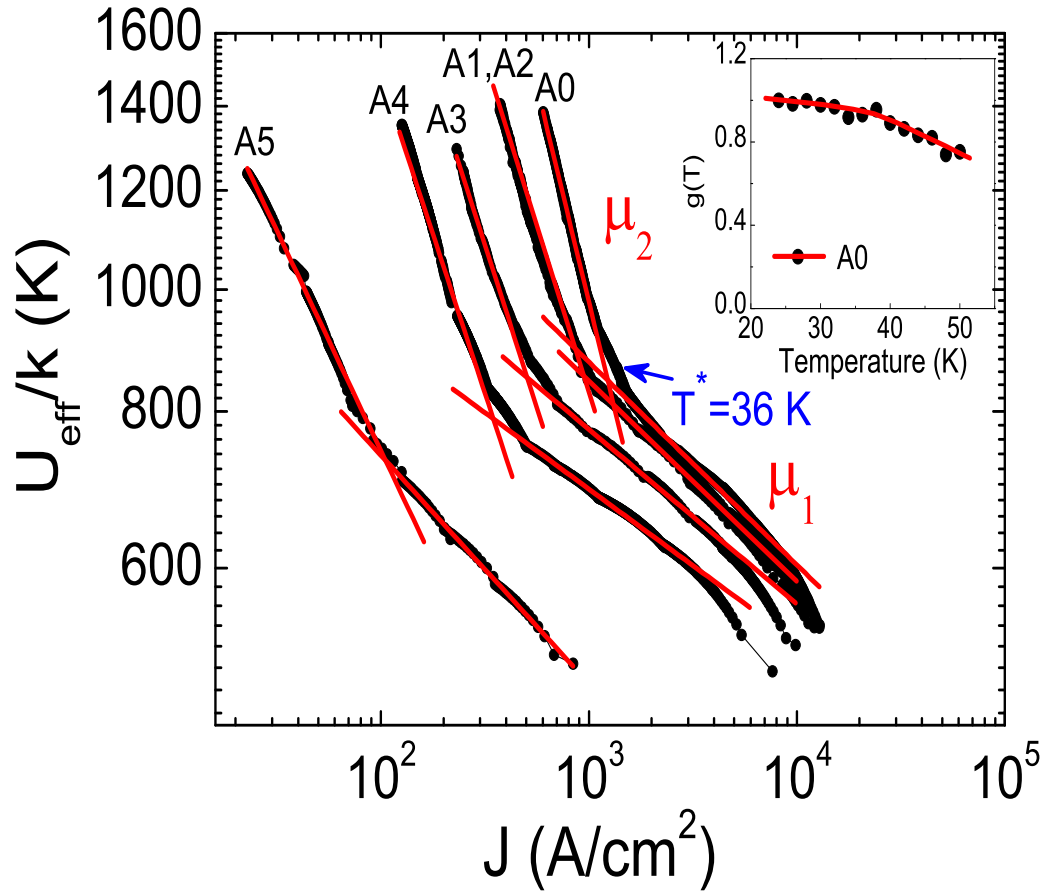


Figure 5.3: The effective energy barrier $U_{eff}(J)$ as a function of the persistent current density J calculated for the as-grown and vacuum annealed BSCCO crystal. The suppression of the current density J_m due to annealing is responsible for the shift of $U_{eff}(J)$ to low current density. The values of the critical exponents $\mu_{1,2}$ are shown in Table 4.1. The inset: Typical curve of the thermal factor $g(T)$ as a function of temperature.

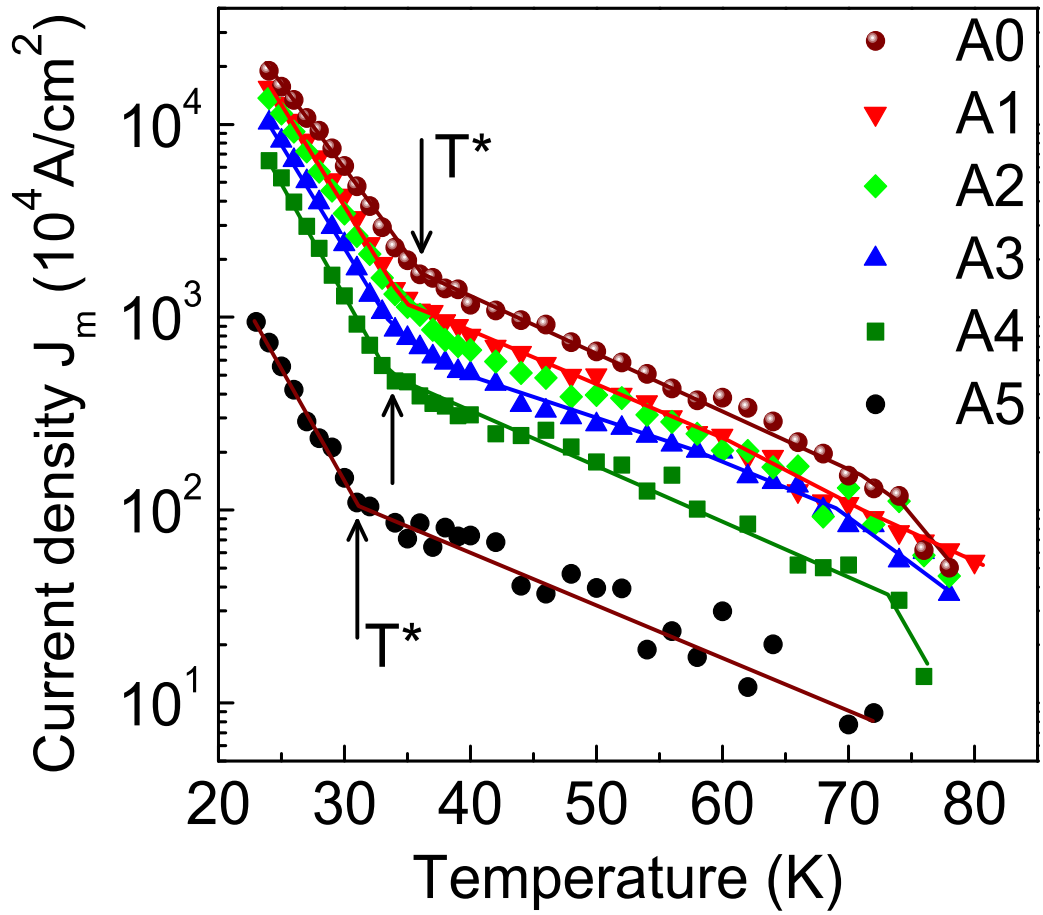


Figure 5.4: Dependence of the persistent current density on temperature 1s after the critical state was established, measured for as-grown and vacuum annealed BSCCO single crystal (Solid lines are guides to the eye).

5.5 Effects of Oxygen

The most interesting results have been obtained for the ring-shaped BSCCO crystal annealed in vacuum at temperatures between 300 and 450 °C. Table 1 summarizes the annealing environment, the annealing time and temperature. Vacuum annealing removes the oxygen from the crystal and subsequently reduces the current density J_m and T_c . After all vacuum annealings, the absolute value of J_m drops by more than 95% (see Figure 4.4), which is associated with a decrease of T_c and T^* by only 5 K. The temperature dependence of J_m , as well as the dependence of J on time are not affected by the vacuum annealing.

Critical exponents $\mu_{1,2}$ obtained from the dependence of U_{eff} on the current density J after each annealing step (see Table 1), show interesting behavior. The change in the microstructure has little effect on the vortex dynamics at temperatures below T^* , where μ_1 fluctuates around the value of $1/7$. On the other hand, at temperatures above T^* the vortex dynamics is strongly affected by the microstructure, where μ_2 displays a monotonic decrease from ~ 0.7 to 0.35 , as the current density drops from a high to a very low value.

According to some collective pinning theories exponent $\mu_1 = 1/7$ has been thought of as a parameter that characterizes the single vortex pinning regime in which the vortices are pinned individually [2, 22]. The experimental value of this exponent changes little with a decreasing oxygen content (an increasing disorder, and a decreasing current density from high to very low values). This result is puzzling. The independence of μ_1 on the microstructure suggests a highly cooperative effect [29] in the vortex structure at temperatures below T^* .

At temperatures above T^* , in the high current density limit, exponent μ_2 is 0.7 in an as-grown ring-shaped BSCCO crystal. This number suggests that the vortices are in the low density limit, i.e., they are far enough apart that bulges can occur in single vortices (or possibly single vortex bundles)[2], and $\mu = (6 - d)/4$. For $d = 3$ (vortices with kinks [28]) $\mu = 3/4$. After all thermal annealings the sample's current density is small, and μ_2 drops to $0.35 \sim 1/3$. By analogy with the Bose glass picture [2] μ

$= 1/3$ has been attributed to the situation where the vortex lines start to wander individually but with the superposition of a random pinning potential and a weak periodic potential reflecting short-range order.

5.6 Conclusions

In summary, the temperature dependence of the persistent current and its dissipation rate due to its interaction with magnetic vortices was investigated in a pure ring-shaped BSCCO single crystal whose microstructure (oxygen content) has been changed by vacuum annealing. This allowed us to obtain information on the value of exponent μ , a parameter showing the dependence of the energy barrier against vortex motion $U_{eff}(J) \propto (J_c/J)^\mu$ and the persistent current density J . Temperature dependence of the persistent current relaxations revealed a crossover in the dissipation rate from a strongly non-logarithmic regime at temperatures below T^* to a logarithmic one at temperatures above T^* . In the former regime the vortex dynamics is governed by the energy barrier $U_{eff}(J)$ with $\mu \simeq 1/7$ which depends little on changes in the microstructure, suggesting highly cooperative effects in the vortex structure. In the latter regime, on the other hand, μ is strongly dependent on the microstructure, with its value dropping from 0.7 in an as-grown crystal down to 0.35 in a disordered crystal.

Bibliography

- [1] J. Jung, K. H. Chow, M. Egilmez, and A. Welsh, Appl. Phys. Lett. **87**, 262506 (2005).
- [2] G. Blatter, M. V. Feigel'man, V. B. Geshkenbein, A. I. Larkin, V. M. Vinokur, Rev. Mod. Phys. **66**, 1125 (1994).
- [3] M. V. Feigel'man, V. B. Geshkenbein, A. I. Larkin, and V. M. Vinokur, Phys. Rev. Lett. **63**, 2303 (1989).
- [4] H. Beidenkopf, N. Avraham, Y. Myasoedov, H. Shtrikman, E. Zeldov, B. Rosenstein, E. H. Brandt, and T. Tamegai, Phys. Rev. Lett. **95**, 257004 (2005).
- [5] M. Liu, Y. W. He, W. J. Wu, and Y. H. Yang, Phys. Rev. B **71**, 224508 (2005).
- [6] Sandeep Tyagi and Yadin Y. Goldschmidt, Phys. Rev. B **70**, 024501 (2004).
- [7] C. J. Olson, G. T. Zimanyi, A. B. Kolton, and N. Gronbech-Jensen, Phys. Rev. Lett. **85**, 5416 (2000).
- [8] D. Darminto, M. O. Tjia, T. Motohashi, H. Kobayashi, Y. Nakayama, J. Shimoyama, and K. Kishio, Phys. Rev. B **62**, 6649 (2000).
- [9] C. P. Bean, Phys. Rev. Lett. **8**, 250 (1962).
- [10] C. P. Bean, Rev. Mod. Phys. **36**, 31 (1994).
- [11] M. Tinkham, Introduction to Superconductivity, 2nd edition, McGraw-Hill, Inc., USA (1996).

- [12] A. Houghton, R. A. Pelcovits, and A. Sudbo, Phys. Rev. B **40**, 6763 (1989).
- [13] L. I. Glazman, A. E. Koshelev, Phys. Rev. B **43**, 2835 (1991).
- [14] D. S. Fisher, Matthew P. A. Fisher and David A. Huse, Phys. Rev. B **43**, 130 (1991).
- [15] P. L. Gammel, L. F. Schneemeyer, J. V. Wasczak, and D. J. Bishop, Phys. Rev. Lett. **61**, 1666 (1988).
- [16] A. Piriou, Y. Fasano, E. Giannini, and O. Fischer, Phys. Rev. B **77**, 184508 (2008).
- [17] V. F. Correa, J. A. Herbsommer, E. E. Kaul, F. de la Cruz, and G. Nieva, Phys. Rev. B **63**, 092502 (2001).
- [18] M. F. Goffman, J. A. Herbsommer, F. de la Cruz, T. W. Li and P. H. Kes, Phys. Rev. B **57**, 3663 (1998).
- [19] T. Verdene, H. Beidenkopf, Y. Myasoedov, H. Shtrikman, M. Rappaport, E. Zeldov, and T. Tamegai, Phys. Rev. Lett. **101**, 157003 (2008).
- [20] Yadin Y. Goldschmidt and Jin-Tao Liu, Phys. Rev. B **76**, 174508 (2007).
- [21] Yadin Y. Goldschmidt and Eduardo Cuansing, Phys. Rev. Lett. **95**, 177004 (2005).
- [22] M. V. Feigel'man, V. B. Geshkenbein and V. M. Vinokur, Phys. Rev. B **43**, 6263 (1991).
- [23] M. P. A. Fisher, Phys. Rev. Lett. **62**, 1415 (1989).
- [24] D. R. Nelson and V. M. Vinokur, Phys. Rev. Lett. **68**, 2398 (1992); Phys. Rev. B **48**, 13060 (1993).
- [25] M. P. Maley and J. O. Willis, Phys. Rev. B **42**, 2639 (1990).

- [26] J. R. Thompson, L. Krusin-Elbaum, L. Civale, G. Blatter, and C. Feild, Phys. Rev. Lett. **78**, 3181 (1997).
- [27] C. J. van der Beek, P. H. Kes, M. P. Maley, M. J. V. Menken and A. A. Menovsky, Physica C **195**, 307 (1992).
- [28] A. Engel and H. J. Trodahl, Phys. Rev. B **66**, 184505 (2002).
- [29] J. C. Phillips, Private communication. Activation Energies of Vortex Glasses and Liquids in Strongly Disordered Superconductors.

Chapter 6

Depinning-induced Transition in Bi-2212 Superconductors

The vortex phase diagram below the vortex melting line of BSCCO superconductors is currently not clear [1, 2]. Vortex depinning transition, 2D-3D crossover, and magnetic relaxations need more investigation. Important information can be found by studying the temperature dependence of the trapped vortex field at temperatures below the saturation line. In this chapter, we investigate the temperature and magnetic field dependence of vortex pinning and its relaxation in $Bi_2Sr_2CaCu_2O_{8+x}$ (BSCCO) single crystal and thin film superconductors.

6.1 Introduction

The lower critical field, $H_{c1}(T)$, and the upper critical field, $H_{c2}(T)$, of type-II superconductors are well-defined functions of temperature, T , and external magnetic field, H . The magnetic phase diagram [1] is commonly plotted as H vs. T . For the BSCCO superconductor [2], the magnetic phase diagram reveals two phases at high fields ($>400\text{Oe}$): a glassy phase at low temperatures (albeit with a pronounced 2D character) with a second order glass transition to a high temperature liquid phase at about 35K. At low fields ($<400\text{Oe}$), there is a Bragg glass (probably 3D) at low

temperatures with a second order glass transition to an ordered crystalline phase at 35-40K and finally a first order melting transition to a liquid at high temperatures. Physically, this magnetic phase diagram represents the vortex structure inside the superconductor, that is, the internal magnetic field. The detailed vortex structure of mixed state is determined by the flux pinning, the external magnetic field and the temperature. Furthermore, according to Bean's critical state model [3], the internal magnetic field in the low T and low H region is not uniform and the local value of H is a strongly varying function of position inside the superconductor even though the external magnetic field is uniform. Therefore, the conventional magnetic phase diagram cannot give proper information about the vortex system by referring to the external magnetic field.

In fact, one should consider the possibility of investigating the trapped magnetic field inside a superconductor. The approach that we use in this thesis is as follows: apply a constant external magnetic field, H_a , to a superconductor at different temperatures, resulting in penetration of the vortices into the bulk of the superconductor. We then reduce H_a to zero and the vortex field trapped in the sample is detected by a Hall probe sensor. At or close to the melting field [4] $B_m(T)$, the superconductor is fully penetrated and the internal magnetic field is expected to be constant over the entire sample volume. Therefore, the vortex structure close to the melting field can be well represented by the measurement of the trapped magnetic field. At a fixed temperature, the trapped magnetic field increases with increasing external magnetic field and finally reaches a saturated value, which corresponds (not equals) to the melting field $B_m(T)$ (external field). Similar to the name "melting line", we will refer to the series of the saturated trapped fields as "saturation line". As the trapped field is monitored as a function of temperature, the behavior of the vortex lattice can be inferred.

Since H_{c1} decreases with increasing temperature, the surface screening effect becomes weak [5], allowing more vortices to enter the bulk of the superconductor [6]. The shear modulus of the vortex lattice $c_{66} \approx (\Phi_0 B)/(\pi\lambda)$, where Φ_0 is the flux

quantum and B is the magnetic field, also decreases with increasing temperature due to an upturn in the penetration depth λ [1]. Consequently, the vortex lines become flexible which allows some parts of the individual flux lines to deviate from an ideal periodic arrangement of the Abrikosov lattice. The vortex lines can then lower their energy by passing through favorable random pinning sites, resulting in more effective pinning. Therefore, one might expect the trapped magnetic field to increase with increasing temperature, eventually reaching a maximum at the saturation line. Some theories suggest that the layer/vortex decoupling transition [7] or vortex depinning transition [8, 9] appears in the pancake-vortex lattice of layered superconductors, such as $Bi_2Sr_2CaCu_2O_{8+x}$ (BSCCO) superconductors, a few degrees below the saturation line. Unfortunately the experiments have not confirmed explicitly these theoretical suggestions, i.e., what happens to the vortex lattice and its pinning at temperatures just below the saturation line? Does the pinning of the vortex-lattice decrease abruptly at the saturation line or does this process occur gradually when the temperature approaches T_m ?

In order to answer these questions, we performed the experiments outlined above on BSCCO crystals and films. A constant magnetic field was applied to the samples at a fixed temperature and subsequently removed after a time interval t^* . This was followed by measurement of the trapped field. The results of these studies revealed a peak in the temperature dependence of the trapped vortex field at temperatures a few degrees below the saturation line. We attribute the peak to the presence of the vortex depinning transition.

6.2 Phase Diagram

The $Bi_2Sr_2CaCu_2O_{8+x}$ single crystal and thin film samples with geometric shape of disks and rings were prepared as detailed in Chapter 2.

The solid lines in Figures 5.1(a) and 5.2(a) show the “saturation line” $H_m(T)$, i.e., the temperature dependence of the maximum field that could be trapped in a sample

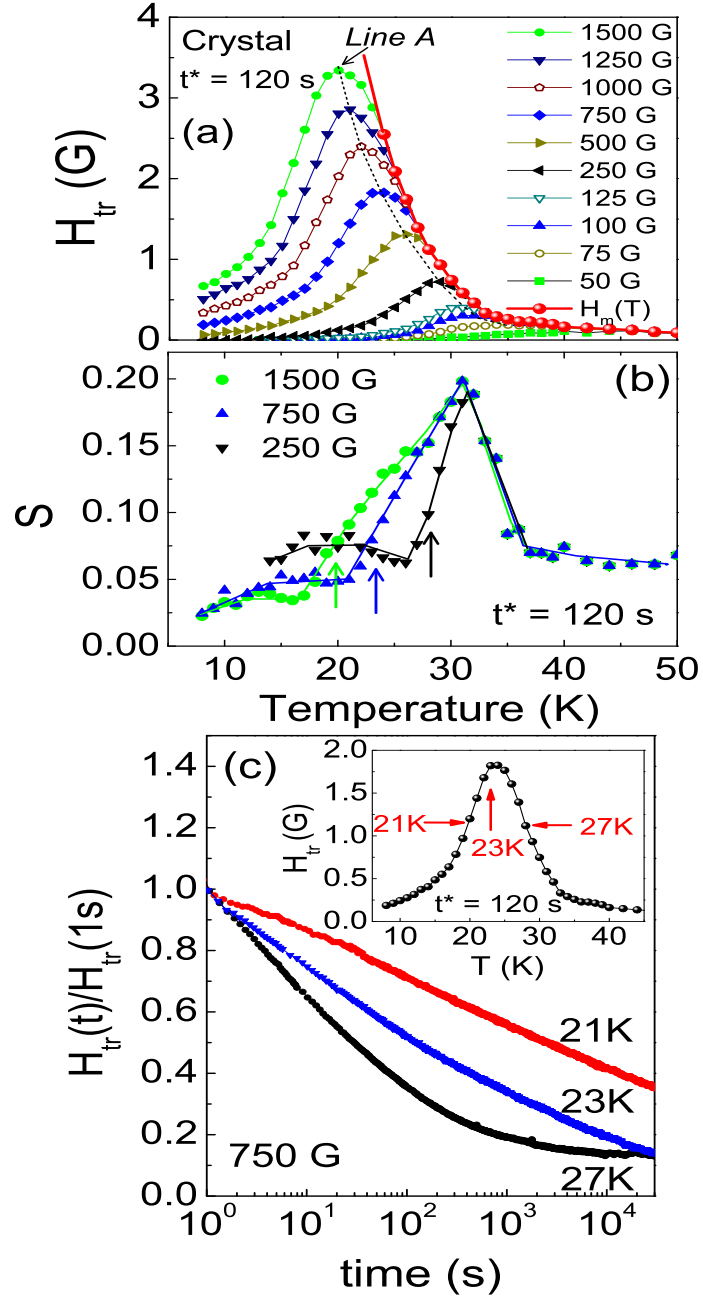


Figure 6.1: (a) Temperature dependence of the field trapped in the BSCCO single crystal by applying different constant magnetic fields between 50 and 1500 G during a time interval t^* of 120 s. $H_m(T)$ represents the temperature dependence of the saturation line. Line A joins the maxima of the trapped field. (b) Temperature dependence of the logarithmic decay rates $S = d(\ln H_{tr})/d(\ln t)$ of the trapped field calculated for a short initial time intervals up to 10-20 s. The arrows indicate temperatures of the maxima in the trapped field. (c) Dependence of the field trapped in the BSCCO crystal on time measured at different temperatures around the trapped field maximum.

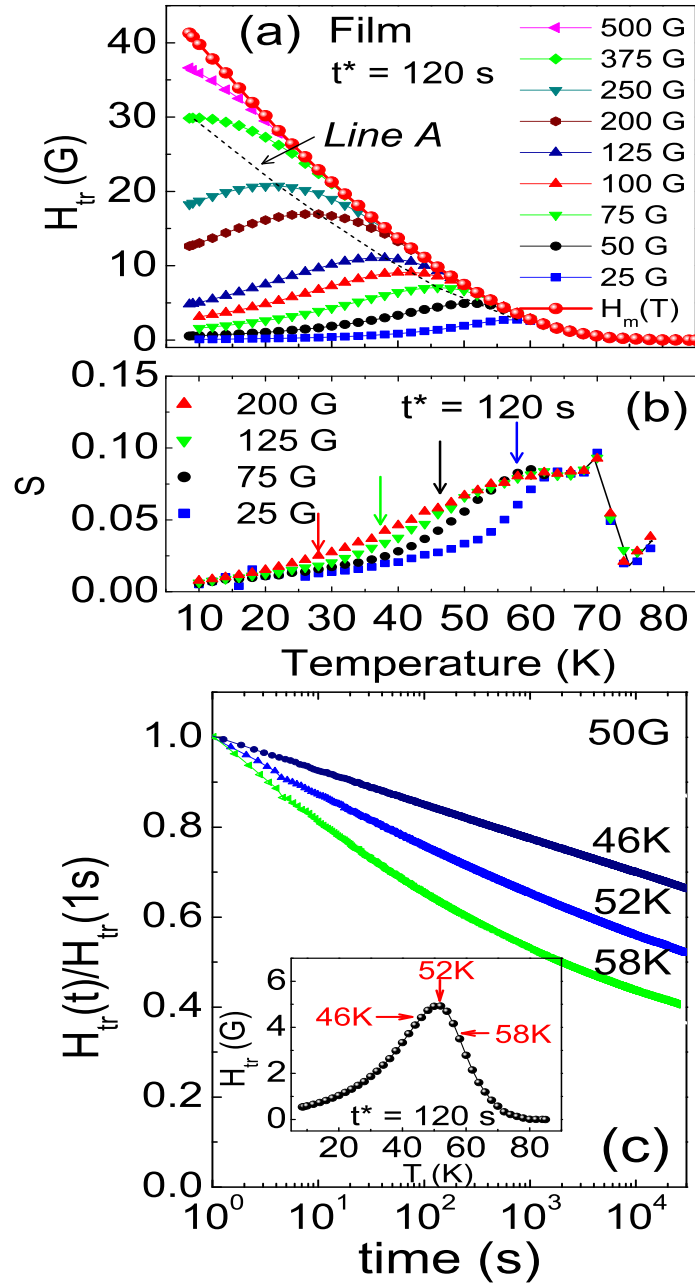


Figure 6.2: (a) Temperature dependence of the field trapped in a BSCCO thin film by applying magnetic fields between 25 and 500 G during a time interval t^* of 120 s. $H_m(T)$ represents the temperature dependence of the saturation line. Line A joins the maxima of the trapped field. (b) Temperature dependence of the logarithmic decay rates $S = d(\ln H_{tr})/d(\ln t)$ of the trapped field calculated for short initial time intervals up to 10-20 s. The arrows indicate temperatures of the maxima in the trapped field. (c) Dependence of the field trapped in the BSCCO film on time measured at different temperatures around the trapped field maximum.

at each temperature, for a crystal and film respectively. Also shown in the figures is the temperature dependence of the trapped field obtained by applying a constant magnetic field to the sample for a fixed time interval, t^* . The temperature dependence of the trapped field H_{tr} , after the magnetic field is applied and subsequently removed, exhibits a maximum at temperatures close to the saturation line. At higher temperatures the trapped fields merge with those at the saturation line. The dashed curves join the maxima of the trapped field. It marks the temperatures above which the pinning of the vortices becomes weak. The maxima of the trapped field follow this curve as the applied field or the time interval t^* increase. The temperature dependence of the trapped field and its maximum at temperatures below the saturation line have been observed to be qualitatively similar for single crystal and thin film disk-shaped samples. We have also found similar effects in single crystals of different geometry, such as in disk and ring-shaped crystals.

6.3 Decay Rates

In a ring, vortices are trapped in the bulk as well as in the ring's inner hole after the external applied field is turned off. In order to maintain the flux trapped in the ring's center, a persistent current circulating around the ring's inner hole must be induced. In this case a Hall sensor measures the magnetic field generated by both the persistent current and the bulk vortices. The persistent current exerts a Lorentz force on the vortices causing them to move in the radial directions out of the ring. This dissipates the current. Therefore, the time decay of the magnitude of the persistent current is directly related to the pinning of the bulk vortices. In a disk, there is no circulating persistent current and only the pinned vortices contribute to the trapped field.

Measurements of the decay of the trapped field H_{tr} , over a time interval of about 3×10^4 s, for all samples revealed that the decays are close to logarithmic only at temperatures below the peak in the temperature dependence of the trapped field (Figures

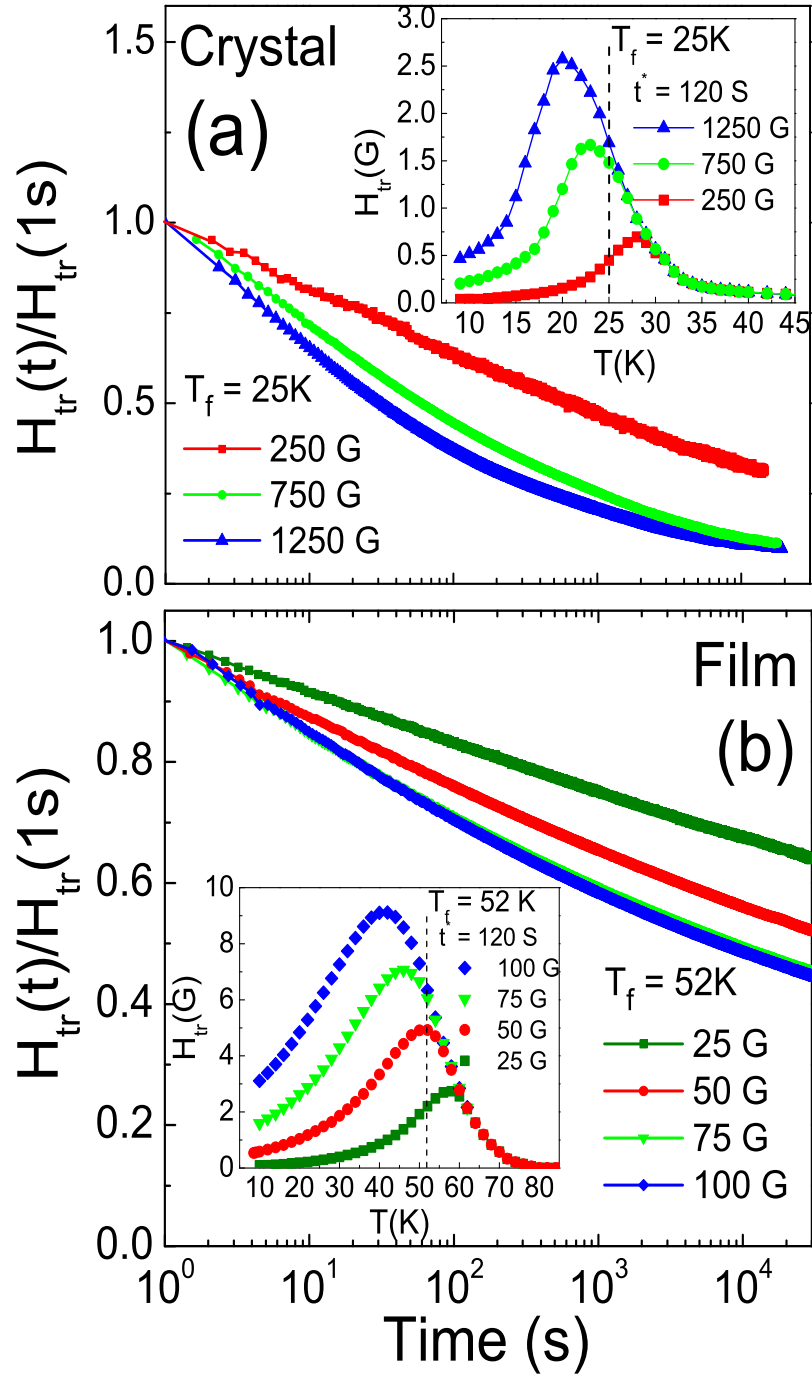


Figure 6.3: (a) Decays of the field trapped at a fixed temperature $T_f = 25$ K in the BSCCO crystal, after applying external fields of 250, 750 and 1250 G. (b) Decays of the field trapped at a fixed temperature $T_f = 52$ K in the BSCCO film, after applying external fields of 25, 50, 75 and 100 G. The insets show the dependence of the trapped field, obtained by applying different external fields, on temperature.

5.1(c) and 5.2(c)). (As discussed below, whether the decay is logarithmic or not provides information on the nature of the vortex interactions.) For temperatures at or above the peak, the decay curves start to deviate from the logarithmic behavior observed below the peak. The decay curves of H_m are also non-logarithmic. Because of the non-logarithmic character of the decay curves, we calculated the decay rates $S=d(\ln H_{tr})/d(\ln t)$ only for very short initial time intervals up to 10-20 s. The dependence of S on temperature for a crystal (S for a disk and a ring are similar) and thin film are shown in Figures 5.1(b) and 5.2(b).

In the following section we discuss possible reasons for our observations. As noted above, the amount of the field trapped inside a superconductor depends on temperature and applied magnetic field. The trapped field increases with increasing temperature reaching a maximum value at a temperature below the saturation line. The trapped field eventually merges with the saturation line at higher temperatures (see Figures 5.1(a) and 5.2(a)). As mentioned before, this behavior is accompanied by changes in the temperature dependence of the relaxation rates (decay rates) of the trapped field, i.e., the maximum in the trapped field separates the low temperature region where the decay rates are logarithmic from the high temperature region where they are non-logarithmic. This property was found to be independent of the sample geometry, i.e., the disk or the ring, and the same for both the single crystal and thin film samples. However, the temperature dependence of the normalized logarithmic decay rates S calculated for the first 10-20 s of decay of the trapped field in a single crystal differs from that obtained for a thin film (see Figures 5.1(b) and 5.2(b)). Particularly, at temperatures below the peak in the $H_{tr}(T)$ diagram, S is approximately constant for the crystal. This behavior has not been observed in the film, where S was found to increase more gradually with temperature.

The observed dependence of the trapped field on temperature could be the result of the interplay between the surface and bulk pinning of the vortices [10, 11, 12]. The effects of surface barriers [3] and geometrical barrier [13, 14, 15, 16] play a dominant role in determining the vortex dynamics in BSCCO single crystals at elevated

temperatures [2]. The saturation line at high temperatures appears to represent a simultaneous melting and decoupling of pancake vortices. The small S value at about 35 K indicates that trapped vortices in this region could be dominated by the strong surface and geometrical barriers.

Our experiments show that the maxima in the trapped field in BSCCO crystals and BSCCO films occur at temperatures several degrees below the saturation line. The presence of the maxima suggests that the partial depinning of magnetic vortices [8, 9] occurs at temperatures above the maxima, leading to a gradual decrease of the trapped field with increasing temperature, which eventually merges with the saturation line. Line A in Figures 5.1(a) and 5.2(a), which joins the maxima of the trapped field, separates two different vortex pinning regimes. This agrees with the observation of two different dependences of the trapped field on time at temperatures below and above the maximum (see Figures 5.1(c) and 5.2(c)). Therefore, we believe that line A can be interpreted as the vortex depinning line. Calculation of the initial relaxation rates S (see Figures 5.1(b) and 5.2(b)) revealed that at temperatures below the maximum of the trapped field, S is substantially reduced.

Our results also show that there is a large difference between the properties of the film and those of the crystal (see Figures 5.1 and 5.2). The saturated field H_m and the 2D-3D crossover temperature T^* of the thin film is considerably higher than that of the crystal. This could be related to the sample purity, i.e., thin films contain more defects than crystals. The impurities in the thin film as well as the interface between the thin film and the substrate act as pinning centers, and consequently the thin film has a saturated field H_m which is higher than that of the crystal. The decay rates in the film are much smaller than those in the crystal, due to the stronger pinning in the film (see Figures 5.1(b) and 5.2(b)). This is consistent with the earlier observation [17] of an increase of the saturated field and of the T^* when artificial defects are introduced into BSCCO by proton irradiation. Figures 5.1(a) and 5.2(a) shows that line A follows the saturation line closely, which confirms that line A is the vortex depinning line, and not the decoupling line.

Table 6.1: Annealing conditions of BSCCO crystal. T and t are the annealing temperature and the annealing time, respectively, in an argon or vacuum environment

Annealing step	Environment	T($^{\circ}$ C)	t(hours)
A0	As-grown	-	-
A1	Argon	300	2
A2	Vacuum	300	5
A3	Vacuum	357	2
A4	Vacuum	400	1
A5	Vacuum	450	1

Figure 5.3 shows the transition of the decay of the trapped vortex field at a fixed temperature T_f , from a logarithmic to a non-logarithmic one, as the applied magnetic field and consequently the trapped field increase. At temperatures below the maximum of the trapped field, the density of the trapped vortex lines is low for all fields that we have applied. This suggests that the vortex lines can be trapped by the random pinning centers and that there is little interaction between the vortices. The decay of this trapped field is logarithmic which is in agreement with classical theories of the vortex creep in the absence of vortex-vortex interaction [18, 19]. Applying a higher magnetic field causes an increase in the trapped field accompanied by a shift of the maximum to temperatures below T_f . In this case, strong vortex-vortex interactions are expected, resulting in faster and non-logarithmic decays of the trapped field. This type of magnetic relaxation in the presence of strong vortex-vortex interactions is in agreement with collective flux creep theories [20, 21, 22] and vortex glass theories [23, 24, 25]. An increasing interaction between the vortices in the vicinity of the saturation line when the density of the trapped vortices increases, could also lead to a depinning of the vortices trapped by the random pinning centers. The shift of line A at low temperatures away from the saturation line observed in Figures 5.1(a) and 5.2(a) as the trapped field increases, may be an indication of this process.

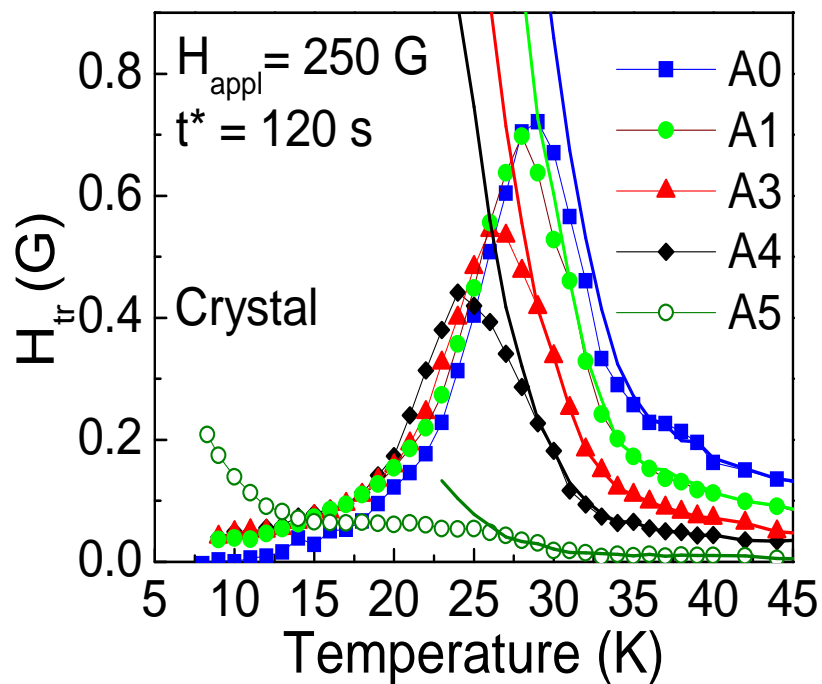


Figure 6.4: Evolution of the temperature dependence of the field trapped in the BSCCO crystal with the annealing temperature in vacuum. The field was trapped by applying a constant magnetic field of 250 G. The results for sample A2 are not shown. They are identical to those for sample A1. Solid curves represent the saturated lines.

6.4 Effects of Vacuum Annealing

In an attempt to identify the lattice defects that could be responsible for the vortex pinning above the maximum in the trapped field, we performed annealing experiments on BSCCO crystals (see Table 5.1). Annealing in vacuum (or in argon) introduces point defects, such as oxygen vacancies and subsequently suppresses the order parameter. In addition, annealing at elevated temperatures of 350-400°C in vacuum adds extra structural defects, such as dislocations and tweed-like dislocation structures into the BSCCO crystals [26, 27, 28]. Annealing at a higher temperature of 450°C causes complete removal of the structural dislocations out of the crystal [28]. It was also found that dislocations could act as strong pinning centers for the vortices, especially for the decoupled pancake vortices [26] in BSCCO crystals.

Figure 5.4 shows that annealing of the BSCCO crystal in vacuum reduces the trapped field (which was trapped by applying and subsequently turning off a constant applied magnetic field of 250 G) at temperatures above the maximum of the trapped field, but not at temperatures below the maximum. Annealing in vacuum shifts the saturation line to low temperatures and reduces the magnitude of the peak in the trapped field. Oxygen vacancies created during vacuum annealing act as random pinning centers which distort the vortex lattice and cause vortex depinning. This process creates a continuous drop of the trapped field after annealing in vacuum. The oxygen deficiency also reduces the hole doping and consequently the order parameter, being responsible for a decrease in T_c and a shift of the 2D-3D crossover temperature T^* and the saturation line (by about 5 K) to lower temperatures. On the other hand, the sudden collapse of the trapped field after annealing at 450°C (due to the annihilation of dislocations) suggests that the vortex pinning by dislocations could also be a substantial contributor to the peak in the dependence of the vortex trapping on temperature at temperatures below T^* . The peak in the trapped field for the BSCCO film was found to be shifted relative to the saturation line a few degrees more than the corresponding maximum in the BSCCO crystal. The stronger vortex-vortex interaction in the film which contains more random pinning defects, is likely

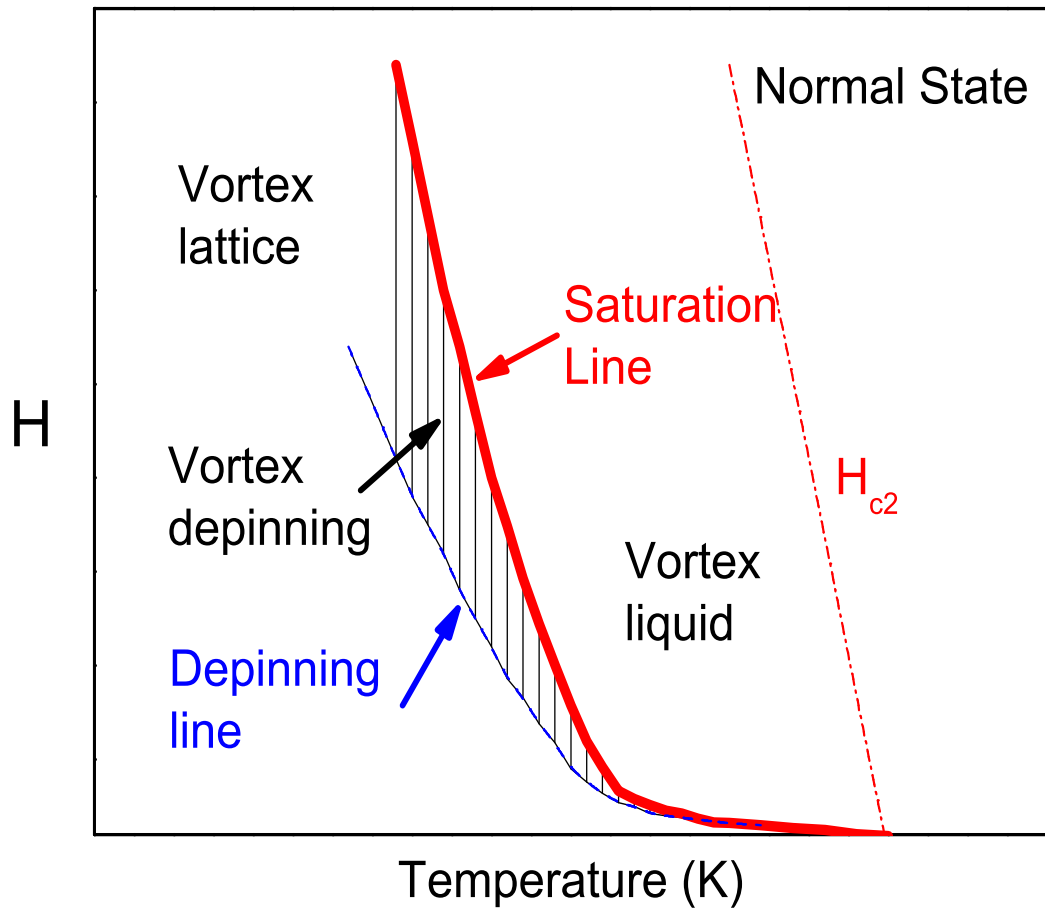


Figure 6.5: Schematic representation of the temperature dependence of the depinning and the saturated lines.

responsible for the depinning of the vortices at lower temperatures as suggested above.

6.5 Conclusions

In summary, we studied evolution of the vortex trapping in BSCCO single crystal and thin film superconductors. We measured the effects of temperature and applied magnetic field on the vortex trapping, as well as the relaxation (decay) of the resulting trapped vortex field. A maximum in the trapped field was observed at temperatures a few degrees below the vortex saturation line. Logarithmic and non-logarithmic decays of the trapped field were detected below and above this maximum, respectively. These

data suggest the presence of a vortex depinning transition in the close vicinity of the vortex saturation line (see Figure 5.5) in agreement with some theories [8, 9].

Bibliography

- [1] G. Blatter, M. V. Feigel'man, V. B. Geshkenbein, A. I. Larkin, V. M. Vinokur, *Rev. Mod. Phys.* **66**, 1125 (1994).
- [2] H. Beidenkopf, N. Avraham, Y. Myasoedov, H. Shtrikman, E. Zeldov, B. Rosenstein, E. H. Brandt, and T. Tamegai, *Phys. Rev. Lett.* **95**, 257004 (2005).
- [3] C. P. Bean, *Phys. Rev. Lett.* **8**, 250 (1962).
- [4] E. Zeldov, D. Majer, M. Konczykowski, V. B. Geshkenbein, V. M. Vinokur and H. Shtrikman, *Nature* **375**, 373 (1995).
- [5] W. Meissner and R. Ochsenfeld, *Naturwissenschaften* **21**, 787 (1933).
- [6] Ch Jooss, J Albrecht, H Kuhn, S Leonhardt and H Kronmuller, *Rep. Prog. Phys.* **65**, 651 (2002).
- [7] M. J. W. Dodgson, V. B. Geshkenbein, G. Blatter, *Phys. Rev. Lett.* **83**, 5358 (1999).
- [8] R. Sugano, T. Onogi, K. Hirata, and M. Tachiki, *Phys. Rev. Lett.* **80**, 2925 (1998).
- [9] R. Sugano et. al., *Physica B* **284**, 803 (2000).
- [10] L. Burlachkov, *Phys. Rev. B* **47**, 8056 (1993).
- [11] S. T. Weir, W. J. Nellis, Y. Dalichaouch, B. W. Lee, M. B. Maple, J. Z. Liu, R. N. Shelton, *Phys. Rev. B* **43**, 3034 (1991).

- [12] N. Chikumoto, M. Konczykowski, N. Motohira, A. P. Malozemoff, Phys. Rev. Lett. **69**, 1260 (1992).
- [13] E. Zeldov, A. I. Larkin, V. B. Geshkenbein, M. Konczykowski, D. Majer, B. Khaykovich, V. M. Vinokur, and H. Shtrikman, Phys. Rev. Lett. **73**, 1428 (1994).
- [14] M. V. Indenbom, G. D'Anna, M. O. Andre, V. V. Kabanov, and W. Benoit, Physica C **235-240**, 201 (1994).
- [15] M. Benkraouda and J. R. Clem, Phys. Rev. B **53**, 5716 (1996).
- [16] E. H. Brandt et al. eds, Physics and material science of vortex state, flux pinning and dynamics., volume 356 of NATO ASI. Kluwer Academic Publisher, the Netherlands, 1999.
- [17] L. Krusin-Elbaum et. al., Appl. Phys. Lett. **64**, 3331 (1994).
- [18] P. W. Anderson, Phys. Rev. Lett. **9**, 309 (1962).
- [19] K. Fossheim and A. Sudbo, Superconductivity Physics and Applications (John Wiley & Sons, Ltd, England, 2004), p.206.
- [20] Y. Yeshurun, A. P. Malozemoff, Phys. Rev. Lett. **60**, 2202 (1988).
- [21] M. V. Feigel'man, V. B. Geshkenbein, and V. M. Vinokur, Phys. Rev. B **43**, 6263 (1991).
- [22] M. V. Feigel'man, V. B. Geshkenbein, A. I. Larkin, and V. M. Vinokur, Phys. Rev. Lett. **63**, 2303 (1989).
- [23] M. P. A. Fisher, Phys. Rev. Lett. **62**, 1415 (1989).
- [24] A. P. Malozemoff and M. P. A. Fisher, Phys. Rev. B **42**, 6784 (1990).
- [25] D. S. Fisher, M. P. A. Fisher, and D. A. Huse, Phys. Rev. B **43**, 130 (1991).
- [26] G. Yang, P. Shang, S. D. Sutton, I. P. Jones, J. S. Abell, and C. E. Gough, Phys. Rev. B **48**, 4054 (1993).

- [27] G. Yang, P. Shang, I. P. Jones, J. S. Abell, and C. E. Gough, *Phys. Rev. B* **48**, 16873 (1993).
- [28] G. Yang, P. Shang, I. P. Jones, J. S. Abell, and C. E. Gough, *Physica C* **282**, 1093 (1997).

Chapter 7

Magnetic Properties in $YBa_2Cu_3O_{6+x}$ Single Crystal

In Chapter 3, we have studied the time dependence of vortex penetration in $Bi_2Sr_2CaCu_2O_{8+x}$ (BSCCO) superconductor [1]. In Chapter 5, we have studied the depinning induced phase transition in BSCCO superconductor [2]. In this chapter, we report the measurements of the vortex penetration and the depinning induced phase transition in a $YBa_2Cu_3O_{6+x}$ (YBCO) single crystal.

7.1 Introduction

Our early studies have shown that the vortex penetration process in BSCCO superconductors is strongly time dependent [1]. The penetration time scale varies and is dependent on the temperature, the applied field and the geometry of the sample. The temperature and magnetic field dependence of the vortex pinning and its relaxation were investigated in BSCCO single crystals and thin films [2]. The experiments revealed a peak in the temperature dependence of the trapped vortex field at temperatures below the vortex saturation line. Logarithmic and non-logarithmic dependence on time were observed in the magnetic relaxations at temperatures below and above the peak, respectively. The results suggest the presence of a vortex-depinning transi-

tion at temperatures below the saturation line of BSCCO.

In this chapter, we used a similar measuring procedure to test the vortex penetration into a YBCO single crystal under various conditions. The results show that a similar phenomena can be observed in the YBCO superconductor, which further confirms that the time dependent vortex penetration process is a universal phenomena in high- T_c superconductors.

7.2 Experimental Details

YBCO single crystal bulk samples with $T_c \simeq 92$ K and size of 2×3 mm came from Osaka University. The measuring procedure is similar to that used in the study of BSCCO superconductors, which is detailed in chapter 2.

In this chapter, we measure the trapped field in both the z -direction and the x -direction of the YBCO crystal, where z -direction is parallel to the c -axis of the crystal and x -direction is parallel to the a - b planes of the crystal.

7.3 Temperature Dependence and Time Dependence of Vortex Penetration

Figure 7.1 shows the temperature dependence of the trapped field obtained by applying a constant magnetic field over different time intervals t , as well as the measurements of the “saturation line”, i.e., the maximum trapped field at each temperature (represented by the solid line in Figures 7.1(a) and (b)). The temperature dependence of the trapped field, after a constant magnetic field is applied and subsequently removed, exhibits a maximum at temperatures close to the saturation line. At higher temperatures the trapped fields merge with those at the saturation line. In both of the x and z components of the trapped field, the maximum and the evolution with increasing t have been observed to be qualitatively similar.

As discussed for the BSCCO superconductors in Chapter 3, the observed depen-

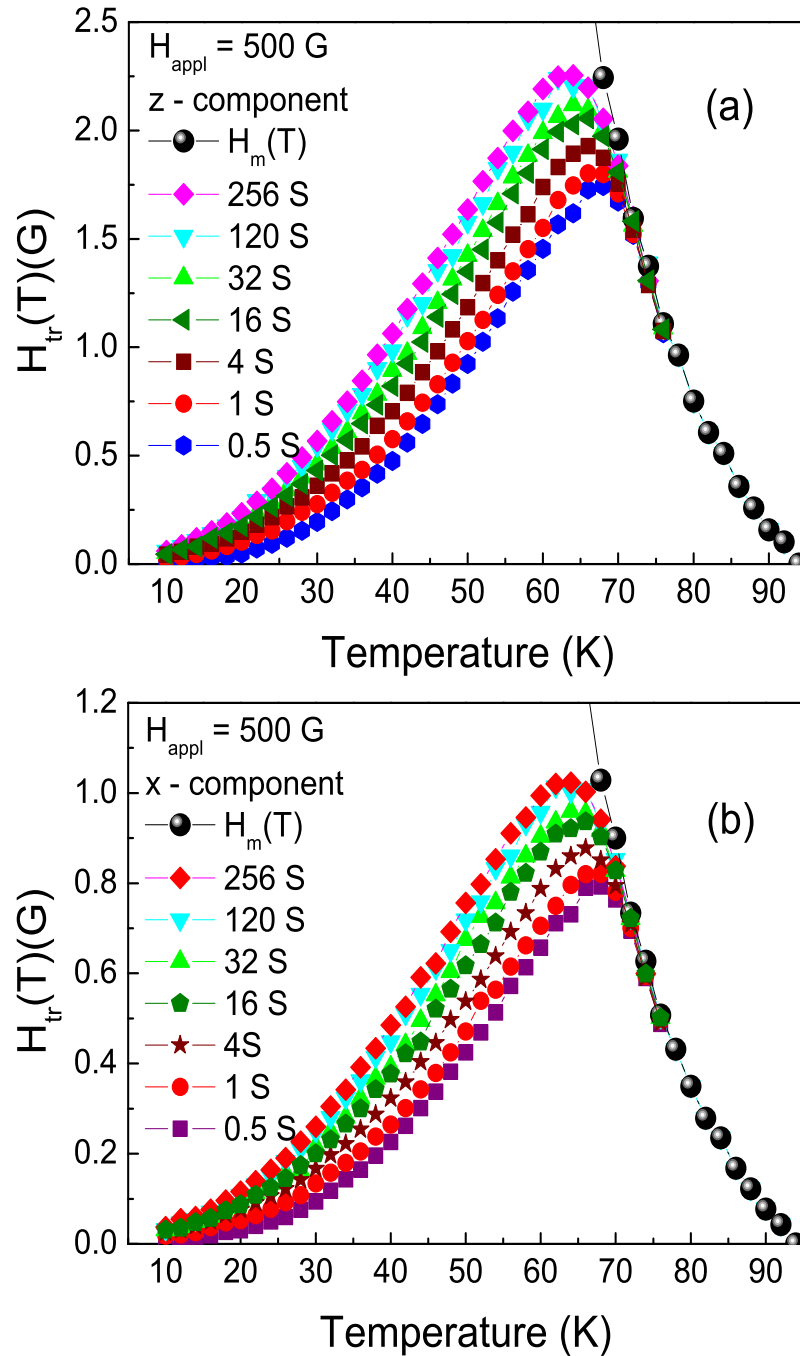


Figure 7.1: (a) Temperature dependence of the z-component of the field trapped in the YBCO single crystal. The field was trapped by applying a constant magnetic field $H_{appl} = 500$ G which was subsequently reduced to zero after a time interval t . $H_m(T)$ is the temperature dependence of the saturation line. (b) Temperature dependence of the x-component of the field trapped in the YBCO crystal after applying a constant field of 500 G.

dence of the trapped field on temperature could be the result of the surface screening effects [3], surface barriers [4, 5, 6, 7, 8, 9, 10, 11], and the softening of vortices [12]. Surface screening effects prevent the vortex penetration into a superconductor. However, the surface screening effect weakens with an increasing temperature, allowing more vortices to be pinned in a superconductor. Therefore, when a constant magnetic field is applied at different temperatures and subsequently removed, the resulting trapped field would gradually increase with an increasing temperature. The presence of the maximum suggests that the partial depinning of magnetic vortices [13, 14] occurs at temperatures above the maximum, which will be further discussed in the following sections.

Figure 7.1 also shows that the trapped magnetic field increases with increasing time t . According to Bean and Livingston [4], a vortex close to a surface (inside the superconductor) feels an attractive image force to the surface as well as a repulsive force from the external field. The sum of these two forces decreases exponentially away from the surface and is, therefore, a short range force which only works at the initial stage of the vortex-penetration process when the vortex is close to the surface. It indicates that, by applying an external magnetic field to a superconductor for a longer time, more vortices can surmount this energy barrier and penetrate into the superconductor and leading to a larger trapped magnetic field. However, it also shows that the time dependence of the vortex penetration in YBCO superconductor is not significant when compared to with that in BSCCO superconductor (see Chapter 3). The reason could be that YBCO superconductor is less anisotropic.

7.4 Phase Diagram

Figure 7.2 (a) and (b) show the magnetic phase diagram of the z -component and the x -component of the YBCO crystal, respectively. The magnetic phase diagrams consist of the trapped field curves measured under different applied magnetic field magnitudes but with the same applied field duration of $t^* = 120$ seconds. The

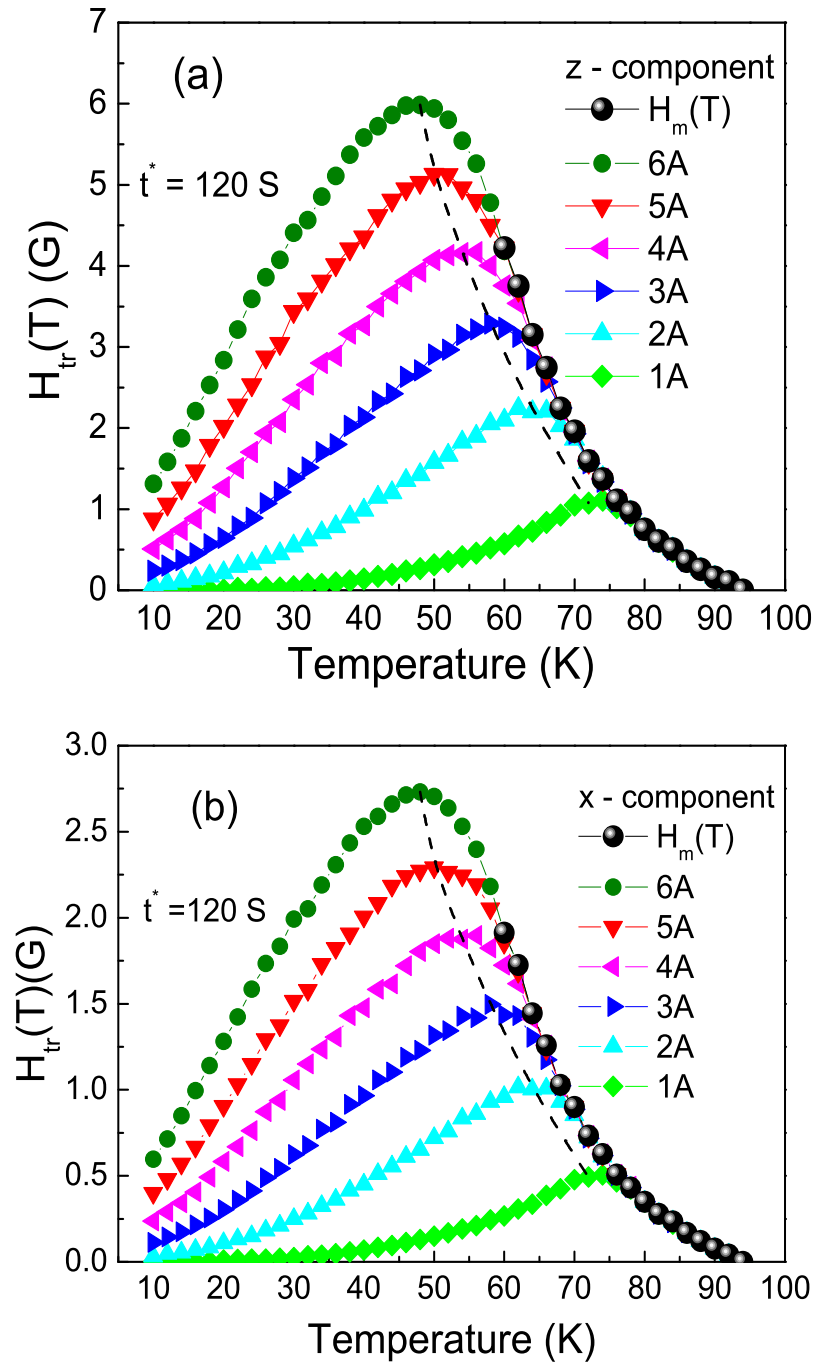


Figure 7.2: (a) Temperature dependence of the z -component of the field trapped in the YBCO single crystal by applying different constant magnetic fields between 250 G and 1500 G during a time interval of $t^* = 120$ s. $H_m(T)$ represents the temperature dependence of the saturation line. (b) The corresponding temperature dependence of x -component of the field trapped in the YBCO crystal by applying magnetic fields between 250 G and 1500 G during a time interval of $t^* = 120$ s.

trapped field curves are the temperature dependence of the trapped field obtained by applying a constant magnetic field to the sample over a fixed time interval t^* . The solid lines are the “saturation line” $H_m(T)$, i.e., the temperature dependence of the maximum field that could be trapped in a sample at each temperature for the z -component and the x -component, respectively, of the YBCO crystal. The trapped field H_{tr} exhibits a maximum at a temperature close to, but not at the saturation line. At higher temperatures the trapped fields merge with those at the saturation line. The maxima of the trapped fields increase with increasing applied field, but shift to lower temperatures. The dashed curves in Figures 7.2 (a) and (b) join the maxima of the trapped field. It marks the temperatures above which the pinning of the vortices becomes different.

The experiments show that the maxima in the trapped field in YBCO crystals occur at temperatures several degrees below the saturation line. The presence of the maximum suggests that the partial depinning of magnetic vortices [13, 14] occurs at temperatures above the maximum, leading to a gradual decrease of the trapped field with increasing temperature, which eventually merges with the saturation line at higher temperatures (see Figure 7.1).

The amount of the field trapped inside a superconductor also depends on the applied magnetic field. When a small field is applied at low enough temperatures, the strong surface screening currents limit the vortex entry into a superconductor. In this case only a small number of vortices can penetrate into the bulk, and their pinning results in a small trapped field. Applying a higher magnetic field causes an increase in the trapped field accompanied by a shift of the maximum to a lower temperature. This is because the density of the trapped vortices increases and an increasing interaction between the vortices in the vicinity of the saturation line lead to a depinning of the vortices trapped by the random pinning centers.

It is also interesting that the magnetic phase diagrams of the z -component and x -component are qualitatively similar even though the external field is only applied in the z -direction.

7.5 Decays

Figure 7.3 shows the decays of both x and z components of the trapped field measured at different temperatures around the peak. At lower temperatures, the decay of the trapped field H_{tr} over a time interval of about 3×10^4 s revealed that the decays are close to logarithmic. For temperatures at and above the peak, the decay curves start to deviate from the logarithmic behavior and become non-logarithmic.

Whether the decay is logarithmic or not provides information on the nature of the vortex interactions. At lower temperatures, the density of trapped vortex lines is low. This implies that all of the vortices could be trapped by random pinning centers and that there is little interaction between them. The decay of this trapped field is logarithmic which is in agreement with classical theories of the vortex creep in the absence of the vortex-vortex interaction [15, 16]. The trapped field at higher temperatures is accompanied by an increase of the decay rate which is again logarithmic. At still higher temperatures the trapped field decreases due to depinning of the trapped vortices. It is known that the random pinning centers can distort the vortex lattice. Consequently, this would increase the elastic energy of the flux lines. According to the collective pinning theory [17], the probability of depinning of a flux line is higher when the line has high elastic energy. Non-logarithmic relaxations of the trapped field at temperatures above the peak could reflect the vortex depinning and are in agreement with collective flux creep theory [18, 19, 20] and vortex glass theory [21, 22, 23].

As mentioned before, the amount of the field trapped inside a superconductor depends on temperature and applied magnetic field. This behavior is accompanied by changes in the time evolution of the trapped field. In other words, the maximum in the trapped field separates the low temperature region where the decays are logarithmic from the high temperature region where they are non-logarithmic.

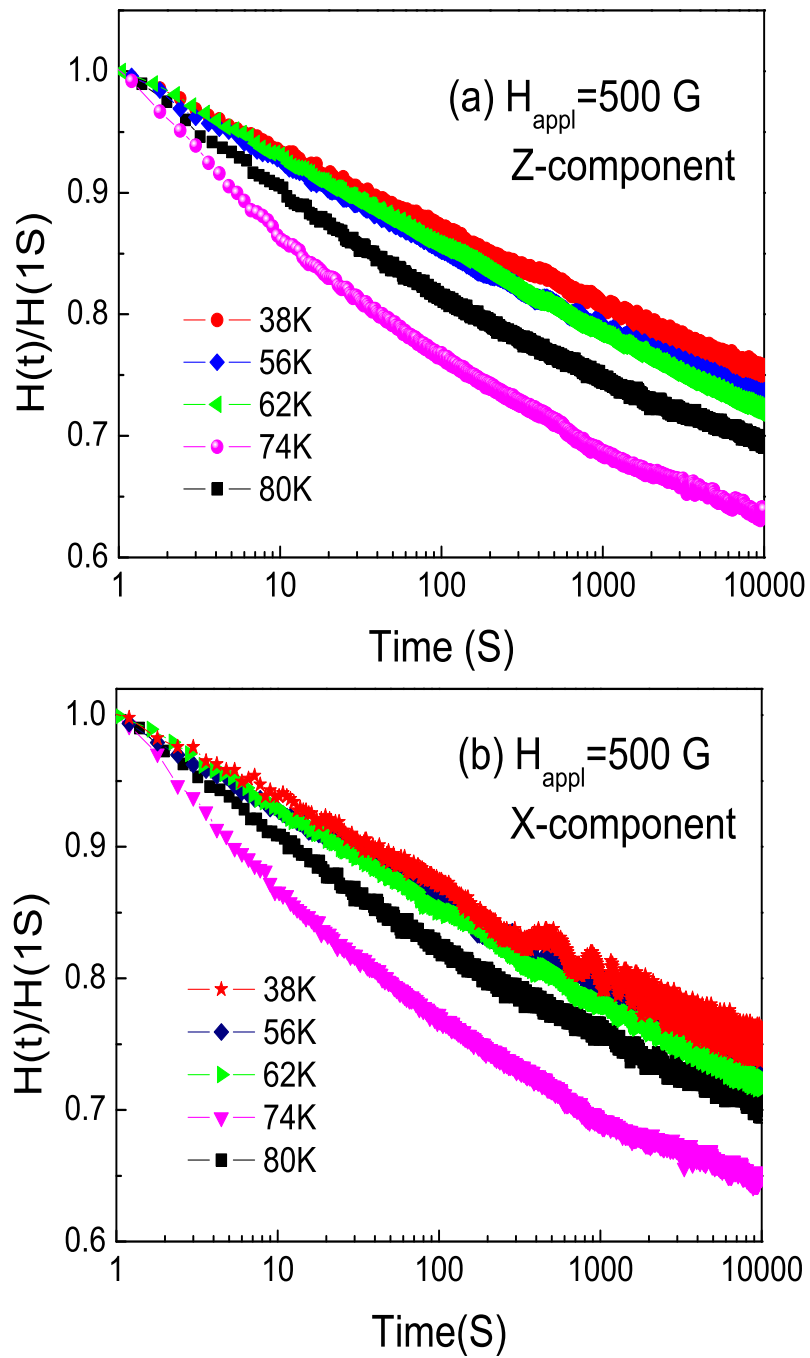


Figure 7.3: (a) Dependence of the z-component of the field trapped in the YBCO crystal on time measured at different temperature around the trapped field maximum. (b) The corresponding time decay curves of the x-component measured for the YBCO crystal.

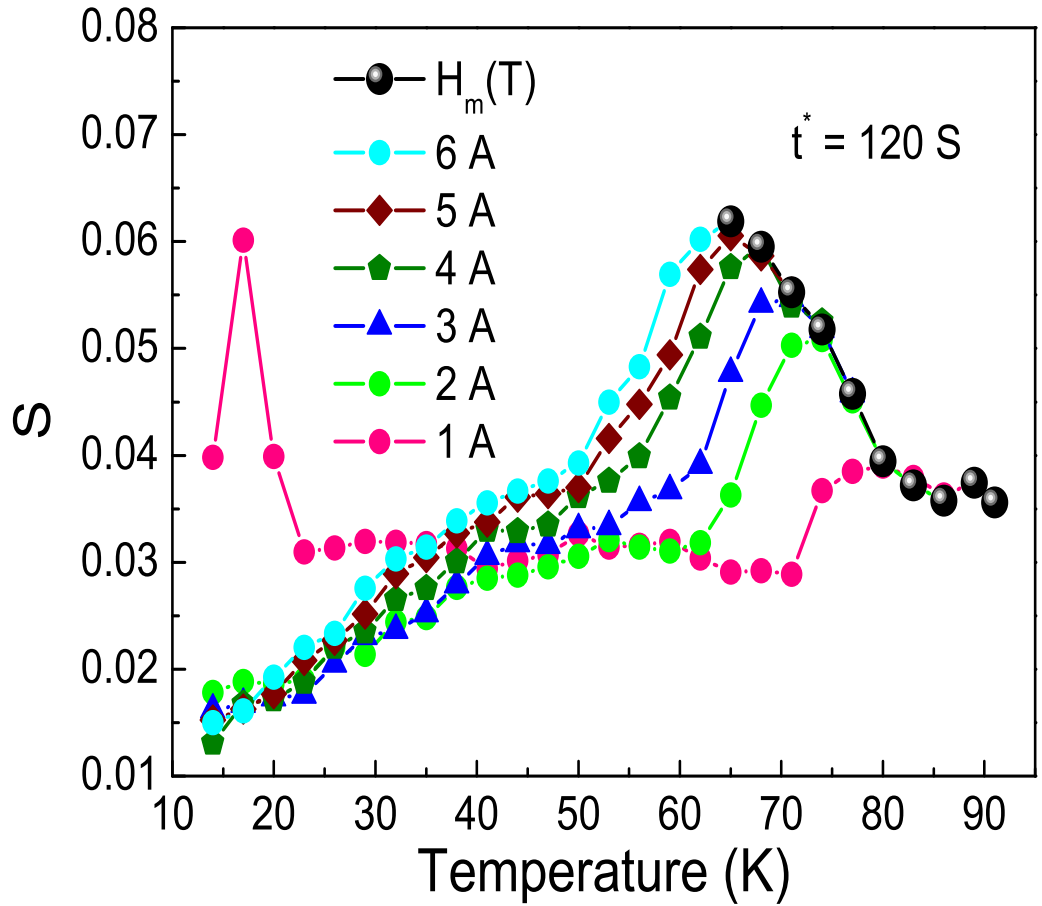


Figure 7.4: Temperature dependence of the logarithmic decay rates $S=d(\ln H_{tr})/d(\ln t)$ of the z -component of the trapped field calculated for a short initial time intervals up to 10-20 s for the YBCO crystal. Decay rates correspond to the points on the phase diagram of z -component.

7.6 Decay Rates

Figure 7.4 shows the decay rates $S=d(\ln H_{tr})/d(\ln t)$ of the z -component of the trapped field as a function of temperature. Because of the non-logarithmic character of the decay curves at the higher temperatures above the peaks (see Figure 6.3), we calculated the decay rates, $S=d(\ln H_{tr})/d(\ln t)$, only for very short initial time intervals of up to 10-20 s. These decay rates correspond to the points on the phase diagram of the z -component. At the temperatures below the peaks in the magnetic phase diagram, S is approximately constant. While at and above the peaks, the decay rates increase quickly, which corresponds to a reduction in the trapped field as shown in Figure 6.2. Finally, the decay rates decrease again and reach a common constant value at higher temperatures.

This result agrees with the observation of two different dependencies of the trapped field on time at temperatures below and above the maximum (see Figure 7.3). It suggests partial depinning of magnetic vortices [13, 14] occurs at temperatures above the maximum, resulting in a gradual decrease of the trapped field with increasing temperature. The line which joins the maxima of the trapped field separates the two different vortex pinning regimes. Therefore, we believe that the line which joins the maxima can be interpreted as the vortex depinning line.

7.7 Conclusions

In summary, we found that the vortex-penetration process in YBCO crystal is time dependent and strongly related to the edge barriers of the sample. Since the same phenomena is also observed in Bi-2212 superconductors, this indicates that the physics revealed in our measurements are not restricted to the specific microstructure of a YBCO or a BSCCO superconductor. Therefore, we conclude that the time dependent vortex-penetration process is a general physical property of type-II superconductors. We also studied the evolution of the vortex trapping in YBCO crystal. We measured the effects of temperature and applied magnetic field on vortex penetration, as well

as the relaxation (decay) of the resultant trapped vortex field. A maximum in the trapped field was observed at temperatures a few degrees below the vortex saturation line. Logarithmic decays of the trapped field were detected below and non-logarithmic decays were found above this maximum. These data suggest the presence of the vortex depinning transition close to the vicinity of the vortex saturation line.

Bibliography

- [1] Rongchao Ma et. al, Time-dependent vortex-penetration in $Bi_2Sr_2CaCu_2O_{8+x}$ superconductor. To be published.
- [2] Rongchao Ma et. al, Depinning-induced transition in Bi-2212 superconductors. To be published.
- [3] W. Meissner and R. Ochsenfeld, *Naturwissenschaften* **21**, 787 (1933).
- [4] C. P. Bean, J. D. Livingston, *Phys. Rev. Lett.* **12**, 14 (1964).
- [5] L. Burlachkov, *Phys. Rev. B* **47**, 8056 (1993).
- [6] S. T. Weir, W. J. Nellis, Y. Dalichaouch, B. W. Lee, M. B. Maple, J. Z. Liu, R. N. Shelton, *Phys. Rev. B* **43**, 3034 (1991).
- [7] N. Chikumoto, M. Konczykowski, N. Motohira, A. P. Malozemoff, *Phys. Rev. Lett.* **69**, 1260 (1992).
- [8] E. Zeldov, A. I. Larkin, V. B. Geshkenbein, M. Konczykowski, D. Majer, B. Khaykovich, V. M. Vinokur, and H. Shtrikman, *Phys. Rev. Lett.* **73**, 1428 (1994).
- [9] M. V. Indenbom, G. D'Anna, M. O. Andre, V. V. Kabanov, and W. Benoit, *Physica C* **235-240**, 201 (1994).
- [10] M. Benkraouda and J. R. Clem, *Phys. Rev. B* **53**, 5716 (1996).

- [11] E. H. Brandt et al. eds, Physics and material science of vortex state, flux pinning and dynamics., volume 356 of NATO ASI. Kluwer Academic Publisher, the Netherlands, 1999.
- [12] G. Blatter, M. V. Feigel'man, V. B. Geshkenbein, A. I. Larkin, V. M. Vinokur, Rev. Mod. Phys. **66**, 1125 (1994).
- [13] Ryoko Sugano, Toshiyuki Onogi, Kazuto Hirata, Masashi Tachiki, Physica B **284-288**, 803 (2000).
- [14] R. Sugano, T. Onogi, K. Hirata, and M. Tachiki, Phys. Rev. Lett. **80**, 2952 (1998).
- [15] P. W. Anderson, Phys. Rev. Lett. **9**, 309 (1962).
- [16] K. Fossheim and A. Sudbo, Superconductivity Physics and Applications (John Wiley & Sons, Ltd, England, 2004), p.206.
- [17] A. I. Larkin and Yu. N. Ovchinnikov, J. Low Temp. Phys. **34**, 409 (1979).
- [18] Y. Yeshurun, A. P. Malozemoff, Phys. Rev. Lett. **60**, 2202 (1988).
- [19] M. V. Feigel'man, V. B. Geshkenbein, and V. M. Vinokur, Phys. Rev. B **43**, 6263 (1991).
- [20] M. V. Feigel'man, V. B. Geshkenbein, A. I. Larkin, and V. M. Vinokur, Phys. Rev. Lett. **63**, 2303 (1989).
- [21] M. P. A. Fisher, Phys. Rev. Lett. **62**, 1415 (1989).
- [22] A. P. Malozemoff and M. P. A. Fisher, Phys. Rev. B **42**, 6784 (1990).
- [23] D. S. Fisher, M. P. A. Fisher, and D. A. Huse, Phys. Rev. B **43**, 130 (1991).

Chapter 8

Summary and Conclusions

The vortex dynamics, such as vortex penetration, vortex relaxation and vortex-depinning transition, has been systematically studied in $Bi_2Sr_2CaCu_2O_{8+x}$ (BSCCO) and $YBa_2Cu_3O_{6+x}$ (YBCO) superconductors with a Hall sensor of sensitivity ± 2 mG. Our results are summarized as follows:

8.1 Vortex Penetration

The time scales of the vortex penetration into $Bi_2Sr_2CaCu_2O_{8+x}$ superconductors were studied under various conditions. The temperature dependence of the trapped field obtained by applying a constant magnetic field over different time intervals t^* shows a maximum at a temperature close to the melting line. At higher temperatures the trapped fields merge with those at the saturation line. The maximum in the trapped field and its evolution with an increasing t^* has been observed to be qualitatively similar in both the single crystal and thin film samples. The observed dependence of the trapped field on temperature could be the result of the interplay between the surface screening effects and the surface and bulk pinning of the vortices.

The measurements of the trapped field as a function of the time interval during which a constant field was applied to the sample indicates that vortex penetration into the BSCCO superconductors is strongly time dependent. The plot of B vs. t (Figure

3.3 and 3.4) shows that the vortex penetration curves have a “concave” shape at short time periods, and subsequently turn into a “convex” shape at some crossover time. The “concave” shape in the vortex penetration curves may be caused by surface screening effects and edge barriers. The vortex close to a surface feels the Bean-Livingston forces, which decrease exponentially away from the surface; therefore, it is a short range force which only works at the initial stage of the vortex-penetration process. Vortex penetration is very fast over the first few seconds and then slows down to approach an upper limit asymptotically. As a vortex penetrates into the interior of the crystal, where $x \gg \lambda$ (λ is the penetration depth), the Bean-Livingston force becomes negligible. It results in a quickly increasing trapped field; the shape of the penetration curve is then changed into the “convex” shape on a longer time scale.

The penetration time scale depends on the applied field, the temperature and the geometry of the sample. For a larger applied magnetic field, the vortices are subjected to a greater driving force, the penetration is faster and the convex-concave shape crossover appears on a shorter time scale. If the applied field is large enough, the crossover is not observed. On the other hand, the surface screening effect weakens with increasing temperature, allowing the vortices to penetrate into the superconductor more quickly at the higher temperatures. The crossover is then also shifted to an earlier point in the penetration process. At a sufficiently high temperature, the crossover is close to zero and finally becomes unobservable. This is further shown in the thin film sample, in which all the vortex penetration curves are “convex” in shape, and there are no “concave” shapes. This is explained by the fact that the thin film sample has a greatly reduced thickness (z -axis), so that the surface barriers perpendicular to z -axis are then very small. With an applied magnetic field parallel to the z -axis, the surface screening effect should be weak, and, therefore, the “concave” shape curves should not be observed.

8.2 Vortex Dynamics with Persistent Currents

The measurements of the temperature dependence of the persistent current density J_m close to the critical state in the ring-shaped as-grown BSCCO crystal show a very sharp drop of J_m with increasing temperature at low temperatures below $T^* = 36$ K, but J_m decreases slowly with increasing temperature at temperatures above T^* . The measurement of the time decays of the persistent current from the critical level shows very fast decays of the persistent current at temperatures below T^* , in contrast to much slower ones at temperatures above T^* .

The temperature dependence of the persistent current J recorded at different times between 1 and 10^4 s after the critical state was established in the ring-shaped as-grown BSCCO crystal was determined. After 10^4 s a giant reduction of the persistent current magnitude by almost 85-90% was detected at temperatures below T^* . This is in contrast to a much smaller drop of the persistent current by about 40% which was detected at temperatures above T^* .

At temperatures below T^* the time decays of the persistent current from the critical level are non-logarithmic over a time period between 1 and 10^4 s; however, above T^* they become quasi-logarithmic. The super-fast non-logarithmic decays are in agreement with the general frameworks of the collective flux creep theory and the vortex-glass theory. The persistent current decay rates dJ/dt have been used to calculate the dependence of the effective energy barrier against vortex motion $U_{eff}(J, T)$ on the persistent current density J over a time period between 1 and 10^4 seconds. The dependence of the effective energy barrier on J could be described by a power-law, i.e., $U_{eff}(J) \propto (J_c/J)^\mu$ with $\mu_1 \simeq 1/7$ and $\mu_2 \simeq 2/3$ below T^* (high currents) and above T^* (low currents), respectively.

After the ring-shaped BSCCO crystal was annealed in vacuum at temperatures between 300 and 450 °C, the absolute value of J_m drops by more than 95%, which is associated with a decrease of T_c and T^* by only 5 K. The temperature dependence of J_m , as well as the dependence of J on time are not affected by the vacuum annealing. Critical exponents $\mu_{1,2}$ are obtained from the dependence of U_{eff} on the current

density J after each annealing step. The change in the microstructure has little effect on the vortex dynamics at temperatures below T^* , where μ_1 fluctuates around the value of $1/7$. The independence of μ_1 on the microstructure suggests a highly cooperative effect in the vortex structure at temperatures below T^* . On the other hand, at temperatures above T^* the vortex dynamics is strongly affected by the microstructure, where μ_2 displays a monotonic decrease from ~ 0.7 to 0.35 , as the current density drops from a high to a very low value. The exponent μ_2 is 0.7 in the as-grown ring-shaped BSCCO crystal, which suggests that the vortices are in the low density limit, i.e., they are far enough apart that bulges can occur in single vortices, and $\mu = (6 - d)/4$. For $d = 3$ (vortices with kinks) $\mu = 3/4$. After all thermal annealings the sample's current density is small, and μ_2 drops to $0.35 \sim 1/3$. By analogy with the Bose glass picture $\mu = 1/3$ has been attributed to the situation where the vortex lines start to wander individually but with the superposition of a random pinning potential and a weak periodic potential reflecting short-range order.

8.3 Vortex Depinning Transition

The vortex depinning transition was studied by measuring the effects of temperature and applied magnetic field on vortex penetration. A maximum in the trapped field was observed at a temperature a few degrees below the vortex melting line. The temperature dependence of the trapped field and its maximum at a temperature below the saturation line is qualitatively similar for single crystal and thin film. The presence of the maximum suggests that partial depinning of magnetic vortices occurs at temperatures above the maximum, leading to a gradual decrease of the trapped field with increasing temperature which eventually merges with the melting line. The line which joins the maxima of the trapped field separates two different vortex pinning regimes. The decays of the trapped field (relaxation) are close to logarithmic only at temperatures below the peak. For temperatures at and above the peak, the decay curves start to deviate from the logarithmic behavior and become non-logarithmic,

which is accompanied by changes in the temperature dependence of the decay rates of the trapped field. This property was found to be the same for both single crystal and thin film samples; therefore, it is independent of the sample geometry.

Our results also show a large difference between the properties of the film and those of the crystal. The melting field H_m and the crossover temperature T^* of the thin film is much higher than that of the crystal. This suggests a relationship to the sample purity, since thin films contain more impurities than crystals. The impurities in the thin film as well as the interface between the thin film and the substrate act as pinning centers, and the thin film will have a melting field H_m which is higher than that of the crystal. The decay rate S in the film is much smaller than those in the crystal, due to stronger pinning within the film.

At a fixed temperature T_f , the decay of the trapped field transits from a logarithmic to a non-logarithmic state as the applied magnetic field and, consequently, the trapped field increase. At a temperature below the peak, the density of the trapped vortex lines are low for all applied fields. The decay of this trapped field is logarithmic which is in agreement with classical theories of vortex creep in the absence of the vortex-vortex interaction. Applying higher magnetic fields causes an increase in the trapped field which is accompanied by a shift of the maximum to temperatures below T_f . In this case, strong vortex-vortex interactions are expected, resulting in faster and more non-logarithmic decays of the trapped field. This type of magnetic relaxation in the presence of strong vortex-vortex interaction is in agreement with collective flux creep theories and vortex glass theories.

Annealing of the BSCCO crystal in vacuum reduces the trapped field at temperatures above the maximum of the trapped field, but not at temperatures below the maximum. Annealing also shifts the melting line to low temperatures and reduces the magnitude of the peak in the trapped field. We suggest that the oxygen vacancies created during vacuum annealing are responsible for the decrease in T_c , the shift of the crossover temperature T^* and the melting line (by about 5 K) to lower temperatures.

8.4 Magnetic Properties in YBCO Crystal

Finally, vortex penetration, vortex relaxation and vortex-depinning transition were studied in a YBCO crystal sample. We measured the effects of temperature and applied magnetic field on the vortex penetration, the relaxation (decay) of the trapped vortex field, and so on. We found that the vortex penetration, vortex depinning transition, and vortex dynamics with persistent currents in YBCO crystal are qualitatively similar to those observed in the Bi-2212 superconductors, indicating that the physics revealed in our measurements is not restricted to the specified microstructure of BSCCO superconductor, but is a general physical property of all type-II superconductors.

8.5 Outlook

Finally, we would like to point out that our studies in Bi-2212 thin films are strongly restricted by fabrication technologies currently available as it is extremely difficult to prepare good thin film samples with high T_c and high J_c . More studies should be carried out on the technique to help improve the performance of the thin films. On the other hand, our measurements are focused on arranging the applied field perpendicular to the layered structure (parallel to the c -axis) of the Bi-2212 superconductor. In most applications of real wires, the applied magnetic fields are arranged parallel to the layered structures of the superconductors. There should be more exploration done by arranging the field parallel to the ab -plane. Furthermore, our results also indicate that the properties observed are not restricted to the special microstructure of Bi-2212 superconductor, so we expect that more interesting results will be observed in other series of superconductors using the same measuring procedures described in this thesis.

Bibliography

- [1] E. Zeldov, A. I. Larkin, V. B. Geshkenbein, M. Konczykowski, D. Majer, B. Khaykovich, V. M. Vinokur, and H. Shtrikman, *Phys. Rev. Lett.* **73**, 1428 (1994).